BOHR MODEL AND DIMENSIONAL SCALING ANALYSIS OF ATOMS AND MOLECULES

A Dissertation

by

KERIM URTEKIN

Submitted to the Office of Graduate Studies of
Texas A&M University
in partial fulfillment of the requirements for the degree of

DOCTOR OF PHILOSOPHY

December 2006

Major Subject: Physics

BOHR MODEL AND DIMENSIONAL SCALING ANALYSIS OF ATOMS AND MOLECULES

A Dissertation

by

KERIM URTEKIN

Submitted to the Office of Graduate Studies of
Texas A&M University
in partial fulfillment of the requirements for the degree of

DOCTOR OF PHILOSOPHY

Approved by:

Chair of Committee,	Marlan Scully
Committee Members,	Siu Chin
	Suhail Zubairy
	Goong Chen
Head of Department,	Edward Fry

December 2006

Major Subject: Physics

ABSTRACT

Bohr Model and Dimensional Scaling Analysis of Atoms and Molecules.

(December 2006)

Kerim Urtekin, B.S., Bogazici University (Istanbul, Turkey)

Chair of Advisory Committee: Dr. Marlan Scully

It is generally believed that the old quantum theory, as presented by Niels Bohr in 1913, fails when applied to many-electron systems, such as molecules, and nonhydrogenic atoms. It is the central theme of this dissertation to display with examples and applications the implementation of a simple and successful extension of Bohr's planetary model of the hydrogenic atom, which has recently been developed by an atomic and molecular theory group from Texas A&M University. This "extended" Bohr model, which can be derived from quantum mechanics using the well-known dimentional scaling technique is used to yield potential energy curves of H_2 and several more complicated molecules, such as LiH, Li_2, BeH, He_2 and H_3, with accuracies strikingly comparable to those obtained from the more lengthy and rigorous "ab initio" computations, and the added advantage that it provides a rather insightful and pictorial description of how electrons behave to form chemical bonds, a theme not central to "ab initio" quantum chemistry. Further investigation directed to CH, and the four-atom system H_4 (with both linear and square configurations), via the interpolated Bohr model, and the constrained Bohr model (with an effective potential), respectively, is reported. The extended model is also used to calculate correlation energies.

The model is readily applicable to the study of molecular species in the presence of strong magnetic fields, as is the case in the vicinities of white dwarfs and neutron stars. We find that magnetic field increases the binding energy and decreases the

bond length.

Finally, an elaborative review of doubly coupled quantum dots for a derivation of the electron exchange energy, a straightforward application of Heitler-London method of quantum molecular chemistry, concludes the dissertation.

The highlights of the research are (1) a bridging together of the pre- and post quantum mechanical descriptions of the chemical bond (Bohr-Sommerfeld vs Heisenberg-Schrödinger), and (2) the reporting of the appearance of new bound states of H_2 in the presence of very strong magnetic fields. The new states emerge above the critical value of 5×10^7 G, and hence cannot be obtained perturbatively.

To Fatma Gultekin

my Friend...

my Teacher...

my Mother...

ACKNOWLEDGMENTS

If stately throngs of words in steady march would pretend power of expression, they should soon acquaint themselves with frustration this day. For I am not in the mood!

Only little children of words are welcome! Artless, happy, little children of words... Their reckless glee and overflowing joy might well fade to an amusing confusion as this goes on.. But never to frustration..

Only with them, yet in their silence are my deep-felt, simple, intense appreciation and gratitude able to find their voice to

intelligent friend...

wise mentor...

and very patient advisor...

Dr. Anatoly Svidzinsky who, to say the very least, suggested the problem as well as directed and guided the research.

It is simply impossible for me to forget Dr. Dudley Herschbach, for more than the very fruitful discussions, much more.. I thank him for the encouragement I had come to need, the example of his intelligent sense of humor, and the perspective of the curious, diligent, “amateur” scientist I can be!

I thank all my thesis committee members, above all, my Chair Dr. Marlan Scully, for bringing me together with these wonderful people and supporting me financially during my studies.

Finally, I’d like to extend my most sincere gratitude to ”Sevgilim” Dorothy ”Zilli” Slater, Seth Andrew Gibson, Catherine Ismini Zachariades, Zoe Elizabeth Sariyanni, Soner Tarim, and, last but not least, Tolga Ciftci for his patient editing of my manuscript and very strange sense of humor.

TABLE OF CONTENTS

CHAPTER Page

LIST OF FIGURES

FIGURE Page

FIGURE Page

FIGURE Page

FIGURE Page

CHAPTER I

INTRODUCTION

> The most beautiful thing we can experience is the mysterious. It is the source of all true art and science. He to whom this emotion is a stranger, who can no longer pause to wonder and stand rapt in awe, is as good as dead: his eyes are closed.
>
> Albert Einstein

When Niels Bohr proposed his shell model of the atom [1], it was in an effort to explain how electrons could have stable orbits around the nucleus. The year was 1913, and a general acknowledgement of a tumulting inadequacy of classical mechanics and electromagnetic theory (due in its final form largely to Maxwell) to successfully treat an increasing host of problems, (e.g. the blackbody radiation originally posed by Gustav Kirchoff as a challenge) had been well under way. The model, though suspect, was a great success, and accurately predicted the discrete spectral lines of atomic hydrogen. This work would later earn Bohr the 1922 Nobel Prize for Physics.

To put Bohr and his work in the better light that it deserves, then it is only fair that we take a quick glance at the different phases through history of the advancement of the idea of atom as the major building block of all matter.

Recorded history details such an idea essentially advanced by the Greek philosopher Democritus of Abdera (c.460—c.370), pupil of Leucippus although there are those who argue that Democritus was not the first to propose an atomic theory, invariably influenced by his teacher Leucippus (whose existence is doubted by some

---

The journal model is Physical Review A.

writers) as well as the atomic system of Anaxagoras of Clazomenae. Democritus atomic model essentially differs from that of Anaxagoras in that he conceives of the atom as that of which all matter is made, and which may not be further subdivided. His view is summarized in [2]:

"Democritus asserted that space, or the Void, had an equal right with reality, or Being, to be considered existent. He conceived of the Void as a vacuum, an infinite space in which moved an infinite number of atoms that made up Being (i.e. the physical world). These atoms are eternal and invisible; absolutely small, so small that their size cannot be diminished (hence the name atomon, or "indivisible"); absolutely full and incompressible, as they are without pores and entirely fill the space they occupy; and homogeneous, differing only in shape, arrangement, position, and magnitude."

Another useful reference is [3]:

"Democritus's theory of the atomic nature of the physical world, developed from that of Leucippus, is known only through the works of critics of the theory such as Aristotle and Theophrastus. It resolved the question of how a world evidently in a state of flux could nevertheless have an underlying nature that was eternal and unchanging. By positing infinitely small things that remained the same but formed different combinations with each other, Leucippus initially, and Democritus in greater detail, managed to answer the question in a way that has been subject to increasingly successful elaboration ever since. One can trace the physical theory of atoms through Epicurus, Lucretius, and Galileo to modern times."

Credit for the first modern atomic theory goes to the English chemist, John Dalton. In his 1808 book, A New System of Chemical Philosophy, Dalton outlined five fundamental postulates about atoms:

1. All matter consists of tiny, indivisible particles, which Dalton called atoms.

2. All atoms of a particular element are exactly alike, but atoms of different

elements are different.

3. All atoms are unchangeable.

4. Atoms of elements combine to form "compound atoms" (i.e., molecules) of compounds.

5. In chemical reactions, atoms are neither created nor destroyed, but are only rearranged.

A key distinguishing feature of Dalton's theory was his emphasis on the weights of atoms. He argued that every atom had a specific weight that could be determined by experimental analysis. Although the specific details of Dalton's proposed mechanism for determining atomic weights were flawed, his proposal stimulated other chemists to begin research on atomic weights.

Dalton's theory was widely accepted because it explained so many existing experimental observations and because it was so fruitful in suggesting new lines of research. But the theory proved to be wrong in many of its particulars. For example, in 1897, the English physicist Joseph J. Thomson showed that particles even smaller than the atom–electrons–could be extracted from atoms. Atoms could not, therefore, be indivisible. The discovery of radioactivity at about the same time showed that at least some atoms are not unchangeable but, instead, spontaneously decay into other kinds of atoms.

In order to explain the results of the experiments on scattering of X-rays by matter Prof. Rutherford has given a theory of the structure of atoms. According to this theory, the atoms consist of a positively charged nucleus surrounded by a system of electrons kept together by attractive forces from the nucleus.... Great interest is to be attributed to this atom-model; for, as Rutherford has shown, the assumption of the existence of nuclei.... seems to be necessary in order to account for the results of the experiments on large angle scattering of the X-rays.

Rutherford's model of the structure of the atom suffered from the apparent instability of the system of electrons, which, according to classical mechanics and electromagnetic theory, should spiral inward, and ultimately collapse into the nucleus through a continuous radiative process, a problem to quote Bohr "purposefully avoided in atom-models previously considered, for instance, in the one proposed by Sir J. Thomson."

As Bohr points out, an elucidation of the principal difference between the atomic models of Thomson and Rutherford, namely the existence, in the former, of configurations and motions of the electrons that allow for a stable equilibrium of the atom, is possible by noticing also the presence of a characteristic length, i.e., the radius of Thomson's positive sphere having the same order of magnitude as the linear extension of the atom whereas such a characteristic length does not appear among the quantities, i.e., the electronic and positive-nuclear charges and masses specifying Rutherford's atom.

With the bearing evidence of the experiments on scattering of the X-rays by matter leaving nothing to puzzle out the mystery of large angle deflections except by an atomic structure that accommodates positively charged nuclei carrying the bulk atomic mass, however, Thomson's model must be discarded, and the difficulties surrounding the Rutherford model, i.e., the implied instability of Keplerian orbits and the absence of a natural parameter with the dimension of length, be addressed squarely. It was, indeed, by this insufficiency of classical electrodynamics to offer a natural parameter by which to ascertain the above-mentioned characteristic length that Bohr was eventually tempted to advance an integration of Planck's theory to considerations of the structure of the atom as such a quantity, i.e., Plank's constant, the elementary quantum of action, does provide the necessary dimension of length. The introduction of this quantity, together with the mass and charge of the particles,

could now be used to determine a length of the required order of magnitude.

Admittedly by Bohr, this was an attempt to show how the application of Planck's theory to Rutherford's atomic model could "afford a basis for a theory of the constitution of atoms", and to further show "that from this theory we are led to a theory of the constitution of molecules".

An early success of the Bohr model was its accurate prediction of the spectral lines of hydrogen for which only an empirical formula (devised by Johannes Rydberg in 1888, and offering no theoretical basis for a physical mechanism) had existed. Bohr maintained that the emission or absorption of radiation could occur only as a result of the system passing from one "state" to another, a term which acquired its broadened meaning in the course of the later more rigorous formulation of quantum mechanics. He asserted that the frequency of such radiation would be related to the energy it imparted, given by Planck's formula, and that in turn this energy would be equal to the difference in energy between the initial and final states.

Decisive evidence for the discrete energy level structure of the atom came from the prizewinning joint experimental work of James Franck and Gustav Hertz that showed that upon collision with an atom, an electron must possess a certain energy in order for that energy to be transferred to the atom (4.9 eV in the case of mercury vapor.) This was a clear demonstration of the quantized inner structure of the atom as foreseen by Niels Bohr, i.e., that energy could be absorbed by atoms only in quanta. Franck and Hertz shared the Nobel Prize for Physics in 1925 for their work.

The success of Bohr's model sparked a genuine interest in Arnold Sommerfeld, who zealously set about exploring avenues of betterment. In particular, Sommerfeld extended the model introducing elliptical orbits. This was a foundation of "old" quantum mechanics which later was substituted by the "new" quantum mechanics due to Schrödinger and Heisenberg.

CHAPTER II

INTERPOLATED BOHR MODEL

A. Bohr model of H_2 molecule

The Bohr model [1] for a one-electron atom played a major historical role and still offers pedagogical appeal. However, when applied to the simple H_2 molecule, the "old quantum theory" proved unsatisfactory [4, 5]. Recently Svidzinsky, Scully and Herschbach [6, 7] found a simple extension of the original Bohr model which describes potential energy curves $E(R)$ of simple molecules with striking accuracy. Such a description provides an insightful picture of how electrons form chemical bonds in molecules. In this introductory section we briefly discuss their findings and consider H_2 molecule as a simplest example.

The Bohr model can be derived from quantum mechanics using dimensional scaling analysis technique developed in quantum chromodynamics. Dimensional scaling analysis provides an unconventional method to treat electronic structure [8, 9, 10, 11, 12]. This method emulates an approach developed in quantum chromodynamics [13], by generalizing the Schrödinger equation to D dimensions and rescaling coordinates [11]. Early work found the tutorial D-scaling procedure of Witten [13] can be dramatically improved; the ground state energy of He was obtained accurate to 5 significant figures by interpolation between the $D = 1$ and $D \to \infty$ limits [8], and to 9 figures by a perturbation expansion in 1/D [14]. However, the scaling procedure which worked well for atoms [8, 10] did not prove successful for two-center problems [11, 12]; e.g., for H_2 that procedure did not yield a bound ground state. In the recently developed D-scaling approach [6], the large-D limit makes contact with the Bohr model [1] which improves the accuracy. In this way we obtain a link between prequantum

and postquantum mechanical descriptions of the chemical bond (Bohr-Sommerfeld vs Heisenberg-Schrödinger).

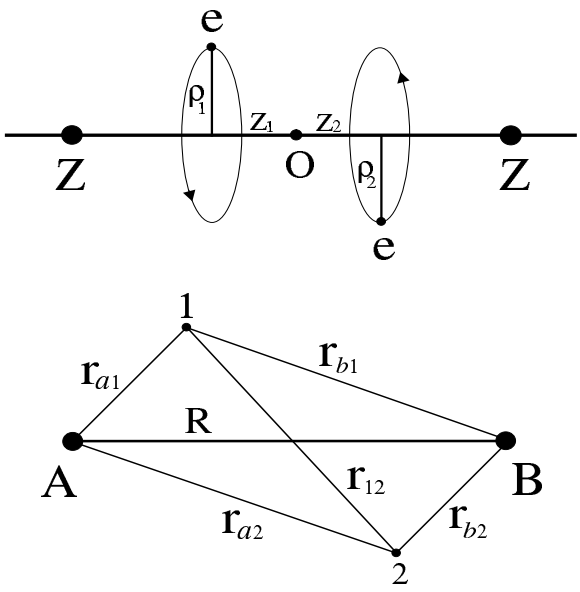

Fig. 1. Cylindrical coordinates (top) and electronic distances (bottom) in H_2 molecule. The nuclei Z are fixed at a distance R apart. In the Bohr model, the two electrons rotate about the internuclear axis z with coordinates ρ_1, z_1 and ρ_2, z_2 respectively; the dihedral angle ϕ between the (ρ_1, z_1) and (ρ_2, z_2) planes remains constant at either $\phi = \pi$ or $\phi = 0$. The sketch corresponds to configuration 2 of Fig. 2, with $\phi = \pi$.

Figure 1 displays the Bohr model for a hydrogen molecule [1, 7, 15], in which two nuclei with charges $Z|e|$ are separated by a fixed distance R (adiabatic approximation) and the two electrons move in the space between them. The model assumes that the electrons move with constant speed on circular trajectories of radii $\rho_1 = \rho_2 = \rho$. The circle centers lie on the molecule axis z at the coordinates $z_1 = \pm z_2 = z$. The separation between the electrons is constant.

The net force on each electron consists of three contributions: attractive interaction between an electron and the two nuclei, the Coulomb repulsion between electrons,

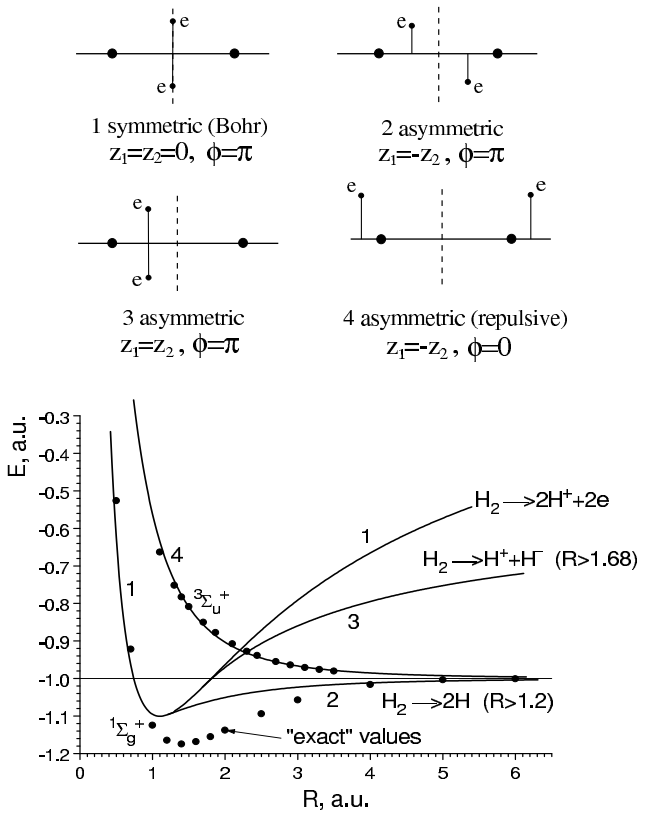

Fig. 2. Energy $E(R)$ of H_2 molecule for four electron configurations (top) as a function of internuclear distance R calculated within the Bohr model (solid lines) and the "exact" ground $^1\Sigma_g^+$ and first excited $^3\Sigma_u^+$ state energy of Ref. [16] (dots). Unit of energy is 1 a.u.= 27.21 eV, and unit of distance is the Bohr radius.

and the centrifugal force on the electron. We proceed by writing the energy function $E = T + V$, where the kinetic energy $T = p_1^2/2m + p_2^2/2m$ for electrons 1 and 2 can be obtained from the quantization condition that the circumference is equal to the integer number n of the electron de Broglie wavelengths $2\pi\rho = nh/p$, so that we have $T = p^2/2m = n^2\hbar^2/2m\rho^2$. All distances we express in terms the Bohr length $a_0 = \hbar^2/me^2$, where m is the electron mass, and take e^2/a_0 as a unit of energy. The

Coulomb potential energy V is given by

$$V = -\frac{Z}{r_{a1}} - \frac{Z}{r_{b1}} - \frac{Z}{r_{a2}} - \frac{Z}{r_{b2}} + \frac{1}{r_{12}} + \frac{Z^2}{R}, \tag{2.1}$$

where r_{ai} $(i = 1, 2)$ and r_{bi} are the distances of the ith electron from nuclei A and B, as shown in Fig. 1 (bottom), r_{12} is the separation between electrons. In cylindrical coordinates the distances are

$$r_{ai} = \sqrt{\rho_i^2 + \left(z_i - \frac{R}{2}\right)^2}, \quad r_{bi} = \sqrt{\rho_i^2 + \left(z_i + \frac{R}{2}\right)^2}, \tag{2.2}$$

$$r_{12} = \sqrt{(z_1 - z_2)^2 + \rho_1^2 + \rho_2^2 - 2\rho_1\rho_2\cos\phi}, \tag{2.3}$$

here R is the internuclear spacing and ϕ is the dihedral angle between the planes containing the electrons and the internuclear axis. The Bohr model energy for a homonuclear molecule having charge Z is then given by

$$E = \frac{1}{2}\left(\frac{n_1^2}{\rho_1^2} + \frac{n_2^2}{\rho_2^2}\right) + V(\rho_1, \rho_2, z_1, z_2, \phi). \tag{2.4}$$

For $n_1 = n_2 = 1$ the energy (2.4) has extrema at $\rho_1 = \rho_2 = \rho$, $z_1 = \pm z_2 = z$ and $\phi = \pi$, 0. These four configurations are pictured in Fig. 2 (upper panel). For example, for configuration 2, with $z_1 = -z_2 = z$, $\phi = \pi$, the extremum equations $\partial E/\partial z = 0$ and $\partial E/\partial \rho = 0$ read

$$\frac{Z(R/2 - z)}{[\rho^2 + (R/2 - z)^2]^{3/2}} + \frac{z}{4[\rho^2 + z^2]^{3/2}} - \frac{Z(R/2 + z)}{[\rho^2 + (R/2 + z)^2]^{3/2}} = 0, \tag{2.5}$$

$$\frac{Z\rho}{[\rho^2 + (R/2 - z)^2]^{3/2}} + \frac{Z\rho}{[\rho^2 + (R/2 + z)^2]^{3/2}} - \frac{\rho}{4[\rho^2 + z^2]^{3/2}} = \frac{1}{\rho^3}, \tag{2.6}$$

which are seen to be equivalent to Newton's second law applied to the motion of each electron. Eq. (2.5) specifies that the total Coulomb force on the electron along the $z-$axis is equal to zero; Eq. (2.6) specifies that the projection of the Coulomb force toward the molecular axis equals the centrifugal force. At any fixed internuclear

distance R, these equations determine the constant values of ρ and z that describe the electron trajectories. Similar force equations pertain for the other extremum configurations.

In Fig. 2 (lower panel) we plot $E(R)$ for the four Bohr model configurations (solid curves), together with "exact" results (dots) obtained from extensive variational calculations for the singlet ground state $^1\Sigma_g^+$, and the lowest triplet state, $^3\Sigma_u^+$ [16]. In the model, the three configurations 1, 2, 3 with the electrons on opposite sides of the internuclear axis ($\phi = \pi$) are seen to correspond to singlet states, whereas the other solution 4 with the electrons on the same side ($\phi = 0$) corresponds to the triplet state. At small internuclear distances, the symmetric configuration 1 originally considered by Bohr agrees well with the "exact" ground state quantum energy; at larger R, however, this configuration's energy rises far above that of the ground state and ultimately dissociates to the doubly ionized limit, $2H^+ + 2e$. In contrast, the solution for the asymmetric configuration 2 appears only for $R > 1.20$ and in the large R limit dissociates to two H atoms. The solution for asymmetric configuration 3 exists only for $R > 1.68$ and climbs steeply to dissociate to an ion pair, $H^+ + H^-$. The asymmetric solution 4 exists for all R and corresponds throughout to repulsive interaction of two H atoms.

The simplistic Bohr model provides surprisingly accurate energies for the ground singlet state at large and small internuclear distances and for the triplet state over the full range of R. Also, the model predicts the ground state is bound with an equilibrium separation $R_e \approx 1.10$ and gives the binding energy as $E_B \approx 0.100$ a.u.$= 2.73$ eV. The Heitler-London calculation, obtained from a two-term variational function, obtained $R_e = 1.51$ and $E_B = 3.14$ eV [17], whereas the "exact" results are $R_e = 1.401$ and $E_B = 4.745$ eV [16]. For the triplet state, as seen in Fig. 2, the Bohr model gives remarkably close agreement with the "exact" potential curve and is in fact much

better than the Heitler-London result (which, e.g., is 30% high at $R = 2$).

B. Introduction into interpolated Bohr model: H_2 molecule

The original Bohr model assumes quantization of the electron angular momentum relative to the molecular axis. This yields very accurate description of the H_2 triplet state $E(R)$. However, ground state $E(R)$ is less accurate at intermediate and larger internuclear separation as seen in Fig. 2. To obtain a better result for the bound states one can use the following observation [7, 18]. At large R each electron in H_2 feels only the nearest nuclear charge because the remaining charges form a neutral H atom. Therefore, at large R the momentum quantization relative to the nearest nuclei, rather than to the molecular axis, must yield a better answer. We call it atomic quantization. This leads to the following expression for the energy of the H_2 molecule

$$E = \frac{1}{2}\left(\frac{n_1^2}{r_{a1}^2} + \frac{n_2^2}{r_{b2}^2}\right) - \frac{Z}{r_{a1}} - \frac{Z}{r_{b1}} - \frac{Z}{r_{a2}} - \frac{Z}{r_{b2}} + \frac{1}{r_{12}} + \frac{Z^2}{R} \tag{2.7}$$

For $n_1 = n_2 = 1$ and $R > 2.77$ the expression (2.7) has a local minimum for the asymmetric configuration 2 of Fig. 2.

We plot the corresponding $E(R)$ in Fig. 3 (curve 2). At $R < 2.77$ the electrons collapse into opposite nuclei, *i.e.*, r_{b1} and/or r_{a2} can vanish because the kinetic energy term does not constrain this separation. As one can see from Fig. 3, the energy function (2.7), which is a natural generalization of Bohr's hydrogen atom to the molecular case, is in good quantitative agreement with the "exact" energy over the range of $R > 2.77$ where the local minimum exists. We plot the corresponding $E(R)$ without the $1/R$ term in Fig. 4 (curve 2).

At small R we apply the quantization condition relative to the molecular axis which yields curve 1 in Fig. 4. To find $E(R)$ at intermediate separation we connect

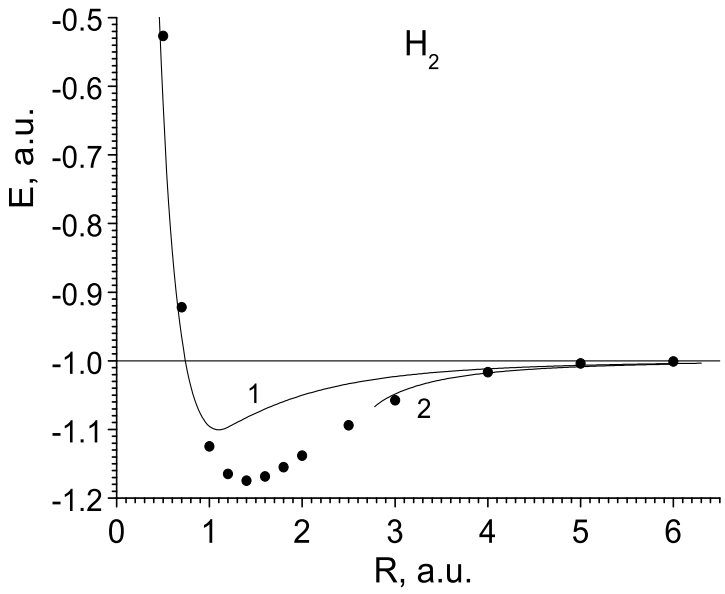

Fig. 3. Potential energy curve of the ground state of the H_2 molecule obtained from the Bohr model with molecular axis quantization (curve 1) and quantization relative to the nearest nucleus (curve 2). Solid circles are the "exact" energies [19].

smoothly the two regions by a third order polynomial (thin line). Addition of the $1/R$ term yields the final potential curve, plotted in Fig. 5. The simple interpolated Bohr model provides a remarkably close agreement with the "exact" potential curve over the full range of R.

C. Interpolated Bohr model of CH

Motivated by the H_2 result, here we calculate the potential energy curve of CH molecule using the interpolated Bohr model.

Figure 6 shows electron configuration of carbon atom in the Bohr model picture. Distances are given in Bohr radii. Carbon atom has six electrons. Outer-shell

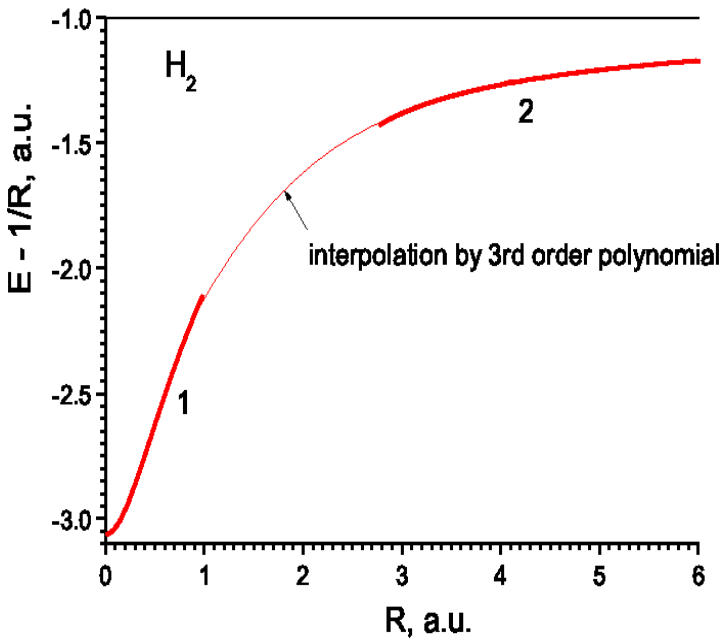

Fig. 4. The Bohr model $E(R)$ for H_2 molecule without $1/R$ term. Curves 1 and 2 are obtained based on the quantization relative to the molecular axis (small R) and the nearest nuclei (large R) respectively. Thin line is the interpolation between two regions.

electrons of carbon form a regular tetrahedron in the Bohr model. This is similar to bond structure of CH_4. Bohr model of carbon yields the ground state energy $E_B = -37.8128$ hartree, which deviates from the "exact" quantum mechanical answer $E_{\rm exact} = -37.8420$ hartree by 0.08% only.

To form the CH molecule we attach one hydrogen atom to carbon. At large R the molecule can be treated as two neutral atoms polarized by Coulomb interactions. Hence, at large R electrons feel only the nearest nucleus and, as in the case of H_2, we apply atomic quantization. To find the potential energy curve we consider only four outer electrons of carbon which have principal quantum number $n = 2$. Contribution of the inner electrons in R-dependence of $E(R)$ is negligible. The simplest version of

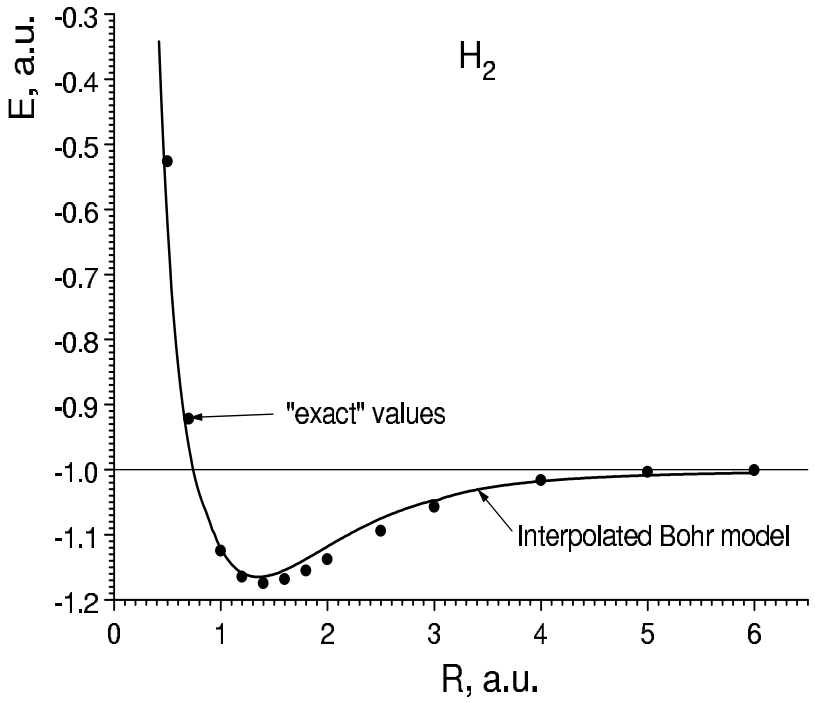

Fig. 5. Ground state $E(R)$ of H_2 molecule as a function of internuclear distance R calculated within the interpolated Bohr model (solid line) and the "exact" energy of Ref. [16] (dots).

the Bohr model we use can not distinguish the difference between p and s electrons of carbon. By symmetry the four outer electrons of carbon are located at equal distanced from the nucleus. We consider a configuration for which the hydrogen electron lies on the molecular axis. Then the Bohr model energy function can be written as

$$E = \frac{2n^2}{r_1^2} + \frac{1}{2r_2^2} + V, \tag{2.8}$$

where r_1 is the spacing between an outer carbon electron and the nucleus and r_2 is the distance between hydrogen electron and the proton. At fixed R the Coulomb potential energy V depends on four parameters: r_1, r_2 and two angles which determine the position of the carbon electrons in space. Minimization of the energy function with respect to these four parameters yields $E(R)$. We performed minimization numerically

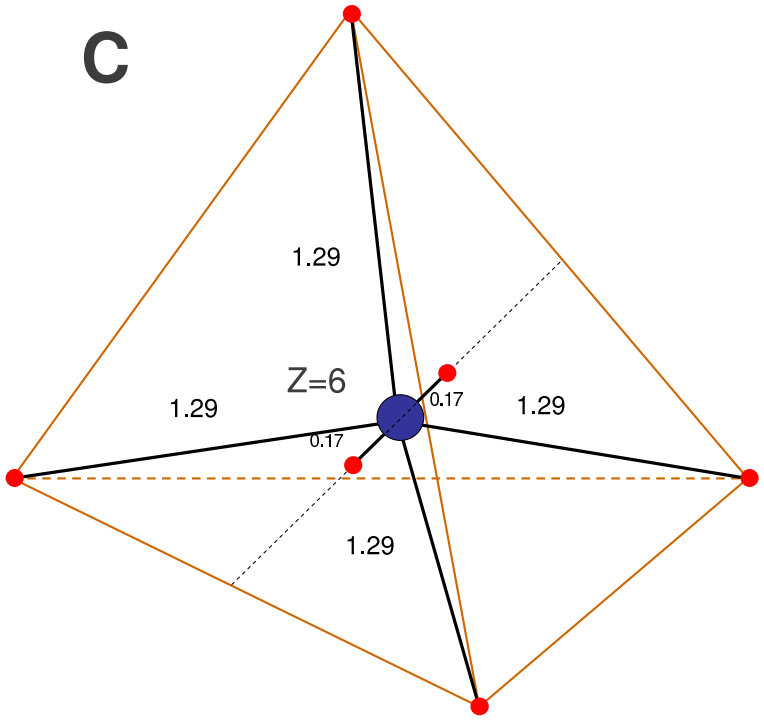

Fig. 6. Electron configuration of carbon atom in Bohr model. Distances are given in Bohr radii.

using Maple. Figure 7 shows our result (curve "Bohr").

The solution for atomic quantization exists at $R > 3.95$ a.u. At smaller R electrons collapse into opposite nucleus. In the region where solution exists the simple Bohr model yields remarkable accuracy as seen from comparison with the "exact" quantum mechanical dots.

To find potential energy curve at very small R we note that at such separation the outer carbon electrons practically does not contribute to change in E if we vary R. Rather then they yield a fix contribution $\Delta E = -0.6$ a.u. (additive constant). Two inner carbon electrons screen the nucleus and effectively reduce it to Be nucleus. Only hydrogen electron gives a substantial contribution into $E(R)$. As a result, at very small R, the CH problem is effectively equivalent to BeH^{4+} problem plus a constant term ΔE. BeH^{4+} molecular ion is a simple one electron two center problem which

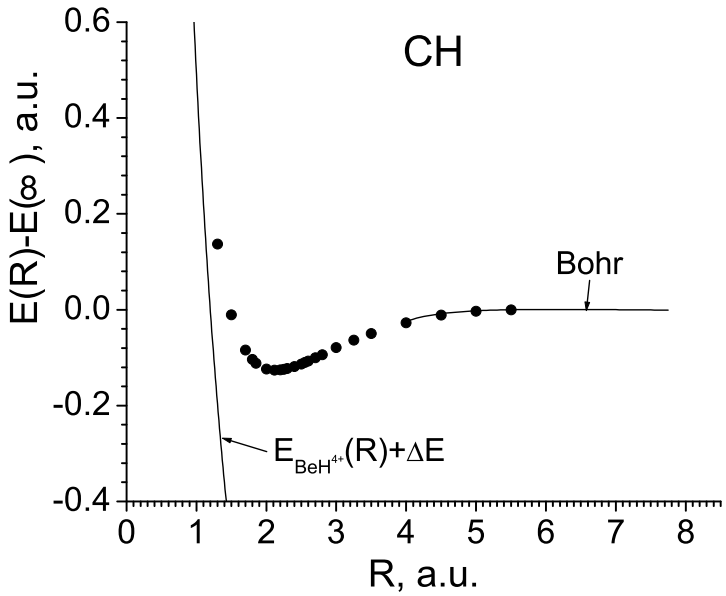

Fig. 7. Finding $E(R)$ in the interpolated Bohr model of CH. At large R we apply the energy function (2.8). At small R we are dealing with the BeH^{4+} problem plus a constant term. Dots are "exact" quantum mechanical result.

allows separation of variables in the Schrödinger equation. The potential energy curve of BeH^{4+} is well known in literature, and we use this information.

Figure 7 shows the potential energy curve of BeH^{4+} plus ΔE. This yields quite accurate description of CH potential curve at small R. In Fig. 8 we plot both the small and large R curves without internuclear repulsion energy $4/R$. This plot shows that indeed small and large R asymptotics can be smoothly connected by a simple polynomial curve. We make the connection using the following fourth order polynomial

$$E = -5.96168 + 3.67843R - 1.29575R^2 + 0.24723R^3 - 0.01901R^4. \qquad (2.9)$$

The result is shown in Fig. 8 as a dashed line.

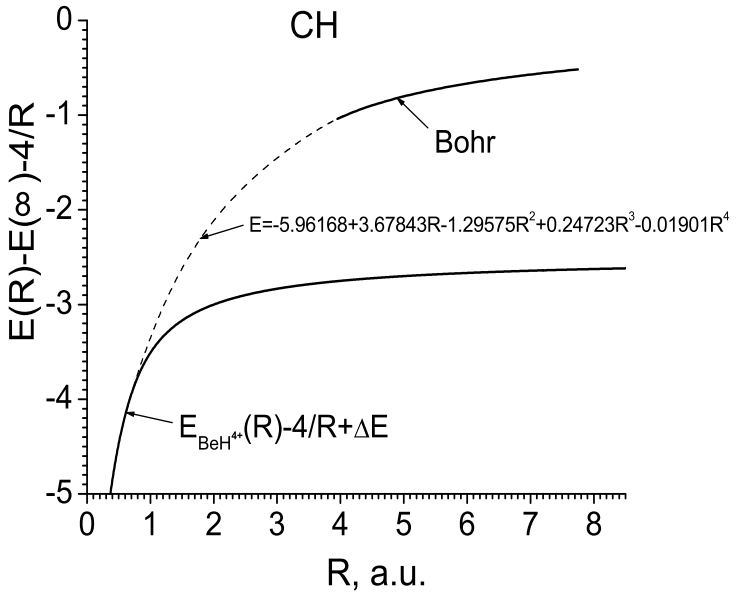

Fig. 8. Interpolated Bohr model of CH. The same as in Fig. 7 but without internuclei repulsion term $4/R$. Dashed line shows connection of the small and large R segments by a fourth order polynomial.

Finally to obtain the potential energy curve for the CH molecule we add back the internuclear repulsion $4/R$ to the interpolation polynomial. This yields solid line in Fig. 9. Dots show "exact" quantum mechanical result. One can see that the simple interpolated Bohr model yet provides quite good accuracy for $E(R)$ at all R. This is remarkable because CH is already an example of a complicated many electron system.

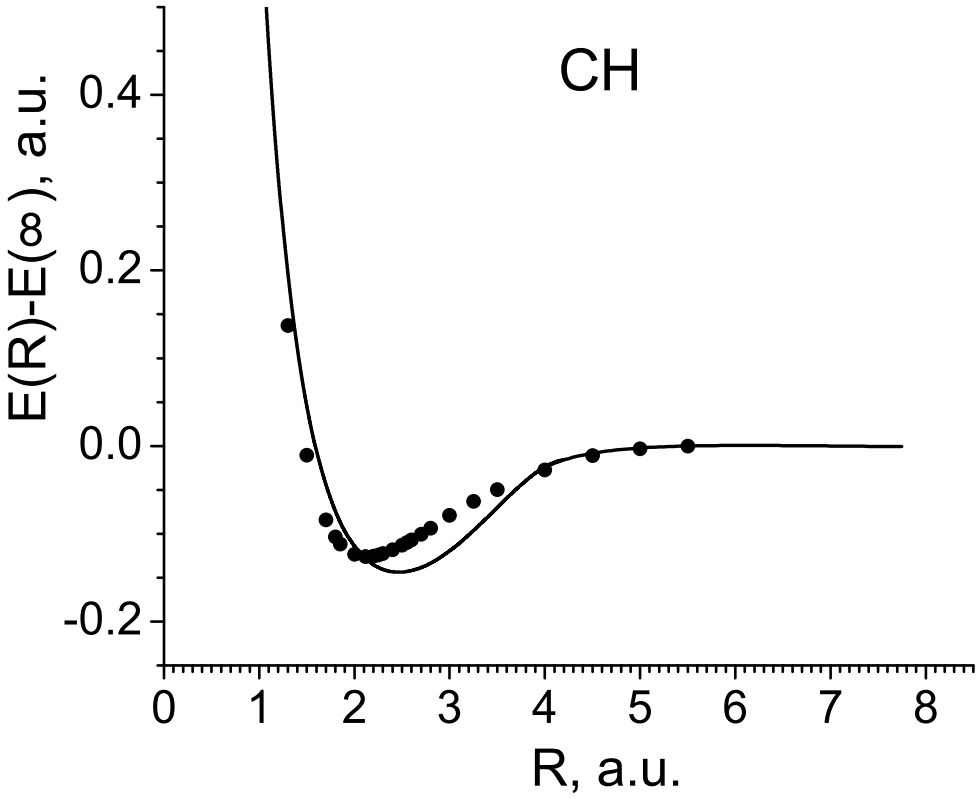

Fig. 9. Ground state energy of CH molecule obtained within Interpolated Bohr model (solid line) and "exact" quantum mechanical result (dots).

CHAPTER III

CONSTRAINED BOHR MODEL APPROACH

The interpolated Bohr model discussed in the previous chapter involves a smooth connection between different asymptotics of $E(R)$. This contains undesired degree of arbitrariness. Here we further study a method which allows us to obtain $E(R)$ at all R without interpolation. The present approach is based on Bohr's molecular model with a constraint imposed by quantum mechanics and was recently proposed by Svidzinsky, Chin and Scully [18]. The approach is as simple and intuitively appealing as the original Bohr model, but, at the same time, it allows us to obtain potential energy curves with the chemical accuracy of a few milli Hartree.

We first introduce the method as applied to H_2 and then extend it for other molecules. Fig. 1 displays electron distances in H_2. The original Bohr model [1] assumes quantization of the electron angular momentum relative to the molecular axis which yields Eq. (2.4) for the ground state energy.

In Fig. 3 (curve 1) we plot ground state $E(R)$ derived from Eq. (2.4), together with "exact" results (dots) obtained from extensive variational wave mechanical calculations [19]. The simplistic Bohr model yields a quite accurate description of the H_2 ground state $E(R)$ at small R, but becomes less accurate at larger internuclear separation. There is a simple means to improve significantly the Bohr model result for large R as discussed in the previous chapter [7]. An improvement emerges if we use quantization of the electron momentum relative to the nearest nuclei, rather than to the molecular axis. This leads to Eq. (2.7) for the H_2 energy. For $n_1 = n_2 = 1$ and $R > 2.77$ expression (2.7) has a local minimum for the top configuration of Fig. 11. We plot the corresponding $E(R)$ in Fig. 3 (curve 2). At $R < 2.77$ the local minimum disappears and electrons collapse into the opposite nuclei. As one can see from Fig.

3, the simple energy function (2.7) provides good quantitative agreement with the "exact" potential curve over the range of R where solution exists. This encourages us to seek a way to extend applicability of Eq. (2.7) over the full range of R.

Svidzinsky, Chin and Scully [18] have shown that a simple algebraic constraint on electron locations obtained from quantum mechanics allows to avoid the collapse problem preserving the simplicity and good accuracy of the energy function (2.7). Next we summarize their derivation of the corresponding constraint equation.

A. Derivation of the effective potential for H_2 molecule: Heitler-London vs Hund-Mulliken

In quantum mechanics electrons are described by a wave function $\Psi(\mathbf{r}_1, \mathbf{r}_2)$; the electron 1 is a charge cloud with a characteristic size r (see Fig. 10).

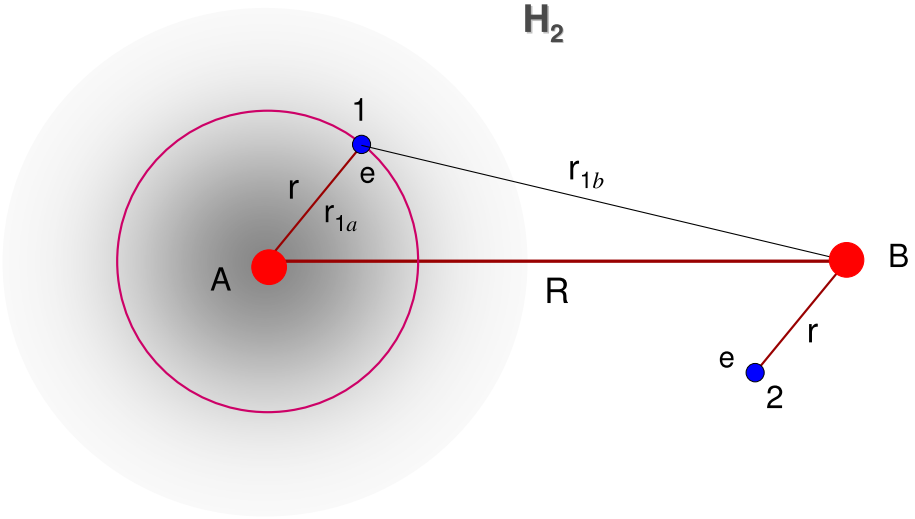

Fig. 10. In quantum mechanics the electron 1 is a cloud with characteristic size r. In the Bohr model we treat electron as a point particle located distance r from the nucleus A.

Let $\Phi(r, R)$ be an interaction potential between the electron cloud and the opposite nucleus B. In the Bohr picture we treat the electron as a point particle located

on a sphere of radius r centered at the nucleus A. Position of the point electron on the sphere gives correct quantum mechanical answer for the particle interaction with the nucleus B if

$$-\frac{1}{r_{\rm b1}} = \Phi(r,R) \equiv \left\langle \Psi \left| -\frac{1}{r_{\rm b1}} \right| \Psi \right\rangle, \tag{3.1}$$

where $r_{\rm b1}$ is the distance between the point electron and the opposite nucleus (see Fig. 1). To avoid electron collapse we impose constraint (3.1) on the electron location. One can derive the effective potential $\Phi(r,R)$ using, for example, Heitler-London (HL) [17] or Hund-Mulliken (HM) [20] variational wave function Ψ. HL wave function is a linear combination of atomic orbitals with coordinate part

$$\Psi = a(1)b(2) \pm b(1)a(2), \tag{3.2}$$

where the sign "+" ("-") corresponds to singlet (triplet) state and

$$a(i) = \sqrt{\frac{\alpha^3}{\pi}}\exp(-\alpha r_{ai}), \quad b(i) = \sqrt{\frac{\alpha^3}{\pi}}\exp(-\alpha r_{bi}), \tag{3.3}$$

$i = 1,\ 2$, and α is a variational parameter. If we take $a(1)$ as a variational wave function for an isolated hydrogen atom A then the variational energy reads: $E = \alpha^2/2 - \alpha$. This expression reduces to the Bohr model energy function of the hydrogen atom if we identify $\alpha = 1/r$, where r is the distance between the point electron and the nucleus. We will also use this assignment for molecules with r being the distance between the electron and the nearest nucleus.

For HL wave function the matrix element in Eq. (3.1) yields

$$\Phi = -\frac{1}{1 \pm S^2}\left\{\int a^2(1)\frac{1}{r_{\rm b1}}d\mathbf{r}_1 \pm 2S\int a(1)b(1)\frac{1}{r_{\rm b1}}d\mathbf{r}_1\right\} \tag{3.4}$$

where the first term is the Coulomb integral, the last term is the exchange integral and $S = \int a(1)b(1)d\mathbf{r}_1$. After integration we obtain the following expression for the

HL singlet effective potential

$$\Phi_{\rm s}(r,R) = -\frac{1}{1+S^2(r,R)}\left[\frac{1}{R} - \exp(-2R/r)\left(\frac{1}{r}+\frac{1}{R}\right) + \right. \tag{3.5}$$

$$\left. \frac{S(r,R)}{r}\exp(-R/r)\left(1+\frac{R}{r}\right)\right], \tag{3.6}$$

where

$$S(r,R) = \exp(-R/r)\left(1+\frac{R}{r}+\frac{R^2}{3r^2}\right). \tag{3.7}$$

Triplet effective potential is

$$\Phi_{\rm t}(r,R) = -\frac{1}{1-S^2(r,R)}\left[\frac{1}{R} - \exp(-2R/r)\left(\frac{1}{r}+\frac{1}{R}\right) - \right. \tag{3.8}$$

$$\left. \frac{S(r,R)}{r}\exp(-R/r)\left(1+\frac{R}{r}\right)\right]. \tag{3.9}$$

Singlet state Hund-Mulliken wave function $\Psi = [a(1)+b(1)][a(2)+b(2)]$ yields HM singlet effective potential:

$$\Phi_{\rm s}(r,R) = -\frac{1}{1+S(r,R)}\left[\frac{1}{R} - \exp(-2R/r)\left(\frac{1}{r}+\frac{1}{R}\right) + \right. \tag{3.10}$$

$$\left. \frac{1}{r}\exp(-R/r)\left(1+\frac{R}{r}\right)\right]. \tag{3.11}$$

For the triplet state, HL and HM wave functions and, hence, the effective potentials are identical.

B. Examples of method application: H_2 molecule

Here we apply the effective potential approach to H_2 molecule. Electron configurations for the ground and triplet states of H_2 are shown in Fig. 11. The energy function has an extremum when $r_{a1} = r_{b2} = r$ and $r_{a2} = r_{b1}$. With the constraint (3.1) the Bohr

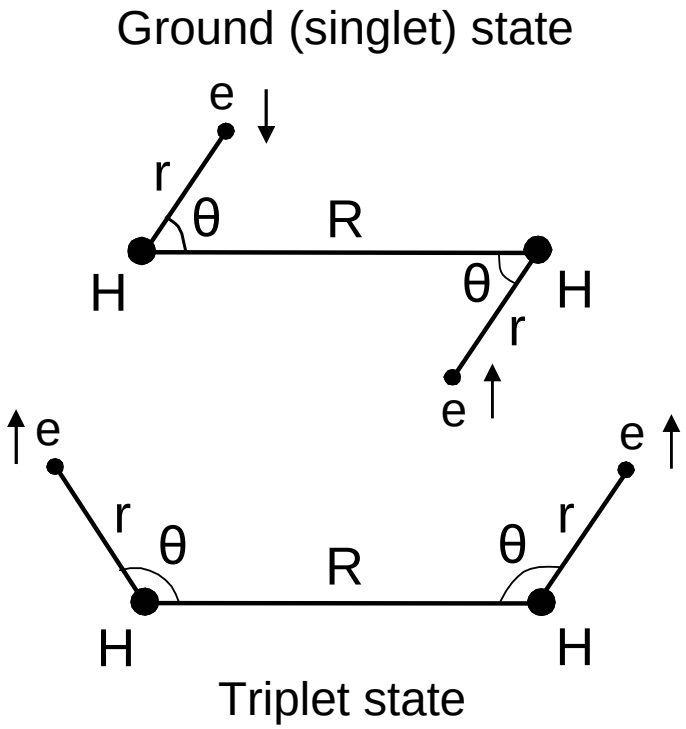

Fig. 11. Electron configuration for the ground (singlet) and triplet states of H_2 molecule.

model energy function reads

$$E(r,R) = \frac{1}{r^2} - \frac{2}{r} + 2\Phi(r,R) + \frac{1}{r_{12}} + \frac{1}{R}, \tag{3.12}$$

where

$$r_{12} = \sqrt{2r^2 - R^2 + \frac{2}{\Phi^2(r,R)}} \tag{3.13}$$

for the singlet configuration and

$$r_{12} = \frac{1}{R\Phi^2(r,R)} - \frac{r^2}{R} \tag{3.14}$$

for the triplet state.

Minimization of the energy function (3.12) with respect to r yields the potential energy curve $E(R)$. Fig. 12 shows the ground state $E(R)$ of H_2 obtained using the Bohr model with the HL (small dots) and HM (lower solid line) singlet effective

potential constraint. Upper solid line is $E(R)$ of the triplet state obtained using the Bohr model with the triplet constraint (3.1), (3.9). Dots are "exact" results [19]. The simple method gives surprisingly accurate $E(R)$ at all R; it yields for the ground state binding energy $E_B = 4.50$ eV (HL potential) and $E_B = 4.99$ eV (HM potential), whereas the "exact" result is $E_B = 4.745$ eV [21]. The Heitler-London effective charge calculation (shown in Fig. 12, dashed curves) gives substantially worse accuracy and predicts $E_B = 3.78$ eV [17, 22]. Accuracy comparable to the constrained Bohr model at all R can be obtained only using trial wave functions with a few variational parameters including configuration interaction.

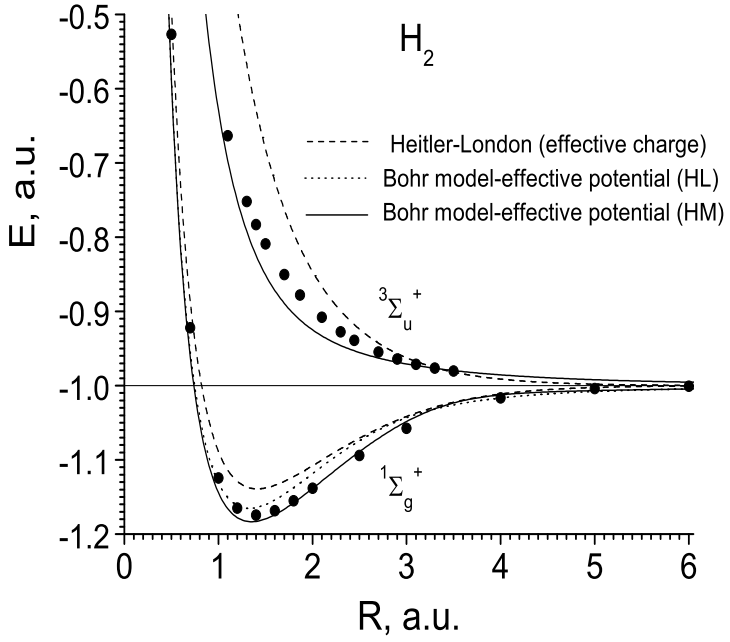

Fig. 12. Potential energy curves of the ground $^1\Sigma_g^+$ and first triplet state $^3\Sigma_u^+$ of the H_2 molecule. Solid lines are obtained from the constrained Bohr model with HM effective potential, while the small dot line is derived with HL potential. Dashed curves are from HL effective charge variational treatment.

Effective potentials (3.6), (3.9) and (3.11) are derived as a solution to the H_2 problem.

Next we show that the approach works for other molecules. Generalization of the constraint (3.1) to the system of several hydrogen atoms is straightforward. Let us consider electron 1 that belongs to the nearest nucleus 1 and denote the distances from the point electron 1 to the nuclei i as r_i ($i = 1, 2, \ldots$). Then the constraint equation reads

$$-\sum_{i>1}\frac{1}{r_i} = \sum_{i>1}\Phi_i(r_1, R_i), \tag{3.15}$$

where R_i is the spacing between the nucleus 1 and i. Mutual spin orientation of electrons 1 and i (that belongs to the nucleus i) determines a specific choice of Φ_i (singlet or triplet) in Eq. (3.15).

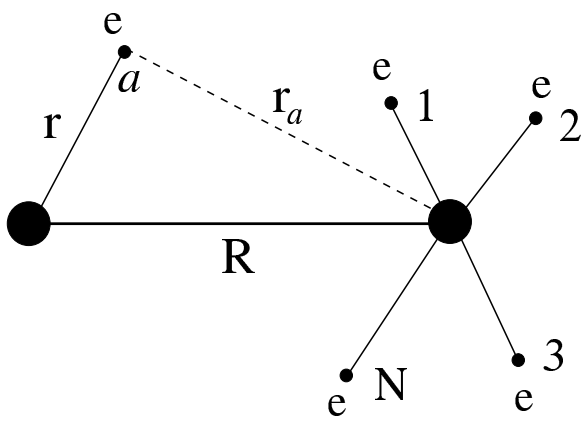

Fig. 13. Electron configuration of a diatomic molecule composed of many-electron atoms.

What about molecules composed of many-electron atoms? One can consider a many-electron atom as a united atom limit of several hydrogen atoms. Then, by continuity, Eq. (3.15) yields the following constraint equation for an electron a in a

diatomic molecule pictured in Fig. 13:

$$-\frac{1}{r_a} = \frac{1}{N}[\Phi_1(r,R) + \Phi_2(r,R) + \ldots \Phi_N(r,R)], \tag{3.16}$$

where N is the number of electrons that belong to the opposite atom. Mutual spin orientation between the electron a and i ($i = 1,\ 2,\ \ldots N$) determines the specific choice of Φ_i (singlet or triplet).

Svidzinsky, Chin and Scully [18] demonstrated that the constrained Bohr model approach works very well, in particular, for such molecules as H_3 and Be_2. The goal of our study is to test their method for more complicated systems. In this chapter we focus on H_4 molecule.

C. H_4 molecule

Next we calculate the ground state $E(R)$ of the four-atomic H_4 molecule using the constrained Bohr model. Free H_4 molecule does not exist in nature, it dissociates into two H_2. However, knowledge of $E(R)$ is useful, e.g., for scattering problems. We consider linear and square configurations shown in Figs. 14 and 16. The spacing between the nearest nuclei is assumed to be the same and equal to R.

1. Linear geometry

Fig. 14 shows distances and spin configuration of the linear H_4 molecule in the ground state. We assume that spins of the nearest neighbor electrons are opposite. Due to symmetry arguments only two distances and two angles are independent, they are determined by minimization of the energy function. We choose r_1, r_2, θ_1 and θ_2 as independent parameters (see Fig. 14). All other distances are expressed in terms of

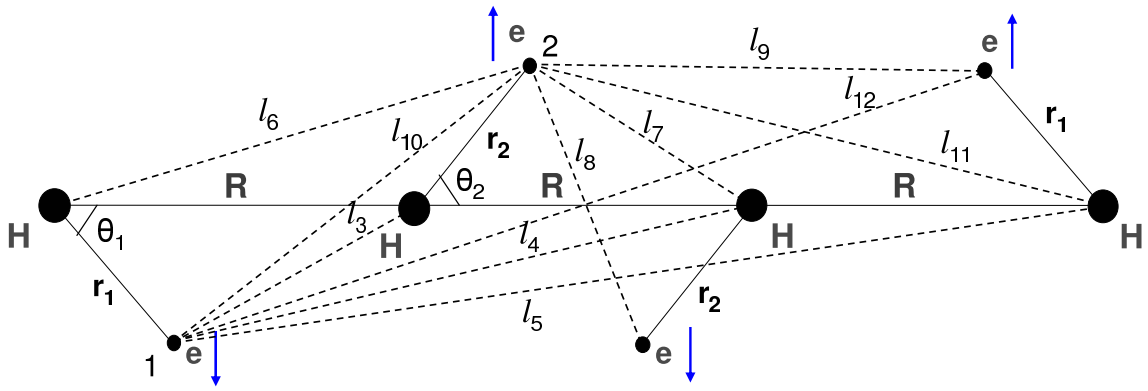

Fig. 14. Electron and spin configuration and distances of the linear H_4 molecule in the ground state. All electrons are in the same plane.

r_1, r_2, θ_1 and θ_2 as follows

$$l_3 = \sqrt{r_1^2 + R^2 - 2r_1 R\cos\theta_1}$$

$$l_4 = \sqrt{r_1^2 + 4R^2 - 4r_1 R\cos\theta_1}$$

$$l_5 = \sqrt{r_1^2 + 9R^2 - 6r_1 R\cos\theta_1}$$

$$l_6 = \sqrt{r_2^2 + R^2 + 2r_2 R\cos\theta_2}$$

$$l_7 = \sqrt{r_2^2 + R^2 - 2r_2 R\cos\theta_2}$$

$$l_8 = 2\sqrt{r_2^2 + R^2/4 - r_2 R\cos\theta_2}$$

$$l_9 = \sqrt{(2R - r_1\cos\theta_1 - r_2\cos\theta_2)^2 + (r_1\sin\theta_1 - r_2\sin\theta_2)^2}$$

$$l_{10} = \sqrt{(R - r_1\cos\theta_1 + r_2\cos\theta_2)^2 + (r_1\sin\theta_1 + r_2\sin\theta_2)^2}$$

$$l_{11} = \sqrt{r_2^2 + 4R^2 - 4r_2 R\cos\theta_2}$$

$$l_{12} = \sqrt{(3R - 2r_1\cos\theta_1)^2 + 4r_1^2\sin^2\theta_1}$$

The Bohr model energy function with the nearest nucleus quantization is given by

$$E(r_1, r_2, \theta_1, \theta_2, R) = \frac{1}{r_1^2} + \frac{1}{r_2^2} - 2\left(\frac{1}{r_2} + \frac{1}{l_3} + \frac{1}{l_4} + \frac{1}{l_5}\right) - 2\left(\frac{1}{r_2} + \frac{1}{l_6} + \frac{1}{l_7} + \frac{1}{l_{11}}\right) +$$

$$+\frac{2}{l_{10}}+\frac{2}{l_9}+\frac{1}{l_8}+\frac{1}{l_{12}}+\frac{13}{3R}. \tag{3.17}$$

To avoid the collapse problem at small enough R we must impose a constraint on electron location. The constraint depends on the mutual spin orientation. Using the prescription discussed in the previous section the constraint equation for electron 1 and 2 read

$$-\frac{1}{l_3}-\frac{1}{l_4}-\frac{1}{l_5}=\Phi_s(r_1,R)+\Phi_t(r_1,2R)+\Phi_s(r_1,3R), \tag{3.18}$$

$$-\frac{1}{l_6}-\frac{1}{l_7}-\frac{1}{l_{11}}=2\Phi_s(r_2,R)+\Phi_t(r_2,2R), \tag{3.19}$$

where l_i are defined in Fig. 14. In the ground state the nearest electrons in the linear H_4 molecule possess opposite spins; this justifies choice of the singlet effective potential $\Phi_s(r_1,R)$ and $\Phi_s(r_2,R)$. If this is the case, the spins of the outermost electrons are also antiparallel and we choose $\Phi(r_1,3R)$ to be singlet. Minimization of the Bohr model energy function (3.17) with the constraints (3.18) and (3.19) yields the potential energy curve. At fixed R we do the minimization with respect to the four independent parameters r_1, r_2, θ_1 and θ_2 using Maple.

Fig. 15 shows the potential energy curve of the linear H_4 molecule obtained within the constrained Bohr model approach (solid line). For Φ_t we use Eq. (3.9) and for Φ_s we take the HL potential (3.6). Dots are "exact" quantum mechanical results. The potential curve, obtained by minimization of an algebraic energy function subject to an algebraic constraint, is surprisingly accurate at all R. This provides an example of a successful application of the constrained Bohr model technique, proposed by Svidzinsky, Chin and Scully [18], for a four-atomic molecule. Such a simple approach yields a clear picture of how electrons form chemical bond in molecules and show that the bond can be treated as electrostatic.

We also calculated the ground state potential curve of linear H_4 molecule taking for Φ_s the HM effective potential (3.11). The result we obtained has substantially

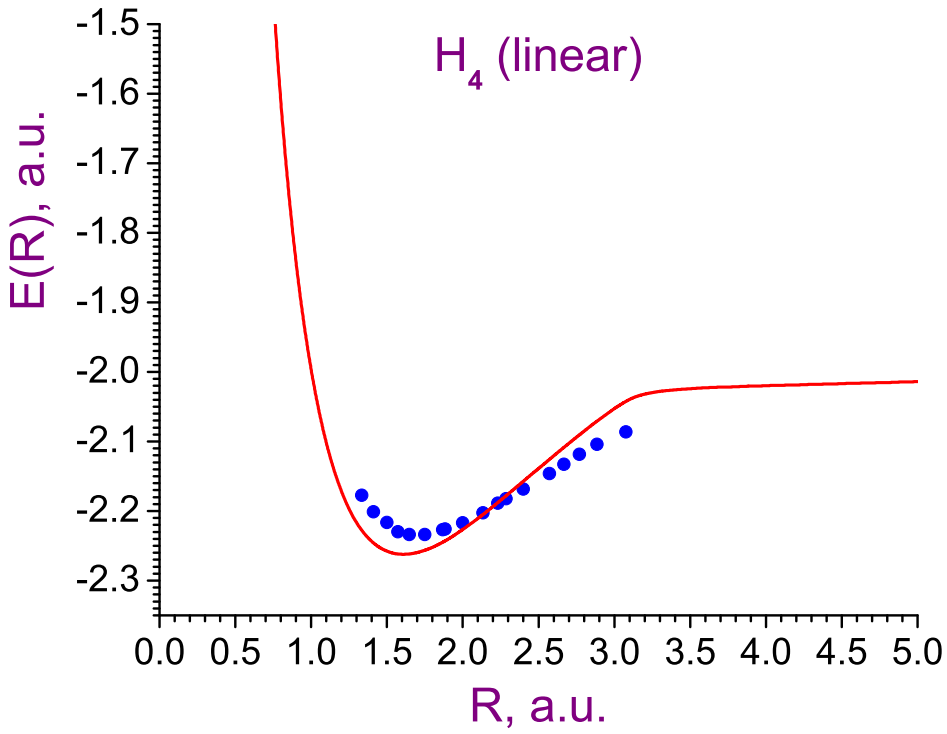

Fig. 15. Ground state $E(R)$ of the linear H_4 molecule obtained from the constrained Bohr model with HL effective potential (solid curve) and "exact" numerical solution of the Schrödinger equation (dots).

worse accuracy as compared to the HL effective potential, we prefer not to discuss it here.

2. Square geometry

Here we study a square configuration of the H_4 molecule in the ground state. As before, the distances between the nearest nuclei are assumed to be the same and equal to R. Fig. 16 shows point electron structure, spin orientation and distances for the square nuclei configuration. We assume that spins of the nearest neighbor electrons are opposite (singlet nearest electron bond). Two opposite electrons lie

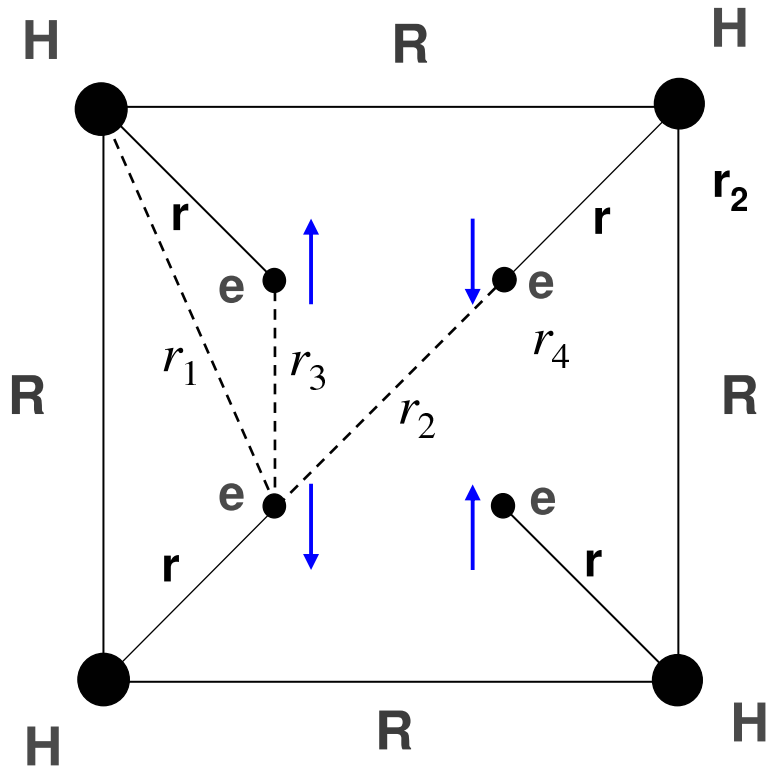

Fig. 16. Electron and spin configuration and distances of the square H_4 molecule in the ground state. Two opposite electrons are above and the other two electrons are below the figure plane.

above, while the other two electrons are below the picture plane. θ is the angle (not shown in the figure) between $\mathbf{r}$ and the molecule plane. By symmetry this angle is the same for all four electrons. Motivated by the symmetry of the nuclei configuration we impose an additional constraint that projections of electrons to the nuclei plane lie on the diagonals of the square. As a result, the electron configuration is fully described by only two independent parameters, which we choose to be r and θ. From this point of view the square geometry is much more simple for numerical analysis as compared to the linear configuration which is described by four degrees of freedom.

In terms of r and θ the other distances shown in Fig. 16 are expressed as

$$r_1 = \sqrt{r^2 \sin^2\theta + R^2 + r^2 \cos^2\theta - \sqrt{2} R r \cos\theta}$$

$$r_2 = \sqrt{(\sqrt{2}R - r\cos\theta)^2 + r^2\sin^2\theta}$$

$$r_3 = \sqrt{4r^2\sin^2\theta + (R - \sqrt{2}r\cos\theta)^2}$$

$$r_4 = \sqrt{2}R - 2r\cos\theta.$$

The Bohr model energy function with atomic quantization is given by

$$E(r,\theta,R) = \frac{2}{r^2} - 4\left(\frac{2}{r_1} + \frac{1}{r_2} + \frac{1}{r}\right) + \frac{2}{r_3} + \frac{2}{r_5} + \frac{2}{r_4} + \frac{4}{R} + \frac{\sqrt{2}}{R}. \tag{3.20}$$

For each electron the constraint equation (3.15) reads

$$-\frac{2}{r_1} - \frac{1}{r_2} = \Phi_s(r,R) + \Phi_t(r,\sqrt{2}R) + \Phi_s(r,R). \tag{3.21}$$

Minimization of the Bohr model energy function (3.20) subject to the constraint (3.21) yields the potential energy curve. Again for Φ_s we take the HL effective potential (3.6). The answer is shown in Fig. 17 (solid line). Dots are quantum mechanical result. The answer we obtained in the Bohr model for the square geometry seems much less accurate then those we got for the linear H_4 case (calculation with the HM effective potential also did not work well for square H_4). The reason for such a discrepancy remains unclear so far. One of the possible explanations is that the ground state of the square H_4 configuration is highly degenerate which makes very hard obtaining a good accuracy in quantum mechanical numerical simulations. It is also possible that the Bohr model may not be accurate for highly degenerate states.

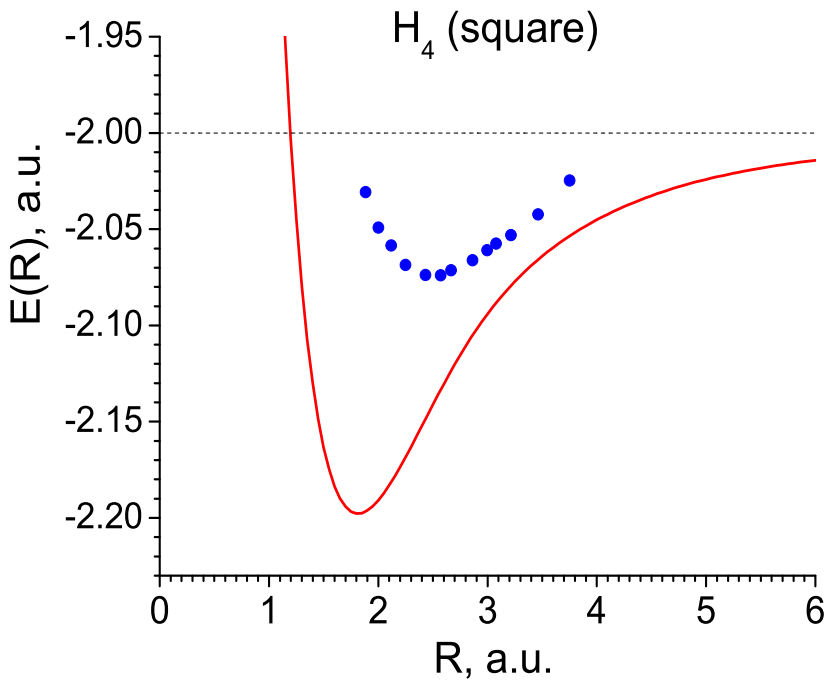

Fig. 17. Ground state $E(R)$ of the square nuclei geometry of the H_4 molecule. Solid curve is the result of the constrained Bohr model with HL effective potential while dots are the quantum mechanical answer.

CHAPTER IV

BOHR MODEL AS A SIMPLE TOOL FOR CALCULATION OF THE CORRELATION ENERGY

The Bohr model can also be applied to calculate the correlation energy for molecules and then improve the Hartree-Fock (HF) treatment [23]. Figure 18 shows the ground state potential curve for H_2 molecule calculated in the Bohr-HF approximation. Such an approximation omits the electron repulsion term $1/r_{12}$ in finding the electron configuration from Eq. (2.4). The difference between the Bohr and Bohr-HF potential curves yields the correlation energy plotted in the insert of Fig. 18.

In Fig. 19 we plot the ground state $E(R)$ for the H_2 molecule obtained with the Heitler-London trial function that has the form of the combination of the atomic orbitals [24]:

$$\Psi = C\left\{\exp[-\alpha(r_{a1}+r_{b2})]+\exp[-\alpha(r_{b1}+r_{a2})]\right\}, \tag{4.1}$$

where α is a variational parameter. Addition of the correlation energy from Fig. 18 improves the Heitler-London result and shifts $E(R)$ close to the "exact" values. The improved potential curve yields the binding energy of 4.63 eV, while the "exact" value is 4.745 eV [16].

Calculation of the correlation energy of the H_2 molecule using the Bohr model was first discussed by Chen et al. [23]. Their approach is based on the simplest formulation of the Bohr model of H_2, namely on the molecular axis quantization. However, such a simple analysis yields worse accuracy for the ground state potential curve then, for example, the constrained Bohr model which combines an atomic quantization and an algebraic constraint derived from quantum mechanics. A natural question rises in this context: can more sophisticated constrained Bohr model improve the accuracy for the correlation energy as compared to the simple molecular axis quantization approach.

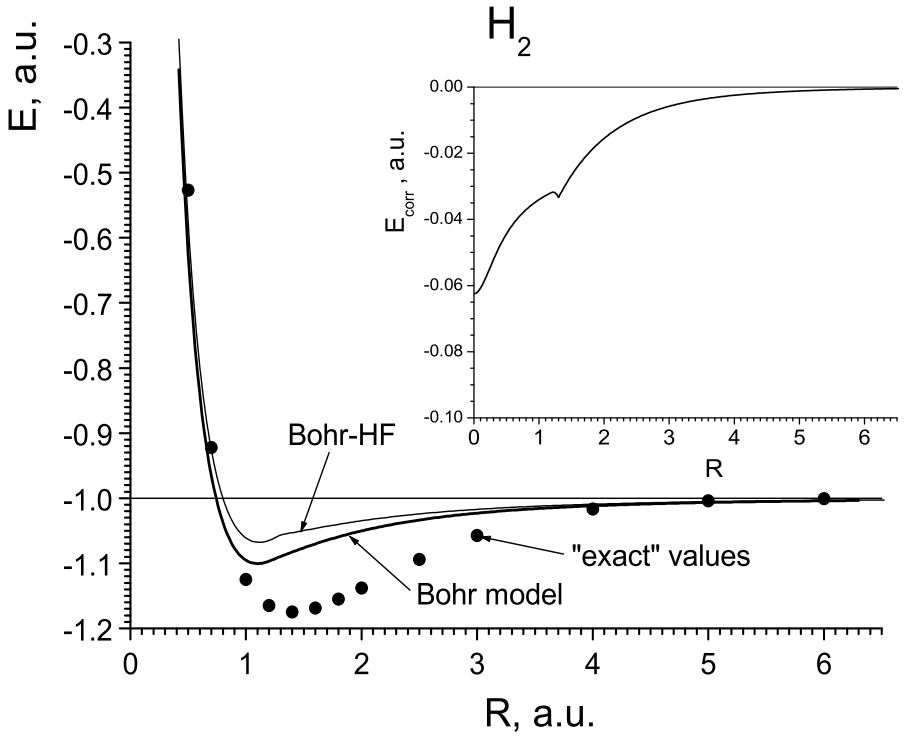

Fig. 18. Ground state $E(R)$ for the H_2 molecule in the Bohr and Bohr-HF models. Insert shows the correlation energy as a function of R.

Here we study this question in detail.

Next we calculate the correlation energy for the ground state of H_2 molecule using constrained Bohr model. We explore both the Heitler-London and Hund-Mulliken effective potentials. In the constrained Bohr model of H_2 the energy function is given by

$$E(r,\theta,R,A) = \frac{1}{r^2} - \frac{2}{r} - \frac{2}{\sqrt{R^2+r^2-2rR\cos(\theta)}} + \frac{1}{2\sqrt{R^2/4+r^2-rR\cos(\theta)}} + \frac{1}{R} + \\ + A\left(2rR\cos(\theta) - R^2 - r^2 + \frac{1}{\Phi_s^2(r,R)}\right)^2, \qquad (4.2)$$

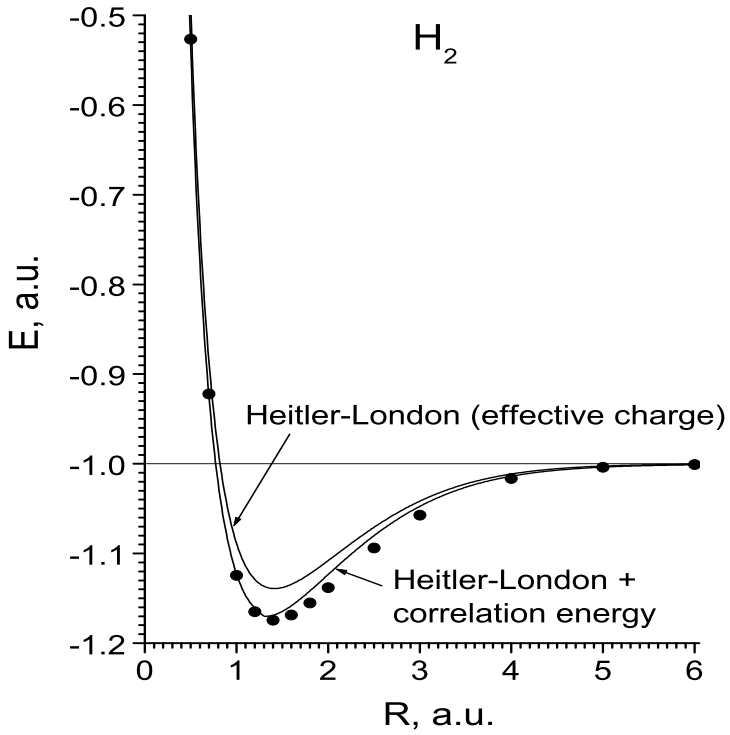

Fig. 19. Ground state energy $E(R)$ of the H_2 molecule in the Heitler-London method and the improved $E(R)$ after the addition of the correlation energy. Dots are the "exact" result from [16].

where A is a large positive constant we introduce to insure satisfaction of the constraint equation $-2rR\cos(\theta) + R^2 + r^2 = \frac{1}{\Phi_s^2(r,R)}$. In numerical calculations we take $A = 1000$. $\Phi_s(r, R)$ is a singlet effective potential given by Eqs. (3.6) or (3.11). At fixed R the energy function (4.2) has to be minimized with respect to r and θ, where r is a separation between the electron and the nearest nucleus and θ is the angle between r and the molecular axis. We minimize the energy function (4.2) using Maple, this gives electron configuration r_0 and θ_0. Then the potential energy curve is obtained as $E(R) = E(r_0, \theta_0, R, 0)$. Please note that when we calculate $E(R)$ we substitute $A = 0$ into the energy function.

In the Bohr-HF approximation we find the electron configuration $r_{\text{B-HF}}$ and $\theta_{\text{B-HF}}$ by minimizing the energy function without electron repulsion term. That is we minimize

$$E_{\text{B-HF}}(r,\theta,R,A) = \frac{1}{r^2} - \frac{2}{r} - \frac{2}{\sqrt{R^2+r^2-2rR\cos(\theta)}} + \frac{1}{R} + \\ +A\left(2rR\cos(\theta) - R^2 - r^2 + \frac{1}{\Phi_s^2(r,R)}\right)^2, \tag{4.3}$$

where again A is a large positive constant. Then the correlation energy is given by $E_{\text{corr}} = E(r_{\text{B-HF}},\theta_{\text{B-HF}},R,0) - E(r_0,\theta_0,R,0)$.

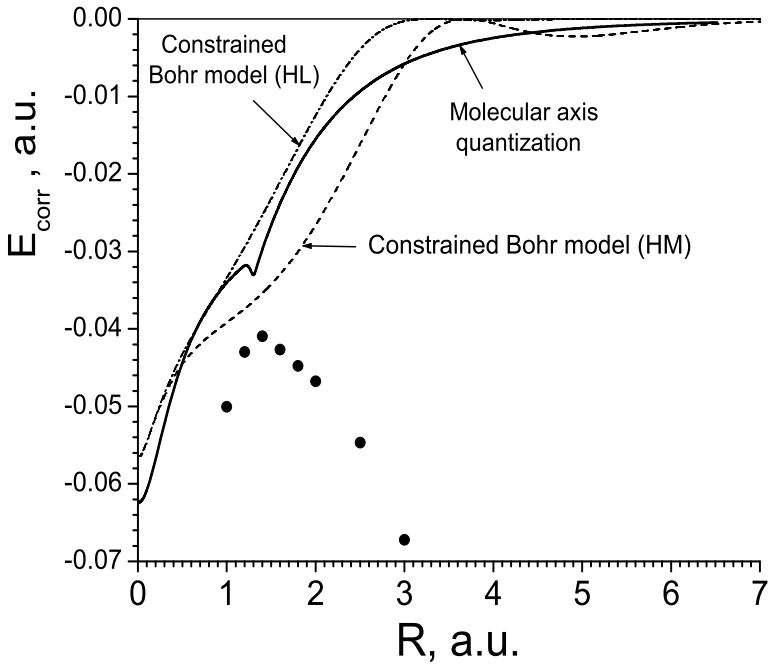

Fig. 20. Correlation energy of H_2 molecule as a function of R obtained in the Bohr model with molecular axis quantization (solid line), constrained Bohr model with Hund-Mulliken (dashed) and Heitler-London effective potential (dash–dot line). Solid dots are obtained by substraction of the result of the self-consistent Hartree-Fock method and "exact" dots from Ref. [16].

Figure 20 shows the correlation energy of H_2 molecule as a function of R obtained in the Bohr model approach for three different cases. Solid line corresponds to the Bohr model with molecular axis quantization which we discussed before. The constrained Bohr model with Hund-Mulliken effective potential yields dashed line. Finally, the constraint with the Heitler-London effective potential gives dash-dot line. One can see that the sophisticated constrained Bohr model approach yields the answer for the correlation energy which is very close to those obtained in a simple molecular axis quantization scheme. Moreover, the Hund-Mulliken effective potential curve lies below, while the Heitler-London curve lies a little above the molecular axis quantization result. From this analysis we conclude that the simple Bohr model with molecular axis quantization yields essentially the same accuracy for the correlation energy as more complicated constrained Bohr model approach. And, therefore, there is no use to go beyond the simple molecular axis quantization technique when we are interested in the correlation energy.

The Hartree-Fock self-consistent method is perhaps the best known method in molecular quantum chemistry and it works for multi-electron and multi-center cases. In computational physics, the Hartree-Fock calculation scheme is a self-consistent iterative procedure to calculate the optimal single-particle determinant solution to the time-independent Schrödinger equation. As a consequence to this, while it calculates the exchange energy exactly, it does not calculate the effect of electron correlation at all. Figure 21 shows the ground state $E(R)$ of H_2 molecule calculated by the self-consistent Hartree-Fock method (solid line). Subtraction of this solid line from a very accurate quantum mechanical calculation (for example of Ref. [16]) yields the "exact" correlation energy. It is shown as solid dots in Fig. 20.

The Bohr model approach we discussed in this chapter can be a useful supplement to the Hartree-Fock self-consistent method as it allows us to calculate the missing

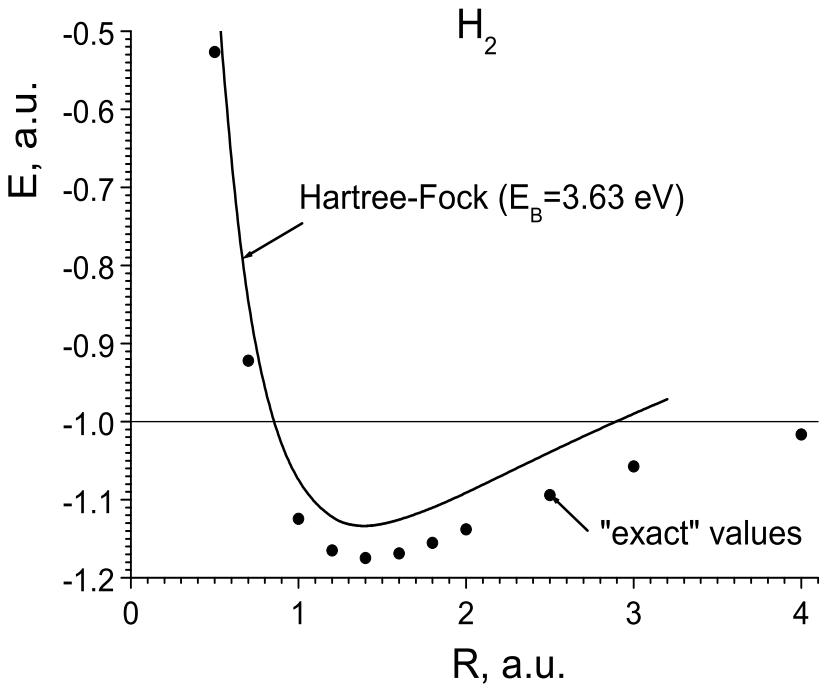

Fig. 21. Ground state $E(R)$ of H_2 molecule calculated by the self-consistent Hartree–Fock method (solid line) and the "exact" energy (dots).

correlation energy in a simple way.

CHAPTER V

MOLECULES IN STRONG MAGNETIC FIELDS

A. Introduction to the model

First brought to the attention of its investigators after the discovery of startling field magnitudes on the surfaces of pulsars—the fields can reach an intensity of 10^{13} G, the study of atomic and molecular phenomena in strong magnetic fields has revealed a large number of unusual and spectacular effects. The physical properties of matter, atomic and molecular systems in particular immersed in strong magnetic fields typical of the vicinities of neutron stars, or white dwarfs are of prime importance as, for instance, remote, natural means of probing neutron star atmospheres and the strength of the particular field prevalent near the suface as well as for monitoring various cosmological processes, such as the intracacies of stellar formation. More specifically, these investigations allow us to consider the possibilities of observing the spectral lines in strong magnetic field regions and, therefore, to estimate the efficiency of methods used for exploring physical conditions close to the surface of a neutron star. Another intriguing consideration may be recognized as the possibility of the catalysis of nuclear reactions now facilitated by the drastically augmented tunneling effects.

Thus, beyond pure theoretical interest, rather practical applications exist in astrophysics and in for instance, the solid-state physics, where laboratory magnetic fields already become "superstrong" for excitons and shallow impurities. (In laboratory conditions this analogous problem, which takes place in semiconductors, concerns excitons represented as hydrogen "quasiatoms", or more interestingly yet as the close solid-state analog of H_2, the excitonic molecule, with a small effective mass and a large dielectric constant. The appropriate dimensionless parameter, which determines the

"strength" of the field, is equal to $\gamma = \mu_B H/R_\infty$, where μ_B is the Bohr magneton, H the field strength (measured in gauss), R_∞ the rydberg (Ry) in the case of atoms, or effective rydberg in the case of excitons.) Last, the motivation for the physical chemist is essentially one based on the need to understand the formation of the various unusual, exotic chemical compounds whose existence is simply impossible without the effects of strong magnetic fields.

The effect of a magnetic field B on the motion of an electron can best be characterized by the energy gap $\hbar eB/m_e c$ between the Landau levels of the electron moving in that field. Landau levels are the energy levels of an otherwise unbound electron interacting with a constant magnetic field. The magnetic field is considered "strong" on the atomic scale when this energy is comparable to the atomic energy unit of 1 Hartree. These energies are exactly equal when the magnetic field is equal to $B_0 = m_e^2 e^3 c/\hbar^3 = 2.350\ 52 \times 10^9 G$. For a brief understanding of the classification of field strengths, let us note that typical white dwarf magnetic fields are in the range $\gamma \sim 10^{-2}$ to 0.5 a.u., whereas fields on the surfaces of pulsars and neutron stars usually fall between $\gamma \sim 10^2$ a.u. and 10^3 a.u..

Research on the behavior of molecular systems in the presence of strong magnetic fields has been confined for the most part to investigations of one-electron systems owing to the siplicity. As such the emphasis hes been the molecular ions. Pioneering work in the study of the properties of matter in strong magnetic fields is that of Schiff and Snyder [25] in their treatment of quadratic Zeeman effect. Experimental work on the nuclear radiofrequency spectra of D_2 and H_2 in intermediate and strong magnetic fields using a molecular beam apparatus, was first carried out by Harrick et al [26]. An early theoretical study of molecular hydrogen and deuterium in magnetic fields may be traced to Ramsey [27]. Ref[28] offers a quantum phase-space treatment of hydrogen molecule in a magnetic field by obtaining analytical Wigner functions.

Detailed calculations of the one-electron molecular ions H_2^+, H_3^{++}, H_4^{3+}, HeH^{++}, He_2^{3+} in a magnetic field ranging from 10^9 G to 4.414×10^{13} G (the Schwinger limit) using trial wave functions with variational parameters may be found in the works of Turbiner et al [29], [30].

A detailed and numerically impressive study came from the authors of ref [31], who have reported their findings based on fully numerical Hartree-Fock calculations regarding their analysis of the singlet $^1\Sigma_g$, triplet $^3\Sigma_u$, and triplet $^3\Pi_u$ states of H_2 molecule in a strong parallel magnetic field.

A list of other useful references may be found in [32], [33], [34], [35], [36], [37], [38] and [39].

We present here a semiclassical approach to study within a field strength range of $10^8$to 10^{10}G, the behavior of hydrogen molecule, and in particular obtain clues as to the formation of new molecular states in response to a strong external magnetic field. We start therefore by first intoducing a reduction via dimensional scaling of a Bohr model admitting of the interaction with a magnetic field.

B. Dimensional scaling analysis of hydrogen atom in a magnetic field

A Bohr model suitable for our purposes is obtained via consideration of the following dimensional scaling analysis of the Schrodinger equation for a hydrogen atom in a magnetic field.The Schrodinger equation in usual three dimensions describing a hydrogen atom in a magnetic field is written (in scaled atomic units)

$$\left(-\frac{1}{2}\nabla^2 - \frac{1}{r} + \frac{\gamma^2\rho^2}{8}\right)\Psi = E\Psi \tag{5.1}$$

where γ ($\equiv B/B_0$), referred to "dimensionless parameter γ" in literature, denotes the strength of a magnetic field incident parallel to the molecular axis, otherwise referred

to internuclear separation vector, and is measured in units of $m_e^2 e^3 c/\hbar^3$ (or c/ea_0^2 in terms of Bohr radius) $\sim 2.350\ 52 \times 10^9 G$, the atomic unit of magnetic field strength.

Before we carry out in detail the necessary scaling transformation to the Hamiltonian and the wave function to extract a useful Bohr model, it is best to briefly describe the utility and procedure of dimensional scaling analyses in general.

Dimensional scaling is still a relatively new field. It is based on the recognition that for certain types of problems it may be useful to consider the spatial dimensionality as a parameter, which ordinarily has the physical value D=3. The reason for taking this unusual approach is that many problems, especially those in electronic structure, simplify dramatically at certain values of D. As may be observed from the application of increased dimensionality to the problem of random walks, for instance, the prolifirating degrees of freedom essentially suppress the dynamic features, which appear in the form of derivatives and in the infinite-dimension limit render a static picture of the interaction between the constituent particles, which now assume fixed positions. For many problems one can also find useful simplifications when the dimensionality is lowered. Several different methods have been developed for utilizing results obtained at non-physical values of D to construct approximate D=3 solutions. One is the method of 1/D expansions, in which the infinite-D limit is used as a starting point, and then systematically corrected by means of perturbation theory. Another approach is to use results obtained at two or more nonphysical values of D to interpolate approximate D=3 solutions. Finally, a third approach is to use only the very simple infinite-D limit solutions explicitly, but to correct these for finite-D effects by means of scale factors derived from the analytic structure of dimensional singularities.

Typically dimensional scaling methods involve four steps:

(1) Generalization of the problem to D-dimensions.

(2) Transforming to a suitably scaled space to remove the major, generic D-dependence of the quantity to be determined.

(3) Evaluatation of the scaled quantity at one or more special D values, such as $D \to \infty$, where the computation is relatively "easy".

(4) Obtaining an approximation for D=3, by relating it to the special D values often by dimensional interpolation or perturbation expansions

Exemplary applications previously studied have included calculations of the radii of gyration of random walks, viral coefficients of hard spheres, correlation energy of two-electron atoms, and resonance energy arising from electronic tunneling in the H_2^+ molecule-ion

We shall chiefly deal with ways to exploit the $D \to \infty$ limit, which is particularly simple to evaluate. In that limit, as stated above, electrons assume fixed positions relative to the nuclei and each other, in the D-scaled space. The large-D electronic geometry and energy correspond to the minimum of an exatly known effective potential and can be determined from classical electrostatics for any atom or molecule.

As might be expected, dimensional scaling results are in general not highly accurate, at least by the standards of modern ab initio calculations. On the other hand, the methods are computationally extremely simple. This renders them useful for treating otherwise insoluble problems. Perhaps even more important, the simplicity of the methods means that one can often use them to gain insight into complex processes. Since the infinite-D limit is in fact a classical limit characterized by localization of the electrons relative to each other, the insights are typically geometric in nature. On the quantitative side, dimensional scaling has proven to be most useful for studying electron correlation (that is, the error associated with the use of the orbital approximation). Electron correlation remains a very challenging problem, even with high-end computational facilities. The fundamental reason that dimensional scaling

has proven to be so useful in treating correlation is that the simplifications that occur in the dimensional limits are not due to dynamical approximations which destroy correlation; thus the dimensional limit solutions upon which the method relies are fully correlated results competitive in accuracy with ab initio calculations are obtained. It is, therefore, a key aspect of dimensional scaling that nonseparable, many-body effects are fully accomodated in the dimensional limits. In other words, the ability to approximate the far more difficult D=3 solution by interpolation or perturbation expansions or other means does not depend on the magnitude, number, or strength of the electronic interactions but only on the dependence on dimension

C. Bohr model for hydrogen atom in a magnetic field

For a derivation of an effective Bohr model description suitable for atomic hydrogen in a magnetic field, we turn our attention to the previously introduced procedure of dimensional scaling. Dimensional scaling essentially establishes a transition from the 3D dynamic picture, expressed in the form of the 3D Schrodinger equation

$$\left(-\frac{1}{2}\nabla^2 - \frac{1}{r} + \frac{\gamma^2\rho^2}{8}\right)\Psi = E\Psi \tag{5.2}$$

via the following set of scaling transformations

$$\nabla^2 = \frac{1}{\rho^{D-2}}\frac{\partial}{\partial\rho}\left(\rho^{D-2}\frac{\partial}{\partial\rho}\right) + \frac{\partial^2}{\partial z^2} + \frac{L^2_{D-2}}{\rho^2} \tag{5.3}$$

$$r \rightarrow \frac{(D-1)^2}{4}r$$

$$\rho \rightarrow \frac{(D-1)^2}{4}\rho$$

$$E \to \frac{4}{(D-1)^2} E$$

$$\gamma \to \frac{8}{(D-1)^3} \gamma$$

$$\Psi = \rho^{-\frac{D-2}{2}} \Phi$$

to the D-scaled Schrodinger equation

$$\left\{ -\frac{1}{2} \left[\frac{1}{\rho^{D-2}} \frac{\partial}{\partial \rho} \left(\rho^{D-2} \frac{\partial}{\partial \rho} \right) + \frac{\partial^2}{\partial z^2} + \frac{L_{D-2}^2}{\rho^2} \right] - \frac{4}{(D-1)^2} \frac{1}{r} + \frac{1}{(D-1)^2} \frac{\gamma^2 \rho^2}{2} \right\} \rho^{-\frac{D-2}{2}} \Phi$$

$$= \frac{4}{(D-1)^2} E \rho^{-\frac{D-2}{2}} \Phi,$$

which in the $D \to \infty$ limit (ground state) gives the static picture energy function

$$E(\rho, z) = \frac{1}{2\rho^2} - \frac{1}{\sqrt{\rho^2 + z^2}} + \frac{\gamma^2 \rho^2}{2} \tag{5.4}$$

which may now be numerically solved for its extrema to yield energy curves with surprising accuracy. Notice that upon performing the scaling transformation, the factor multiplying $\gamma^2 \rho^2$ is $\frac{1}{2}$, and not $\frac{1}{8}$.

$$\frac{B^2 \rho_i^2}{8} \xrightarrow{D \to \infty} \frac{B^2 \rho_i^2}{2} \tag{5.5}$$

This is essential for the projection of the similar model to be applied to the molecule instead. It is a simple, yet crucial recipe that tells us to replace all such factors with their counterparts in writing the Bohr model energy function, and this is what we do in the next section.

D. Hydrogen molecule in a magnetic field

The Bohr model approach to molecular systems dealt with so far have been endowed with two types of quantization initiative to which it has been agreed to refer as radial quantization and molecular-axis quantization. Inspired by the above simple yet subtle analysis, we proceed to replace the Schrodinger equation describing a hydrogen molecule in a magnetic field

$$\left(-\frac{1}{2}\nabla_1^2-\frac{1}{2}\nabla_2^2-\frac{1}{r_{1a}}-\frac{1}{r_{1b}}-\frac{1}{r_{2a}}-\frac{1}{r_{2b}}+\frac{1}{|\overrightarrow{r_1}-\overrightarrow{r_2}|}+\frac{1}{R}+\frac{B^2\rho_1^2}{8}+\frac{B^2\rho_2^2}{8}\right)\Psi=E\Psi \tag{5.6}$$

by the energy function

$$E\left(\overrightarrow{r_1},\overrightarrow{r_2}\right)=\frac{1}{2}\frac{n_1^2}{\rho_1^2}+\frac{1}{2}\frac{n_2^2}{\rho_2^2}-\frac{1}{r_{1a}}-\frac{1}{r_{1b}}-\frac{1}{r_{2a}}-\frac{1}{r_{2b}}+\frac{1}{|\overrightarrow{r_1}-\overrightarrow{r_2}|}+\frac{1}{R}+\frac{B^2\rho_1^2}{2}+\frac{B^2\rho_2^2}{2} \tag{5.7}$$

to construct a molecular-axis quantized Bohr Model, and by the energy function

$$E\left(\overrightarrow{r_1},\overrightarrow{r_2}\right)=\frac{1}{2}\frac{n_1^2}{r_{1a}^2}+\frac{1}{2}\frac{n_2^2}{r_{2b}^2}-\frac{1}{r_{1a}}-\frac{1}{r_{1b}}-\frac{1}{r_{2a}}-\frac{1}{r_{2b}}+\frac{1}{|\overrightarrow{r_1}-\overrightarrow{r_2}|}+\frac{1}{R}+\frac{B^2\rho_1^2}{2}+\frac{B^2\rho_2^2}{2} \tag{5.8}$$

to similarly construct a radially quantized Bohr Model.

Our first approach will be via enforcing quantization with regard to the molecular axis. We do this by considering two spatial configurationinitiatives for the electrons, to which we shall refer henceforth as the UP-UP and the UP-DOWN configurations. These are shown in Fig. 11. The figure shows the spatial positions of the electrons in the up-up and up-down configurations. Prepared in this dissociation limit the axially quantized model has provided an excellent energy-curve description of the antibonding $^3\Sigma_u$ triplet state of the hydrogen molecule in the absence of field as well as the lowest energy $^1\Sigma_g$ singlet (ground) state. Once again, the configurations take

their name intuitively after the positions of the electrons relative to the molecular axis.

In what follows we also take $n_1 = n_2 = 1$ for reasons of greater reliability, and hence focus primarily on the lower energy states this entails.

The defining simplifications of the UP-UP configuration are

$$\rho_1 = \rho_2 = \rho \tag{5.9}$$

$$\theta_1 = \theta_2 = \theta \tag{5.10}$$

$$r_{1a} = r_{2b} = \frac{\rho}{\sin\theta} \tag{5.11}$$

$$r_{2a} = r_{1b} \tag{5.12}$$

with angle θ as shown in Fig. 11 so that the energy function whose extrema are sought for varying R is given by

$$E(\rho,\theta) = \frac{1}{\rho^2} - \frac{2\sin\theta}{\rho} - \frac{2}{\sqrt{\left(R - \frac{\rho}{\tan\theta}\right)^2 + \rho^2}} + \frac{1}{\left|R - \frac{2\rho}{\tan\theta}\right|} + \frac{1}{R} + B^2\rho^2 \tag{5.13}$$

It should be noted that this may in turn be regarded as an extremization of the energy function (5.7) subject to such constraint as implied by equations (5.9)-(5.12).

The UP-DOWN configuration is similarly prepared by setting

$$\rho_1 = \rho_2 = \rho \tag{5.14}$$

$$\theta_1 = \theta_2 = \theta \tag{5.15}$$

$$r_{1a} = r_{2b} = \frac{\rho}{\sin\theta} \tag{5.16}$$

$$r_{2a} = r_{1b}, \tag{5.17}$$

where now the angle θ is measured as shown in Fig. 11. The corresponding energy function whose extrema for varying R yield the potential energy curves is now given

by

$$E(\rho,\theta)=\frac{1}{\rho^2}-\frac{2\sin\theta}{\rho}-\frac{2}{\sqrt{\left(R-\frac{\rho}{\tan\theta}\right)^2+\rho^2}}+\frac{1}{\sqrt{\left(R-\frac{2\rho}{\tan\theta}\right)^2+4\rho^2}}+\frac{1}{R}+B^2\rho^2 \quad (5.18)$$

In order of presentation our findings are:

(i) A description via potential energy curves of the behavior of the ground state in response to a magnetic field corresponding to a range of field strength values from 0.1 a.u. to 0.8 a.u.. This is done within the axially quantized model and coincides with the UP-DOWN configuration. The potential energy curves corresponding to these configurations are shown in Fig. 22.

(ii) In particular the effect of the magnetic field on the binding energy and the bond length are shown. Molecular binding energies for the ground state correponding to incrementally increased field strengths are calculated for a range of fields from 0 to 4.0 a.u.. The result is shown in figure 23 and, predicts a deepening of the potential well. Hence, the state becomes more strongly binding.

(iii) The bond length identified as the value of the internuclear seperation yielding the minimum of the energy curve is similarly calculated for the same range of incrementally advanced field strengths. The result shown in Fig. 24 is a prediction of the shortening of the bondlength for this state.

(iv) The axially quantized model set in the up-up configuration was shown to provide an accurate description of the lowest triplet state in the absence of magnetic field, and as such now reliably presents a description of the evolution of this state as a parallel magnetic field is introduced. The model predicts that the triplet state remains unbinding. The potential energy curves for a range of field strengths are indicated in Fig. 25.

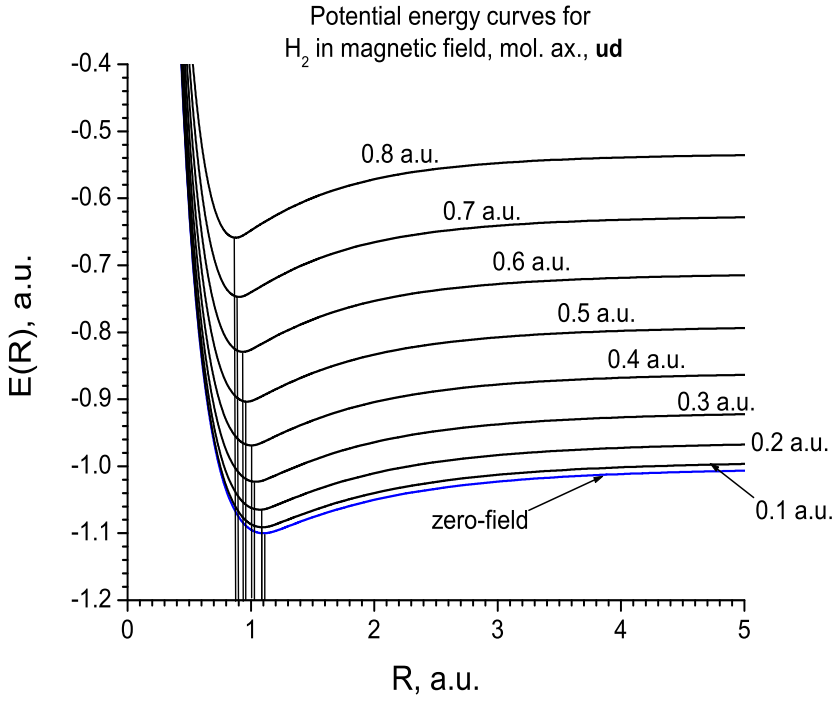

Fig. 22. The energy curves calculated at field strengths of $\gamma = 0.2$ a.u., 0.4a.u., 0.6 a.u., and 0.8 a.u. are shown and compared to the zero-field curve. Notice that aside from the expected increase in the dissociation limit energy, the curves also tend to bunch up with minima shifted to smaller internuclear distances, and the well form becomes more pronounced.

(v) A straightforward application of the previously discussed concept of an effective potential as a safeguard against the "collapse" in intuitive terms of an electron into the "other" nucleus yields the potential energy curves below (see Fig. 26). Typically of all binding, the curves descend as R is decreased, a prelude to forming themselves into a well, but the descent is rather too sharp and decidedly premature. The individual descents continue until a rendezvous with a curve that rather closely contours the potential curve for the zero-field triplet state whereupon they instantly

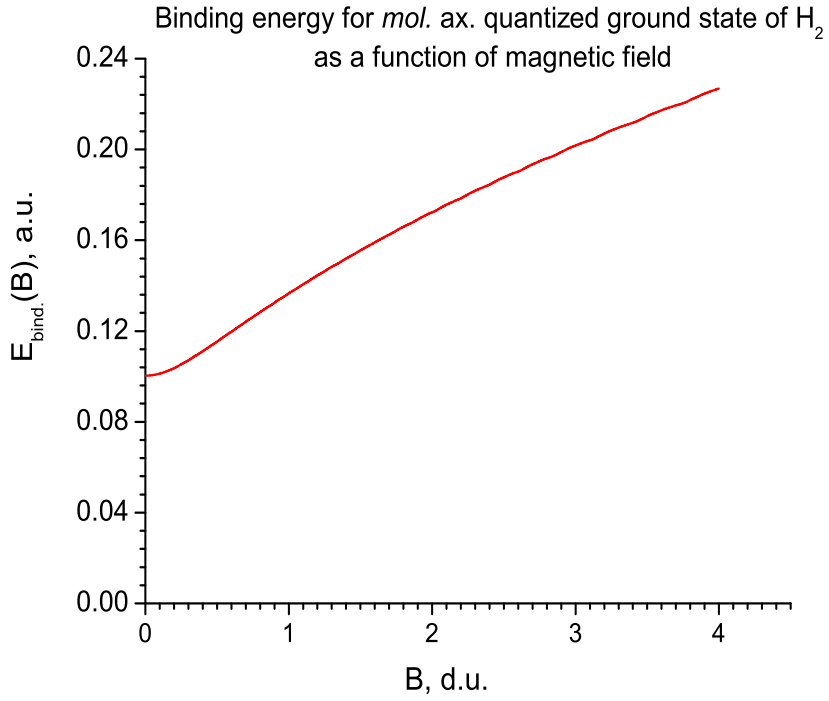

Fig. 23. The numerically obtained field strength dependence of molecular binding energy associated with the axially modelled $^1\Sigma_g$ singlet state of H_2 molecule is shown. Characteristic of this and later plots is the form of the dependence in the weak- and strong-field limits.

merge. Attempts at obtaining solutions past the point of line-crossing that would be natural extensions of the original curves have so far failed. Although it may be argued that the effective potential employed in the calculation is not one that inherently acknowledges the presence of the magnetic field, it still does not explain how solutions to the extremization of an energy function prepared in one configuration (up-down) may be identified as solutions also to one in another configuration (up-up).

(vi) Of particular interest is the emergence of a new state that exists only above a critical value of the magnetic field strength. This is predicted by the radially

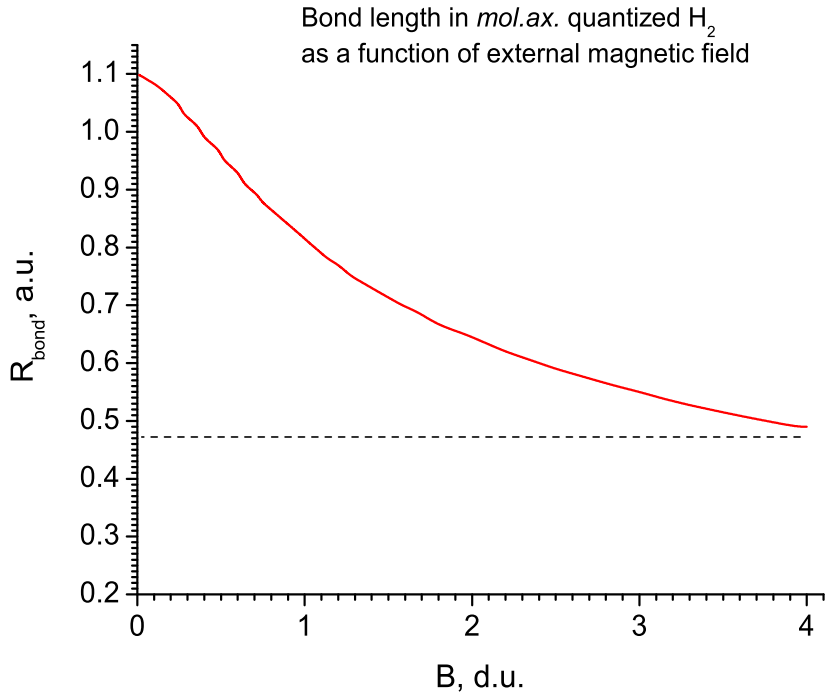

Fig. 24. The internuclear separation corresponding to the minimum of the energy curve is identified as bondlength. Here we see the progression of the bondlength to smaller values with increasing magnetic field.

quantized model fashioned in the UP-DOWN configuration and without an effective potential (see Fig. 27). Potential energy curves corresponding to a range of magnetic field strengths from 0.1 a.u. to 0.8 a.u. have been plotted. These are shown in the figure 28.

Here, too, we notice at once the shift in the location of the minimum of the energy curve as well as a deepening of the potential well as the strength of a parallel magnetic field is increased. The former implies that the effective bondlength is shorter for more intense fields whereas the latter indicates stronger binding. The bond lengths identified over a range of incrementally varied field strengths from 0 a.u

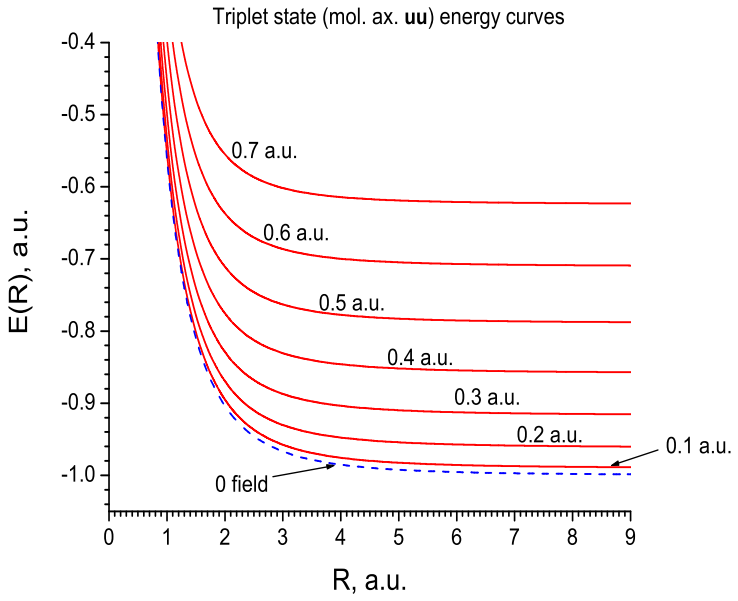

Fig. 25. The energy curves calculated at field strengths of $\gamma = 0.1$ a.u. through 0.7 a.u. in steps of 0.1 a.u., are shown and compared to the zero-field curve. Notice that aside from an expected increase in the R$\rightarrow \infty$- limit energy, the model predicts that the triplet state remains antibonding.

to 1.5 a.u. exhibit a marked difference in their dependence on the field from those obtained using the axially quantized model. This is agreeably so and not surprising given the observation that this state, unlike the axially treated ground state, is not always present, but rather springs into existence above the critical field strength value of 0.020179 a.u.. Below this value the extremization does not admit of a numeric solution.

A comparison of the dependence on field strength of binding energies reveals a similarity, though in qualitative terms, between the axially treated ground state and the radially treated "new state". Despite their different intercepts the curves resemble each other up to a rescaling of magnitudes both in the weak- and the strong-field

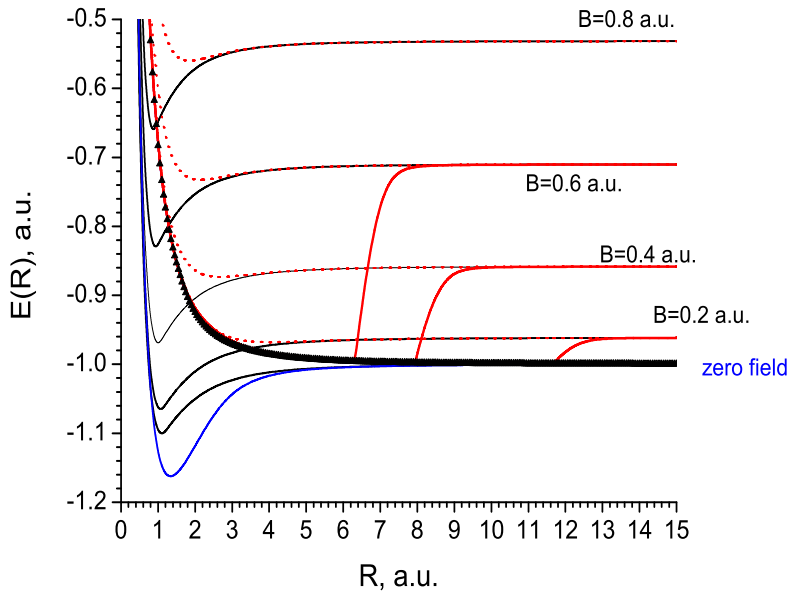

Fig. 26. Crossing of energy lines.

limits. A highlight of the comparison in weak field is best summarized in the figures below.

To gain an insight to the beginnings of this newly predicted state, it is instructive to also examine the associated energy curve in its relationship to other curves. The figure below compares energy curve of the new state at the field value of 0.1 a.u. with those of the field-advanced (γ=0.1 a.u.) triplet, field-advanced (γ=0.1 a.u.) singlet, zero-field triplet, and zero-field singlet states.

A broad-range field dependence of the binding energy associated with the radially quantized "new" state is best described in Fig. 29. For a field dependence of the bondlength associated with this state the reader is refered to Fig. 30. The weak-field dependence of the binding energy is suspectedly parabolic. A close-up may be seen in Fig. 31. The same parabolic dependence of the binding energy associated with the

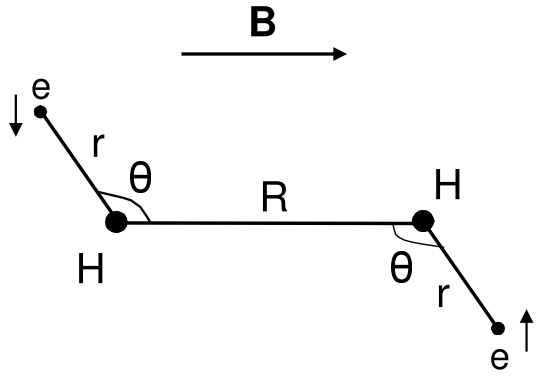

Fig. 27. Electron configuration for a new state that appears in magnetic field.

axially modelled $^1\Sigma_g$ state in the weak-field limit is described in Fig. 32, which one may now compare to that of the "new" state. An essential and detailed comparison of the energy curve associated with this newly predicted state with four other related curves those of is presented in Fig. 33. A family picture of all the potential energy curves so far obtained and their relationship to one another is best summarized in Figs. 34 and 35.

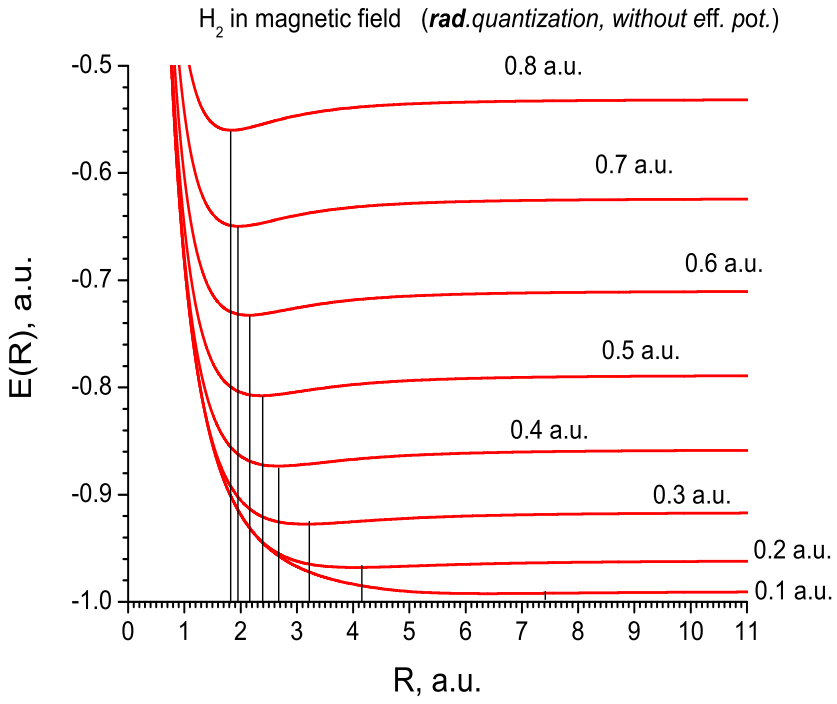

Fig. 28. The potential energy curves for the newly predicted states are shown. An increase in binding energy, and a shortening of bond length can be seen.

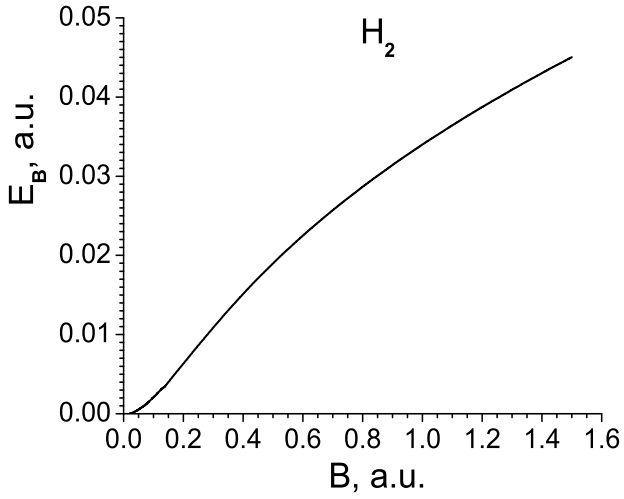

Fig. 29. The figure shows a broad range field dependence of the binding energy associated with the radially quantized new state.

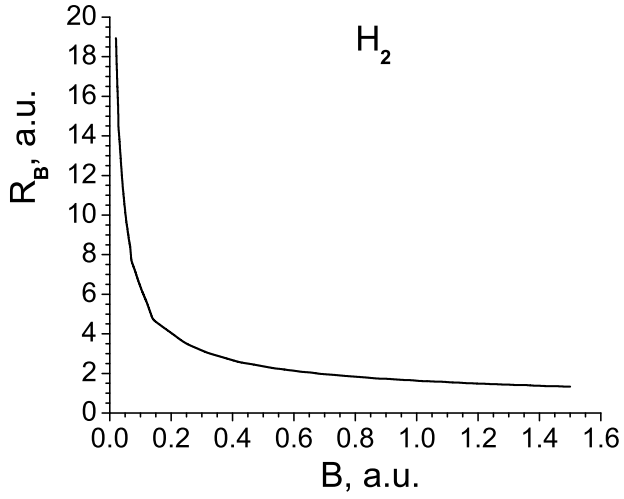

Fig. 30. The curve shows the field dependence of the bond length associated with the radially modelled new state.

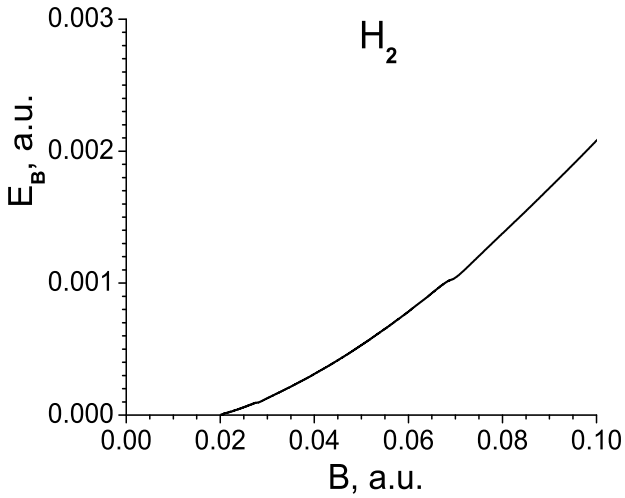

Fig. 31. A close-up shows the almost parabolic weak-field dependence of binding energy associated with the radially quantized new state.

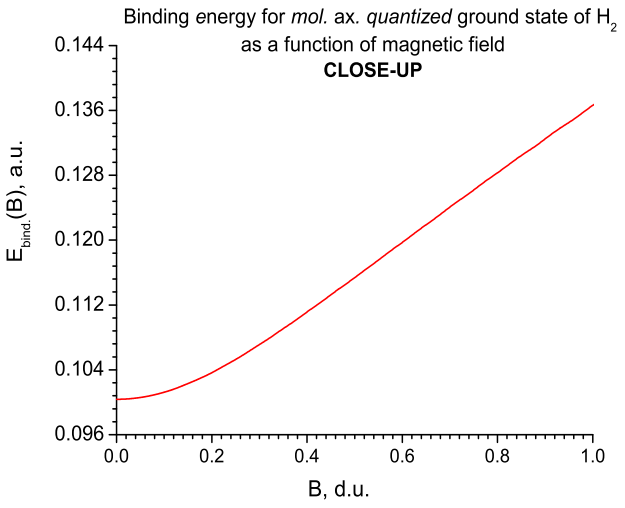

Fig. 32. This close-up shows a similar parabolic dependence on weak-field of the binding energy associated with the axially modelled $^1\Sigma_g$ state.

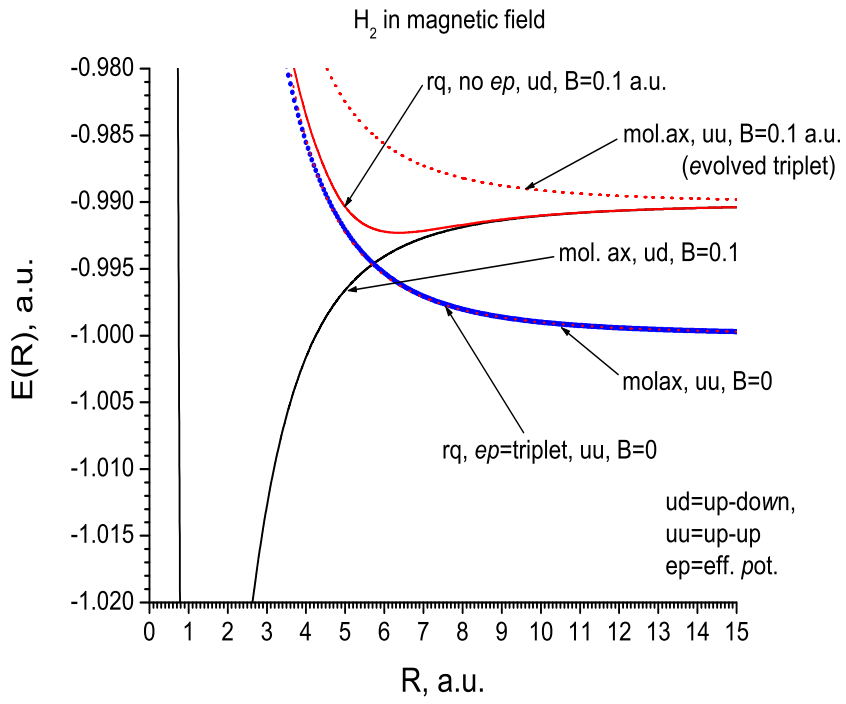

Fig. 33. Figure shows a comparison of the energy curve associated with the newly predicted state with four other related curves.

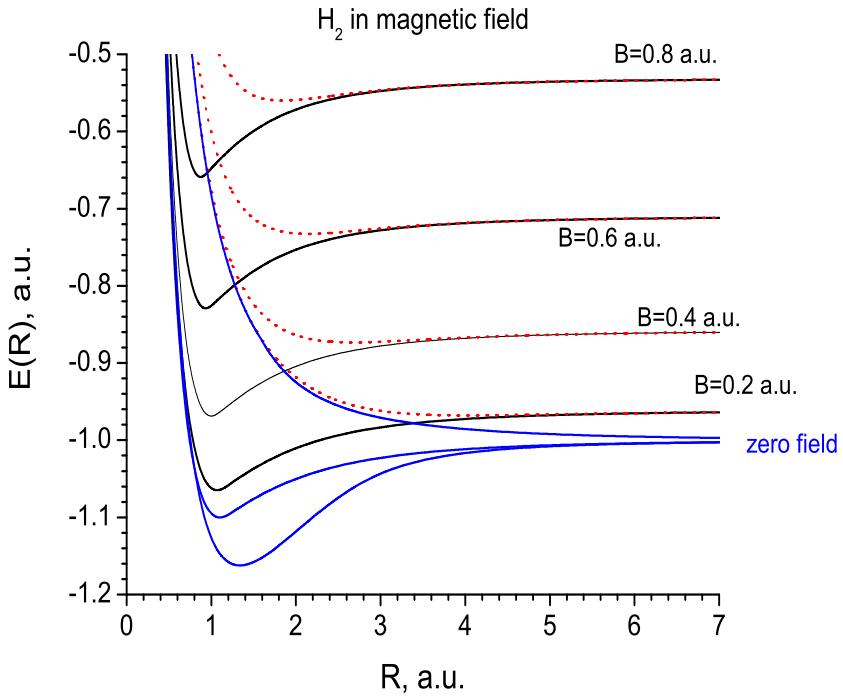

Fig. 34. The figure shows the potential energy curves for the ground state $^1\Sigma_g$ obtained both via an effective potential-radially-quantized model, and by using axial quantization, and for all field-advanced forms of the same state, together with axially treated zero-field and field-advanced triplet $^3\Sigma_u$ states, and the newly predicted states of the radially quantized model set in the up-down dissociation configuration.

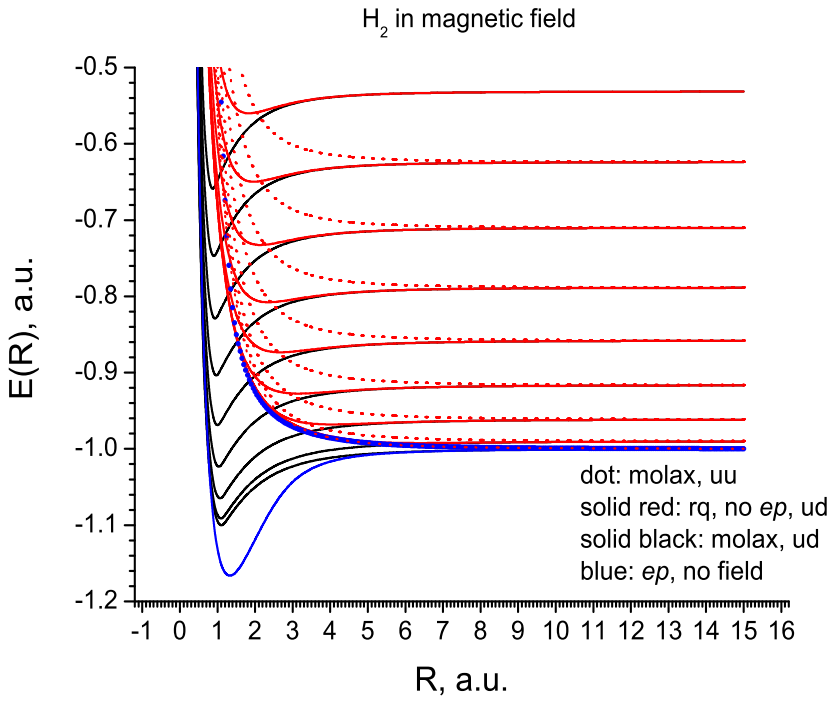

Fig. 35. A larger family picture of energy curves summarizing our findings.

CHAPTER VI

QUANTUM DOT COMPUTING GATES

A. Introduction

The design and construction of the quantum computer (QC) is a major scientific undertaking of the 21^{st} Century. According to DiVincenzo [40], five requirements must be satisfied in order to obtain a reliable QC system: (1) be scalable, (2) the ability to initialize qubits, (3) relatively long decoherence times (longer than the gate operation times), (4) a qubit-specific read-out capability, and (5) a universal set of quantum gates.

Building devices to store and process computational bits quantum-mechanically (qubits) is a challenging problem. In a typical field-effect transistor (FET) in an electronic computer chip, $10,000$ to $100,000$ electrons participate in a single switching event. It is impossible to isolate, out of such a complex system, two quantum mechanical states that would evolve coherently to play the role of a qubit.

Quantum dot(s) (QD) fabrication is a major segment of contemporary nanotechnology. QD devices, including diode lasers, semiconductor optical amplifiers, IR detectors, mid-IR lasers, quantum-optical single-photon emitters, etc., are being developed and considered for a wide variety of applications. QD are also a promising candidate for the future QC technology. In this chapter, we hope to elucidate the connection between the physics of QD and the basic mathematics of quantum gate operations. We have put a certain emphasis on the mathematical derivations but we also hope to explain some rudimentary science and technology of QD.

We begin by introducing what QDs are. QDs consist of nano-scale crystals from a special class of semiconductor materials, which are crystals composed of chemical

elements in the periodic groups II-VI, III-V, or IV-IV. The size of QD ranges from several to tens of nanometers (10^{-9}m) in diameter, which is about 10-100 atoms'. A QD can contain from a single electron to several thousand electrons since the size of the quantum dot is designable. QD are fabricated in semiconductor material in such a way that the free motion of the electrons is trapped in a quasi-zero dimensional "dot". Because of the strong confinement imposed in all three spatial dimensions, a QD behaves similarly to atoms and is often referred to as artificial atoms or giant atoms.

If an electron travels far enough to be scattered by impurities or other electrons, it will lose its phase coherence, which is called *dephasing*. The length in which an electron travels yet can keep its phase coherent is called the *phase coherence length*. The motion of the electron of coherent phase is regarded as a wave motion since it has an interference effect. It is well-known that only standing wave exists within a confined regime because of the destructive interference. Thus, the electron states are not continuous but discrete. Therefore, energy quantization or momentum quantization is observed if the motion of the electron is restricted within a very small regime. This phenomenon is known as the *size quantization effect*.

In natural bulk semiconductor material, the overwhelming majority of electrons occupy the valence band. However, an extremely small percentage of electrons may occupy the conduction band, which has higher energy levels. The only way for an electron in the valence band to be excited and be able to jump to the conduction band is to acquire enough energy to cross the *bandgap*. If such a jump or transition occurs, a new electric carrier in the valence band, called a *hole*, is generated. Since the hole moves in the opposite direction of the electron, the charge of a hole is regarded as positive. The pair of raised electron and hole is called an *exciton*. The average physical separation between the electron and the hole is called the exciton Bohr radius.

Exciton moves freely in bulk semiconductor. However, an exciton is trapped by high energy barriers as an electron is. The size quantization effect is optically observable.

If the device length is smaller than the phase coherence length of the electron or exciton Bohr radius, the energy levels are discrete and the size quantization effect is observed. Since the energy levels are discrete, the three-dimensional energy band becomes lower-dimensional depending on the number of confinement directions. If there is only one directional length of device shorter than the phase coherence length, the device is regarded as a two-dimensional device, called a *quantum well*. The phase coherence length of a quantum well is about 1.62μm for GaAs and about 0.54μm for Si at low temperature. However, since the phase coherence length depends on impurity concentration, temperature and so on, it can be modified for electronic applications. The exciton Bohr radius of GaAs is about 13 nanometers.

There are two approaches to fabricate nano-scale QD: *top-down* and *bottom-up*. The semiconductor processing technologies, such as metal organic chemical vapor deposition, molecular beam epitaxy and e-beam lithography, etc., are used in the top-down approach. Surface and colloid chemistry such as self-assembly, vapor-liquid-solid techniques are used in the bottom-up approach.

There are many methods to synthesize QD in the bottom-up approach, e.g., chemical reactions in colloidal solutions, long time annealing in solid state, chemical vapor deposition on solid surface, wet or dry etching of thin film on solid surface, etc.

As mentioned above, several semiconductor processing technologies can be applied to QD fabrication in the top-down approach. Usually, a quantum well is the starting point of the quantum dot fabrication. Thus, let us first describe the technology of the quantum well fabrication.

By molecular beam epitaxy and metal organic chemical vapor deposition techniques, an ultra-thin single crystalline layer can be deposited on a bulk substrate.

The development of these advanced epitaxy techniques makes it possible to fabricate quantum wells with a very fine boundary. There are two types of quantum wells. One is formed by depositing several single crystalline layers through molecular beam epitaxy, or through the metal organic chemical vapor deposition technique. The other is by depositing single crystalline layers with modulated impurity concentration. The former is usually chosen for optoelectronic devices such as laser where electrons and holes need to be confined at the same time, and the latter is for electronic devices where only either the electron or the hole needs to be confined.

Recent advances in epitaxial growth technology have lead to confinement of single electrons in semiconductor QDs. In QD based "single-electron transistors" (SET), the position of a single electron governs the electrical conductance. However, the same factors that make single-electron detection simple also complicate construction of a quantum computer based on sensing an electron's position. Electrons are easily delocalized by stray electric fields due to Coulomb interaction, and electrons placed in delicate entangled quantum states rapidly lose quantum coherence. The localization of a single dot can be achieved either by advanced epitaxial growth techniques or by using novel optical manipulation techniques such as near-field optical probe.

It was first predicted in 1938 that any two materials with different lattice constants would result in the formation of islands instead of flat layers beyond a critical thickness [41]. The growth of first strain induced islands were reported by Goldstein, *et al.* [42] in 1985 where InAs islands were formed on GaAs. These islands can have sizes in the range of a few nanometers and can confine charge carriers both in the conduction band and in the valence band. Whatever we use the QD system for and whatever the fabrication technology we use, there will always be a statistical distribution of QD size and composition. This statistical distribution in turn produces inhomogeneous broadening of the QD optical response such as transition

frequencies: This favors the distinction of one qubit from the others since the energy-domain discrimination is facile. Access to a specific qubit is achieved by positioning the excitation/ probe beam spot onto the desired location where a number of qubits with different frequencies can be accessed. Access to specific qubits can therefore be achieved by position selective addressing combined with frequency discrimination.

As a single photon generation source, single photons were first generated in a completely different kind of quantum dots, colloidal quantum dots, which are synthesized in solutions [43]. These dots tend to suffer from blinking and bleaching, improvements in their stability is required if practical devices are to be built with these dots, their properties are currently closer to those of molecules than to those of Stranski-Krastanow QD. But because of the advantages of Stranski-Krastanow grown QD, most research has concentrated on epitaxially grown QD. However, one advantage of colloidal dots over epitaxially grown dots is that they still emit efficiently at room temperature.

The recombination of an electron-hole pair leading to the emission of a photon with a specific energy is uniquely determined by the total charge configuration of the dot [44]. If a QD is optically pumped with a pulsed laser leading to the creation of several electron hole pairs in the dot, then it is possible to spectrally isolate the single photon emitted by recombination of the last electron-hole pair [45]. QDs offer several advantages as sources for single photons. They have large oscillator strengths, narrow spectral linewidths, high photon yield, and excellent long-term stability. The materials used to make QDs are compatible with mature semiconductor technologies, allowing them to be further developed and integrated with other components. The usefulness of most QD single-photon sources, though, is limited by their low efficiencies. The dots radiate primarily into the high-index substrates in which they are embedded, and very few of the emitted photons can be collected. The source

efficiency can be increased by placing a dot inside a microscopic optical cavity.

In addition, single-electron devices have a unique mechanism known as the *Coulomb blockade* which is different from size quantization. Single electron tunneling occurs at the ultra-small junction. Electron *cannot* pass through the ultra-small junction due to electrostatic charging energy, which is the Coulomb blockade. Only when the electrostatic charging energy can be lowered by electron tunneling, a single electron can then tunnel through the ultra-small junction, called a single electron junction. Quantitatively, when the capacitance of the junction is much smaller than e^2/k_BT, where e is the absolute charge of electron, k_B is the Boltzmann constant and T is the temperature, single-electron tunneling is observed.

Near-field optical spectroscopy can be used for quantum computation as this probing technique is highly selective and has been utilized for exciting a single quantum dot system. In GaAs based quantum dots the linewidth of emission from single quantum dots has been observed to be less than few μeV. In GaN based quantum dots the linewidth is broader due to larger longitudinal optical (LO) phonon scattering rate and electron effective mass which leads to homogeneous broadening.

QD designs allow for tunable bandgap through the choices of QD sizes, shapes and semiconductor materials. For quantum gate logic operations one can utilize *energy levels*, *spins*, or *excitonic levels* of confined electrons in quantum dots. At present, there exist three major designs of the quantum-dots based QC, due to

(i) Sherwin, Imamoglu and Montroy [46]: The idea is similar to a cavity-QED design [47, 48] by trapping single electrons in quantum dot microcavities;

(ii) Burkard, Loss and DiVincenzo [49, 50]: It utilizes electron spins and their interactions via the electromagnetic effect of tunneling;

(iii) Piermarocchi, Chen, Dale, and Sham [51]: It is based on coherent optical control

of two electron-hole pairs (called a *biexciton*) confined in a single QD. Efforts are being made to couple two of more QD in order to make this design scalable.

In this chapter we focus on the design due to Burkard, Loss and DiVincenzo.

B. Coupled electron spins in an array of quantum dots

1. Electron spin

The electron spin is a "natural" representation of a qubit since it comprises exactly two levels. Unlike for charge (energy-level) states in an atom or quantum dot, there are no additional degrees of freedom into which the system could "leak". Another great advantage of spins as compared to charge qubits is that in typical semiconductor materials like gallium arsenide (GaAs) or silicon (Si), the time over which the spin of a conduction-band electron remains phase coherent can be several orders of magnitude longer than the corresponding charge decoherence times. Of course these numbers have to be compared with the time it takes to perform an elementary gate operation. Even considering this, single spins seem to be very well suited as qubits. The transverse decoherence time T_2, which is most relevant in the context of quantum computing, is defined as the characteristic time over which a single spin which is initially prepared as a coherent superposition of "spin up" and "spin down" coherently precesses about an external magnetic field. The transverse dephasing time of an ensemble of spins in n-doped GaAs can exceed 100ns, as demonstrated by optical measurements [52], while switching times are estimated to be on the order of 10-100ps. The longitudinal (energy) relaxation time T_1 determines how long it takes for a non-equilibrium spin configuration to relax to equilibrium. T_1 can be much longer than T_2 (and particularly long in confined structures), but while suppression of spin relaxation is necessary for quantum computation, it is not sufficient.

There are two main schemes for achieving qubits in quantum dots using electron spin:

1. Single-qubit rotations: In principle, spin-flip Raman transition could rotate the electron spin in $\tau_{gate} \sim 10\text{ps} \ll \tau_{decoh} \sim 1\mu\text{s}$.

2. Two-qubit gates: the real challenge in most schemes. In this case, the spin decoherence during gate operation is a problem.

Spintronics requires the fabrication of ferromagnetic nanostructures that at room temperature can transport spin-polarized carriers, and which can be assembled into addressable hierarchies on a macroscopic chip. Most efforts have been directed towards the mixing of transition-metal atoms (such as Ni, Fe and Mn, which have permanent magnetic moments) into semiconductor devices based on compounds from groups II-VI (such as CdS) or III-V (GaAs) of the periodic table. Superstructures consisting of alternating ferromagnetic/diamagnetic, metallic/oxide thin films have also received attention; like spin valves, spin-polarized currents can be injected into them and transported. An all-electrically controlled quantum dot array can be used for switching qubits.

Recently, a new class of diluted magnetic semiconductor based on III-V system is being studied due to it large intrinsic magnetic dipole moment. Gd doped GaN materials are reported to have a strong intrinsic spin dipole moment. The tunneling in quantum dot based diluted magnetic semiconductor can also be enhanced by using a nanoscale electrode on a diluted magnetic semiconductor system.

2. The design due to D. Loss and D. DiVincenzo

In this section, we study questions related to the spintronics design [49]. The basics of the Loss and DiVincenzo scheme is quite mathematically elegant. For a linear array

of quantum dots a single electron is injected into each dot. The electron's spin up and down constitute a single qubit. Each quantum dot is coupled with its (two) next neighbors through gated tunneling barriers. The overall Hamiltonian of the array of coupled quantum dots is given in [50]:

$$H = \sum_{j=1}^{n} \mu_B g_j(t) \boldsymbol{B}_j(t) \cdot \boldsymbol{S}_j + \sum_{1 \le j < k \le n} J_{jk}(t) \boldsymbol{S}_j \cdot \boldsymbol{S}_k, \tag{6.1}$$

where the first summation denotes the sum of energy due to the application of a magnetic field $\boldsymbol{B}_j$ to the electron spin at dot j, while the second denotes the interaction Hamiltonian through the tunneling effect of a gate voltage applied between the dots, and $\boldsymbol{S}_j, \boldsymbol{S}_k$ are the spin of the electric charge quanta at, respectively, the j-th and k-th quantum dot.

Quantum dots themselves may be viewed as artificial atoms as both manifest similar behaviors. Coupled quantum dots, in this connection, may be considered to a certain extent as *artificial molecules* [49]. Thus, Burkard, Loss and DiVincenzo applied naturally the Heitler-London and Hund-Mulliken methods in molecular quantum chemistry to evaluate the "exchange energy" J, which in terms of our notation in (6.7) later in Section 3, is

$$J = \frac{\hbar}{2} \omega(t).$$

J is a function of B, E and a, among others, where

$$J = J(B, E, a), \tag{6.2}$$

with

$B =$ the magnetic field strength,

$E =$ the electric field strength, and

$a =$ tunneling barrier height or, equivalently, inter-dot distance,

by varying which we will be lead to, respectively, the effects of wave function suppression, level detuning, and the suppression of tunneling between the dots [49]. The determination of $\omega(t)$ or, equivalently, J, is important. Technologically, the tailoring, design and implementation of the control pulse $\omega(t)$ are also perhaps the most challenging.

The coupling between two quantum dots consists of the usual Coulomb repelling potential between the two electrons located within each dot and, in addition, a quartic potential

$$V(x,y) = \frac{m\omega_0^2}{2}\left[\frac{1}{4a^2}(x^2-a^2)^2 + y^2\right]. \tag{6.3}$$

to model the effect of tunneling. Using the Heitler-London approach (likening the coupled quantum dots as the H_2 dimer), Burkard, Loss and DiVincenzo obtained the exchange energy as

$$J = \frac{\hbar\omega_0}{\sinh(2d^2(2b-\frac{1}{b}))}\left[c\sqrt{b}\left(e^{-bd^2}I_0(bd^2) - e^{d^2(b-\frac{1}{b})}I_0\left(d^2\left(b-\frac{1}{b}\right)\right)\right)\right.$$
$$\left. + \frac{3}{4b}(1+bd^2) + \frac{3}{2}\frac{1}{d^2}\left(\frac{eBa}{\hbar\omega_0}\right)^2\right], \tag{6.4}$$

where

$$b \equiv \frac{\Omega}{\omega_0}, \quad d = (m\omega_0/\hbar)^{1/2}a$$

and

$$\Omega \equiv \sqrt{\omega_0^2 + \left(\frac{eB}{2mc}\right)^2}.$$

The above result given in [50] is very commendable but its calculation is lengthy. Its derivations require special techniques and carefulness but details were not available in [50]. We fill in such mathematical technical details in Appendices A and B, which are our main results obtained in this chapter.

3. Model of two identical laterally coupled quantum dots

For the model given by Loss and DiVincenzo in [50], the underlying assumptions leading to the main result (6.4) are itemized below:

(1) The *geometry* of the two coupled dots. The electron confinement is based on single GaAs heterostructure quantum dots formed in a 2DEG (2-dimensional electron gas). The electric and magnetic fields are

$$\boldsymbol{B} = B\boldsymbol{e}_z, \quad \text{with choice of vector potential } \boldsymbol{A}(x, y, 0) = \frac{B}{2}(-y\boldsymbol{e}_x + x\boldsymbol{e}_y) \tag{6.5}$$

$$\boldsymbol{E} = E\boldsymbol{e}_x \tag{6.6}$$

(2) The quartic potential (6.3) for tunneling was motivated by the experimental fact from [53] that the spectrum of single dots in GaAs is well described by a parabolic confinement potential, e.g., with $\hbar\omega_0 = 3meV$ ([50, 53]). (The quartic potential (6.3) separates into two harmonic wells centered at $x = \pm a$.) The constant a, the half interdot distance, satisfies

$a \gg a_B$,

where $a_B = [\hbar/(m\omega_0)]^{1/2}$ = the effective Bohr radius of a single isolated harmonic well,

μ_B: is the Bohr magneton;

$g_j(t)$: is the effective g-factor;

$\boldsymbol{B}_j(t)$: is the applied magnetic field;

$J_{jk}(t)$: the time-dependent exchange constant [see [10] in the References therein], with $J_{jk}(t) = 4t_{jk}^2(t)/u$, which is produced by the turning on and off of the tunneling matrix element $t_{ij}(t)$ between quantum dots i and j, with u being the charging energy of a single dot. Moreover, $J_{jk}(t) \equiv 0$ if $|j-k| > 1$.

Note that for

$$\boldsymbol{S}_j = \sigma_x^{(j)}\boldsymbol{e}_x + \sigma_y^{(j)}\boldsymbol{e}_y + \sigma_z^{(j)}\boldsymbol{e}_z, \qquad j = 1, 2, \ldots, n,$$

and

$$\boldsymbol{B}_j(t) = b_x^{(j)}(t)\boldsymbol{e}_x + b_y^{(j)}(t)\boldsymbol{e}_y + b_z^{(j)}(t)\boldsymbol{e}_z, \qquad j = 1, 2, \ldots, n,$$

where

$$\boldsymbol{e}_x = \begin{bmatrix} 1 \\ 0 \\ 0 \end{bmatrix}, \quad \boldsymbol{e}_y = \begin{bmatrix} 0 \\ 1 \\ 0 \end{bmatrix}, \quad \boldsymbol{e}_z = \begin{bmatrix} 0 \\ 0 \\ 1 \end{bmatrix}$$

and $\sigma_x^{(j)}, \sigma_y^{(j)}$ and $\sigma_z^{(j)}$ are the standard Pauli spin matrices (at dot j):

$$\sigma_x^{(j)} = \begin{bmatrix} 0 & 1 \\ 1 & 0 \end{bmatrix}, \quad \sigma_y^{(j)} = \begin{bmatrix} 0 & -i \\ i & 0 \end{bmatrix}, \quad \sigma_z^{(j)} = \begin{bmatrix} 1 & 0 \\ 0 & -1 \end{bmatrix},$$

the dot products are defined by

$$\boldsymbol{S}_j \cdot \boldsymbol{S}_k = \sigma_x^{(j)}\sigma_x^{(k)} + \sigma_y^{(j)}\sigma_y^{(k)} + \sigma_z^{(j)}\sigma_z^{(k)},$$

$$\boldsymbol{B}_j(t) \cdot \boldsymbol{S}_j = b_x^{(j)}(t)\sigma_x^{(j)} + b_y^{(j)}(t)\sigma_y^{(j)} + b_z^{(j)}(t)\sigma_z^{(j)}.$$

From the universal quantum computing point of view, as the collection of 1-bit

and 2-bit quantum gates are universal, it is sufficient to study a system with *only two coupled quantum dots*, whose Hamiltonian may now be written as ([54, 47])

$$H(t) \equiv \frac{\hbar}{2}[\mathbf{\Omega}_1(t) \cdot \boldsymbol{\sigma} + \mathbf{\Omega}_2(t) \cdot \boldsymbol{\tau} + \omega(t)\boldsymbol{\sigma} \cdot \boldsymbol{\tau}], \tag{6.7}$$

followed by rewriting the notation

$$\boldsymbol{S}_1 = \boldsymbol{\sigma}, \quad \boldsymbol{S}_2 = \boldsymbol{\tau}; \quad \mu_B g_j(t)\boldsymbol{B}_j(t) = \frac{\hbar}{2}\mathbf{\Omega}_j(t), \qquad j = 1, 2; \quad J_{12}(t) = \frac{\hbar}{2}\omega(t).$$

The $\mathbf{\Omega}_1(t)$, $\mathbf{\Omega}_2(t)$ and $\omega(t)$ are the *control pulses*. Thus, varying $\mathbf{\Omega}_1(t)$ and $\mathbf{\Omega}_2(t)$ will generate complete 1-bit Rabi-rotation gates for the first and second qubits, respectively ([47]). However, in order to generate the *entangling* controlled-not (CNOT) gate or a quantum phase gate, both being 2-bit gates, the coupling term $\omega(t)\boldsymbol{\sigma} \cdot \boldsymbol{\tau}$ in (6.7) is indispensable. Therefore,

(3) The Coulomb interaction between the two electrons is described by

$$C = \frac{e^2}{\kappa|\boldsymbol{r}_1 - \boldsymbol{r}_2|}, \qquad \boldsymbol{r}_1 = x_1\boldsymbol{e}_x + y_1\boldsymbol{e}_y, \boldsymbol{r}_2 = x_2\boldsymbol{e}_x + y_2\boldsymbol{e}_y. \tag{6.8}$$

Here we assume that the screening length λ satisfies

$$\lambda/a \gg 1.$$

(4) The ratio between the Zeeman splitting (due to the magnetic field $\boldsymbol{B}$) and the relevant orbital energies (see (5) below) is small for all values of B of interest here. The spin-orbit effect can be neglected since the spin-orbit coupling isgiven by

$$H_{\text{spin-orbit}} = \left(\frac{\omega_0^2}{2mc^2}\right)\boldsymbol{L} \cdot \boldsymbol{S} \tag{6.9}$$

and the ratio of its magnitude to the characteristic energy is

$$H_{\text{spin-orbit}}/(\hbar\omega_0) \approx 10^{-7},$$

where $\hbar\omega_0 = 3\text{meV}$ represents the characteristic energy.

Consequently, the dephasing effects by potential or charge fluctuations can couple only to the charge of the electron, instead of the "holes."

Under conditions (1)–(4) above, the total orbital Hamiltonian of the coupled system may be given as

$$H_{\text{orb}} = h_1 + h_2 + C, \tag{6.10}$$

where

$$h_j = \frac{1}{2m}\left|\boldsymbol{p}_j - \frac{e}{c}\boldsymbol{A}(\boldsymbol{r}_j)\right|^2 + ex_jE + V(\boldsymbol{r}_j), \text{ for } j = 1, 2. \tag{6.11}$$

(5) Assume further the cryogenic condition $kT \ll \hbar\omega_0$, so we need only consider the two lowest orbital eigenstates of the orbital Hamiltonian H_{orb}, which are, respectively, the (symmetric) *spin-singlet* and the (antisymmetric) spin-triplet. A perturbation approximation then leads to the effective Heisenberg spin Hamiltonian

$$H_s = J\boldsymbol{S}_1 \cdot \boldsymbol{S}_2 \qquad \text{(cf. } J \text{ in (6.2))}$$

$$J \equiv \epsilon_t - \epsilon_s = \text{ the difference between the triplet and singlet energies.} \tag{6.12}$$

A self contained account for the derivation of J involves rather technical mathematical analysis of the Fock-Darwin Hamiltonians and states, and clever simplifications of the various integrals in the exchange energy. We put together such work in Appendices A and B.

Next we briefly reproduce the proof from literature of the universality and availability of the quantum computational operations that are supported by this physical set-up. Without the identification of physical processes inherent to the set-up as corresponding to universal quantum gate operations, there would be no point to such design.

The universality of the Loss–DiVincenzo QD quantum gates can now be pre-

sented. We first show how to choose the control pulse $\mathbf{\Omega}_1(t)$ in order to obtain the 1-bit unitary rotation gate $U_{\theta,\phi}$.

Theorem B.1. *([47, p. 111-112]) Let $\phi, \theta \in [0, 2\pi]$ be given. Denote $\boldsymbol{e}(\phi) = \cos\phi \boldsymbol{e}_x + \sin\phi \boldsymbol{e}_y + 0\boldsymbol{e}_z$ for the given ϕ. Let $U_{1,\mathbf{\Omega}_1}(t)$ be the time evolution operator corresponding to the quantum system*

$$i\hbar\frac{\partial}{\partial t}|\psi(t)\rangle = H(t)|\psi(t)\rangle, \quad T > t > 0, \quad \textit{cf. } H(t) \textit{ in } (6.7) \tag{6.13}$$

where the pulses are chosen such that

$$\mathbf{\Omega}_1(t) = \Omega_1(t)\boldsymbol{e}(\phi), \quad \mathbf{\Omega}_2(t) = 0, \quad \omega(t) = 0, \qquad t \in [0, T], \tag{6.14}$$

with $\Omega_1(t)$ satisfying

$$\int_0^T \Omega_1(t)dt = 2\theta, \quad \textit{for the given } \theta. \tag{6.15}$$

Then the action of $U_{1,\mathbf{\Omega}_1}(t)$ on the first qubit satisfies

$$U_{1,\mathbf{\Omega}_1}(t) = U_{\theta,\phi}, \ \textit{the 1-bit unitary rotation gate.} \tag{6.16}$$

Proof. We have

$$\begin{aligned}
U_{\theta,\phi} &= \begin{bmatrix} \cos\theta & -ie^{-i\phi}\sin\theta \\ -ie^{i\phi}\sin\theta & \cos\theta \end{bmatrix} \\
&= \cos\theta\mathbf{1} - ie^{-i\phi}\sin\theta\left(\frac{\sigma_x - i\sigma_y}{2}\right) - ie^{i\phi}\sin\theta\left(\frac{\sigma_x - i\sigma_y}{2}\right) \\
&= \cos\theta\mathbf{1} - i\sin\theta\cos\phi\sigma_x - i\sin\theta\sin\phi\sigma_y \\
&= \cos\theta\mathbf{1} - i\sin\theta(\cos\phi\sigma_x + \sin\phi\sigma_y) \\
&= \cos\theta\mathbf{1} - i\sin\theta\boldsymbol{e}(\phi)\cdot\boldsymbol{\sigma} \\
&= e^{-i\theta\boldsymbol{e}(\phi)\cdot\boldsymbol{\sigma}},
\end{aligned} \tag{6.17}$$

noting that in the above, we have utilized the fact that the 2×2 matrix

$$\boldsymbol{e}(\phi) \cdot \boldsymbol{\sigma} = \begin{bmatrix} 0 & \cos\phi - i\sin\phi \\ \cos\phi + i\sin\phi & 0 \end{bmatrix} \tag{6.18}$$

satisfies $(\boldsymbol{e}(\phi) \cdot \boldsymbol{\sigma})^{2n} = \mathbf{1}$ for $n = 0, 1, 2, \ldots$, where $\mathbf{1}$ is the 2×2 identity matrix.

With the choices of the pulses as given in (6.14), we see that the second qubit remains steady in the time-evolution of the system. The Hamiltonian, now, is

$$H_1(t) = \frac{\hbar}{2}\Omega_1(t)\boldsymbol{e}_1(\phi) \cdot \boldsymbol{\sigma} \tag{6.19}$$

and acts only on the first qubit (where the subscript 1 of $\boldsymbol{e}_1(\phi)$ denotes that this is the vector $\boldsymbol{e}(\phi)$ for the first bit). Because $\Omega_1(t)$ is scalar-valued, we have

$$H_1(t_1)H_1(t_2) = H_1(t_2)H_1(t_1) \quad \text{for any} \quad t_1, t_2 \in [0, T]. \tag{6.20}$$

Thus

$$\begin{aligned} U_{1,\boldsymbol{\Omega}_1}(T) &= e^{-\frac{i}{2}\int_0^T \Omega_1(t)\boldsymbol{e}_1(\phi)\cdot\boldsymbol{\sigma}\ dt} \\ &= e^{\left[-\frac{i}{2}\int_0^T \Omega_1(t)dt\right]\boldsymbol{e}_1(\phi)\cdot\boldsymbol{\sigma}} \\ &= e^{-i\theta\boldsymbol{e}_1(\phi)\cdot\boldsymbol{\sigma}}, \qquad \text{(by (6.15))} \end{aligned} \tag{6.21}$$

using (6.17). The proof is complete. □

We may define $U_{2,\boldsymbol{\Omega}_2}$ in a similar way as in Theorem B.1.

Next, we derive the 2-bit quantum phase gate Q_π and the CNOT gate. This will be done through the square root of the swap gate U_{sw}:

$$U_{sw}(|ij\rangle) = |ji\rangle, \quad \text{for } i, j \in \{0, 1\}. \tag{6.22}$$

Theorem B.2. *([47, p. 110-111]) Denote by $U(t)$ the time evolution operator for the*

quantum system (6.7) *for the time duration* $t \in [0, T]$. *Choose* $\mathbf{\Omega}_1(t) = \mathbf{\Omega}_2(t) = 0$ *in* (6.7) *and let* $\omega(t)$ *therein satisfies*

$$\int_0^T \omega(t)dt = \frac{\pi}{2}. \tag{6.23}$$

Then we have $U(T) = -e^{\pi i/4}U_{\text{sw}}$, *i.e.,* $U(T)$ *is the swapping gate (with a nonessential phase factor* $-e^{\pi i/4}$.*)*

Proof. By assumptions, we have now

$$H(t) = \omega(t)\boldsymbol{\sigma} \cdot \boldsymbol{\tau}/2. \tag{6.24}$$

Since $\omega(t)$ is scalar-valued, we have the commutativity

$$H(t_1)H(t_2) = H(t_2)H(t_1), \quad \text{for any} \quad t_1, t_2 \in [0, T]. \tag{6.25}$$

Therefore

$$\begin{aligned} U(T) &= e^{-i\int_0^T H(t)dt/\hbar} = e^{\left[-\frac{i}{2}\int_0^T \omega(t)dt\right]\boldsymbol{\sigma}\cdot\boldsymbol{\tau}} \\ &= e^{-i\phi\boldsymbol{\sigma}\cdot\boldsymbol{\tau}} \qquad\qquad \left(\phi \equiv \frac{1}{2}\int_0^T \omega(t)dt\right) \\ &= \cos(\phi\boldsymbol{\sigma}\cdot\boldsymbol{\tau}) - i\sin(\phi\boldsymbol{\sigma}\cdot\boldsymbol{\tau}), \end{aligned} \tag{6.26}$$

where $e^{-i\phi\boldsymbol{\sigma}\cdot\boldsymbol{\tau}}$, $\cos(\phi\boldsymbol{\sigma}\cdot\boldsymbol{\tau})$ and $\sin(\phi\boldsymbol{\sigma}\cdot\boldsymbol{\tau})$ are 4×4 matrices. Since

$$\boldsymbol{\sigma}\cdot\boldsymbol{\tau} = \begin{bmatrix} 1 & 0 & 0 & 0 \\ 0 & -1 & 2 & 0 \\ 0 & 2 & -1 & 0 \\ 0 & 0 & 0 & 1 \end{bmatrix}$$

has a 3-fold eigenvalue $+1$ (triplet) and a single eigenvalue (singlet) -3, the associated

projection operators can be easily found to be

$$\boldsymbol{P}_1 = \frac{1}{4}(3\mathbf{1} + \boldsymbol{\sigma}\cdot\boldsymbol{\tau}) \text{ and } \boldsymbol{P}_2 = \frac{1}{4}(\mathbf{1} - \boldsymbol{\sigma}\cdot\boldsymbol{\tau}); \quad \boldsymbol{P}_j\boldsymbol{P}_k = \begin{cases} 0, & j \neq k, \\ \boldsymbol{P}_j, & j = k. \end{cases} \tag{6.27}$$

Thus, from (6.26) and (6.27), we obtain

$$U(T) = e^{-i\phi\boldsymbol{\sigma}\cdot\boldsymbol{\tau}} = e^{-i\phi}\cdot\frac{1}{4}(3\mathbf{1} + \boldsymbol{\sigma}\cdot\boldsymbol{\tau}) + e^{-3i\phi}\cdot\frac{1}{4}(\mathbf{1} - \boldsymbol{\sigma}\cdot\boldsymbol{\tau}). \tag{6.28}$$

With a little manipulation, (6.28) becomes

$$\begin{aligned} U(T) &= e^{i\phi}\left[\cos(2\phi)\mathbf{1} - i\sin(2\phi)\frac{\mathbf{1} + \boldsymbol{\sigma}\cdot\boldsymbol{\tau}}{2}\right] \\ &= e^{i\phi}[\cos(2\phi)\mathbf{1} - i\sin(2\phi)U_{\text{sw}}], \end{aligned} \tag{6.29}$$

by the fact that

$$U_{sw} = \begin{bmatrix} 1 & 0 & 0 & 0 \\ 0 & 0 & 1 & 0 \\ 0 & 1 & 0 & 0 \\ 0 & 0 & 0 & 1 \end{bmatrix} = \frac{1}{2}(\mathbf{1} + \boldsymbol{\sigma}\cdot\boldsymbol{\tau}).$$

Choosing $\phi = \pi/4$, we obtain the desired conclusion. □

Corollary B.3. *([47, p. 110-111]) The square roots of the swapping gate, $U_{\text{sw}}^{1/2}$, are*

$$U_{\text{sw}}^{1/2} = \frac{e^{\pm\pi i/4}}{\sqrt{2}}(\mathbf{1} \mp iU_{\text{sw}}). \tag{6.30}$$

Proof. From (6.29), we first obtain

$$U_{\text{sw}} = ie^{-\frac{\pi i}{4}}U(T). \tag{6.31}$$

Then use $\phi = \pm\pi/8$ in (6.29) to obtain

$$U_{\text{sw}}^{1/2} = (ie^{-\frac{\pi i}{4}})^{1/2}e^{\pm\pi i/8}\left[\frac{1}{\sqrt{2}}(\mathbf{1} \mp iU_{\text{sw}})\right] \tag{6.32}$$

and the desired conclusion. (Note that these two square roots of U_{sw} reflect the choices of $\sqrt{1} = 1$ and the square root of $-1 = \pm i$ for the square roots of the eigenvalues of U_{sw}.) □

Corollary B.4. *([47, p. 112]) The quantum phase gate Q_π is given by*

$$Q_\pi = (-i)U_{1,\mathbf{\Omega}_1^{(2)}} U_{2,\mathbf{\Omega}_2} U_{\text{sw}}^{1/2} U_{1,\mathbf{\Omega}_1^{(1)}} U_{\text{sw}}^{1/2}, \tag{6.33}$$

where

$$\begin{cases} \int \mathbf{\Omega}_1^{(1)}(t)\, dt = -\pi \boldsymbol{e}_{1z}, \\ \int \mathbf{\Omega}_1^{(2)}(t)\, dt = \pi \boldsymbol{e}_{1z}/2, \\ \int \mathbf{\Omega}_2(t)\, dt = -\pi \boldsymbol{e}_{2z}/2, \end{cases} \tag{6.34}$$

and $\boldsymbol{e}_{1z}, \boldsymbol{e}_{2z}$ denote the $\boldsymbol{e}_z$ vector of, respectively, the first and the second qubit.

Remark 1. In order to realize this succession of gates, only one of the $\mathbf{\Omega}(t)$ in (6.34) is nonzero at any given instant t, with the duration when $\mathbf{\Omega}_1^{(1)}(t) \neq 0$ earlier than that when $\mathbf{\Omega}_2(t) \neq 0$, and that when $\mathbf{\Omega}_1^{(2)}(t) \neq 0$ even later. Earliest is the period when $\omega(t) \neq 0$ for the first $U_{\text{sw}}^{1/2}$, and another period when $\omega(t) \neq 0$ is intermediate between those when $\mathbf{\Omega}_1^{(1)}(t) \neq 0$ and $\mathbf{\Omega}_2(t) \neq 0$.

Proof. Define

$$U_{\text{XOR}} \equiv e^{\frac{\pi i}{4}\sigma_z} e^{-\frac{\pi i}{4}\tau_z} U_{\text{sw}}^{1/2} e^{i\frac{\pi}{2}\sigma_z} U_{\text{sw}}^{1/2}, \tag{6.35}$$

with $U_{\text{sw}}^{1/2} = \frac{e^{-\frac{\pi}{4}i}}{\sqrt{2}}(\mathbf{1} + iU_{\text{sw}})$ chosen from (6.30). Then it is straightforward to check that

$$\begin{aligned} U_{\text{XOR}}|00\rangle &= |00\rangle(i), \quad U_{\text{XOR}}|01\rangle = |01\rangle(i), \\ U_{\text{XOR}}|10\rangle &= |10\rangle(i), \quad U_{\text{XOR}}|11\rangle = |11\rangle(-i), \end{aligned} \tag{6.36}$$

so that

$$U_{\mathrm{XOR}} = i(|00\rangle\langle 00| + |01\rangle\langle 01| + |10\rangle\langle 10| - |11\rangle\langle 11|)$$
$$= iQ_{\pi}. \tag{6.37}$$

□

As a final comment of this section, we note that the two quantum dots in coupling are assumed to be identical. However, the state-of-the-art of fabrication of quantum dots with uniform size and characteristics is far from being perfected in contemporary technology. A more refined mathematical treatment for the modeling of two non-identical quantum dots in coupling is needed.

4. Laterally coupled and vertically coupled arrays

Here we provide some details of quantum dot array arrangement. In coupled quantum dots, there exists the combined action of the Coulomb interaction and the Pauli exclusion principle. Two coupled electrons in absence of a magnetic field have a spin-singlet ground state, while the first excited state in the presence of strong Coulomb repulsion is a spin triplet. Higher excited states are separated from these two lowest states by an energy gap, given either by the Coulomb repulsion or the single-particle confinement. For lateral coupling, the dots are arranged in a plane, at a sufficiently small distance, say $2a$, cf. (6.2)-(6.4), such that the electrons can tunnel between the dots (for a lowered barrier) and an exchange interaction J between the two spins is produced. Lateral coupling amongst quantum dots lying in a single plane can be achieved two different techniques. First by controlling the material system, by having spatial correlation between adjoining dots that can lead to splitting of eigenstates within a single dot into symmetric and antisymmetric states. Or secondly by using

a near-field probe that can induce an electromagnetic coupling between neighboring QDs. In the absence of tunneling between the dots we still might have direct Coulomb interaction left between the electrons. However, this has no effect on the spins (qubit) provided the spin-orbit coupling is sufficiently small, which is the case for s-wave electrons in III-V semiconductors with unbroken inversion symmetry (this would not be so for hole-doped systems since the hole has a much stronger spin-orbit coupling due to its p-wave character). Finally, the vanishing of J in (6.1) or (6.2) can be exploited for switching by applying a constant homogeneous magnetic field to an array of quantum dots to tune J to zero (or close to some other desirable value). Then, for switching J on and off, only a small gate pulse or a small local magnetic field is needed.

The exchange interaction is not only sensitive to the magnitude of the applied fields, but also to their direction. An in-plane magnetic field $B_{\|}$ suppresses J exponentially; a perpendicular field in laterally coupled dots has the same effect. The exchange coupling J until both electronic $E_{\perp}$ orbitals are magnetically compressed to approximately the same size, i.e. from this point, J decreases weakly, as for identically sized dots. A perpendicular electric field detunes the single-dot levels, and thus reduces the exchange coupling; the very same finding was made for for laterally coupled dots and an in-plane electric field. An in-plane electric field $E_{\|}$ and different dot sizes provide another switching mechanism for J.

Physical implementations of qubits using QD are fundamentally limited by the interaction of the qubits with their environment and the dephasing. These interactions of the qubits set the maximum time of coherent operation and an upper boundary for the number of quantum gate operations to be applied on a single qubit; therefore understanding the origin of decoherence is critical to control or reduce it, in order to implement quantum logic gates.

Because of their strong localization in all directions, electrons confined in quantum dots are strongly coupled to longitudinal optical (LO) vibrations of the underlying crystal lattice. If the coupling strength exceeds the "continuum width" the energy of keeping the LO phonons delocalized a continuous Rabi oscillation of the electron arises, that is, an everlasting emission and absorption of one LO phonon. As a result, electron-phonon entangled quasi-particles known as polarons form; these play a substantial role in the rapid decoherence of the spin-based quantum dot qubits. The decoherence time for an exciton typically ranges from 20ps to 100ps, which is considerably shorter than the decoherence times of nuclear or electron spin. This is a problem since gate operations take approximately 40ps to perform. However, implementing ultrafast (femtosecond) optoelectronics may eventually enable us to bypass this problem. Read-out on the QDs can be achieved by placing the excitation and probe beam spots on a specific location where a number of qubits with different excitonic frequencies can be accessed. The somewhat randomized distribution of the QD size and composition allow qubits with different excitation frequencies to exist, making it easier to identify specific qubits by singling out the different frequencies.

CHAPTER VII

TWO ELECTRONS IN A RING

The quantum mechanical problem of two electrons confined to motion in a ring of radius R is described by the following Schrödinger equation

$$\left\{-\frac{\hbar^2}{2m_e}\frac{1}{R^2}\frac{\partial^2}{\partial\theta_1^2}-\frac{\hbar^2}{2m_e}\frac{1}{R^2}\frac{\partial^2}{\partial\theta_2^2}+\frac{e^2}{\sqrt{2R^2\left(1-\cos\left(\theta_1-\theta_2\right)\right)}}\right\}\Psi=E\Psi. \tag{7.1}$$

We introduce

$$\theta\equiv\frac{\theta_1+\theta_2}{2} \tag{7.2}$$

$$\varphi\equiv\frac{\theta_1-\theta_2}{2}. \tag{7.3}$$

Then

$$\frac{\partial}{\partial\theta_1}=\frac{1}{2}\frac{\partial}{\partial\theta}+\frac{1}{2}\frac{\partial}{\partial\varphi} \tag{7.4}$$

$$\frac{\partial}{\partial\theta_2}=\frac{1}{2}\frac{\partial}{\partial\theta}-\frac{1}{2}\frac{\partial}{\partial\varphi} \tag{7.5}$$

$$\frac{\partial^2}{\partial\theta_1^2}+\frac{\partial^2}{\partial\theta_2^2}=\frac{1}{2}\frac{\partial^2}{\partial\theta^2}+\frac{1}{2}\frac{\partial^2}{\partial\varphi^2} \tag{7.6}$$

and therefore the original equation reads

$$\left\{-\frac{\hbar^2}{4m_e}\frac{1}{R^2}\left(\frac{\partial^2}{\partial\theta^2}+\frac{\partial^2}{\partial\varphi^2}\right)+\frac{e^2}{\sqrt{2R^2\left(1-\cos 2\varphi\right)}}\right\}\overline{\Psi}=E\overline{\Psi} \tag{7.7}$$

or

$$\left\{-\frac{\hbar^2}{4m_e}\frac{1}{R^2}\left(\frac{\partial^2}{\partial\theta^2}+\frac{\partial^2}{\partial\varphi^2}\right)+\frac{e^2}{\sqrt{4R^2\sin^2\varphi}}\right\}\overline{\Psi}=E\overline{\Psi}, \tag{7.8}$$

where $\overline{\Psi}\left(\theta,\varphi\right)\equiv\Psi\left(\theta_1,\theta_2\right)$. Further simplification is the following

$$\left\{-\frac{\hbar^2}{4m_e}\frac{1}{R^2}\left(\frac{\partial^2}{\partial\theta^2}+\frac{\partial^2}{\partial\varphi^2}\right)+\frac{e^2}{2R\left|\sin\varphi\right|}\right\}\overline{\Psi}=E\overline{\Psi} \tag{7.9}$$

$$-\frac{\hbar^2}{4m_e}\frac{1}{R^2}\frac{\partial^2\overline{\Psi}}{\partial\theta^2}-\frac{\hbar^2}{4m_e}\frac{1}{R^2}\frac{\partial^2\overline{\Psi}}{\partial\varphi^2}+\frac{e^2\overline{\Psi}}{2R\left|\sin\varphi\right|}=E\overline{\Psi} \tag{7.10}$$

$$-\frac{\hbar^2}{4m_e}\frac{1}{R^2}\Phi\frac{d^2\Psi_{cm}}{d\theta^2}-\frac{\hbar^2}{4m_e}\frac{1}{R^2}\Psi_{cm}\frac{d^2\Phi}{d\varphi^2}+\frac{e^2\Psi_{cm}\Phi}{2R\left|\sin\varphi\right|}=E\Psi_{cm}\Phi \tag{7.11}$$

After separation of variables $\overline{\Psi}\left(\theta,\varphi\right)=\Psi_{cm}\left(\theta\right)\Phi\left(\varphi\right)$ we obtain

$$-\frac{\hbar^2}{4m_e}\frac{1}{R^2}\frac{1}{\Psi_{cm}}\frac{d^2\Psi_{cm}}{d\theta^2}-\frac{\hbar^2}{4m_e}\frac{1}{R^2}\frac{1}{\Phi}\frac{d^2\Phi}{d\varphi^2}+\frac{e^2}{2R\left|\sin\varphi\right|}=E. \tag{7.12}$$

Dividing by $\Psi_{cm}\left(\theta\right)\Phi\left(\varphi\right)$ yields

$$-\frac{\hbar^2}{4m_e}\frac{1}{R^2}\frac{1}{\Psi_{cm}}\frac{d^2\Psi_{cm}}{d\theta^2}\equiv E_{cm} \tag{7.13}$$

where $E=E_{cm}+E_{rel}$ and

$$-\frac{\hbar^2}{4m_e}\frac{1}{R^2}\frac{1}{\Phi}\frac{d^2\Phi}{d\varphi^2}+\frac{e^2}{2R\left|\sin\varphi\right|}=E_{rel.} \tag{7.14}$$

$$-\frac{1}{\Psi_{cm}}\frac{d^2\Psi_{cm}}{d\theta^2}=\lambda\equiv\frac{4m_eR^2E_{cm}}{\hbar^2} \tag{7.15}$$

Single-valuedness and periodic boundary conditions imply

$$\Psi_{cm}\sim e^{in\theta} \tag{7.16}$$

and

$$\lambda=n^2, \tag{7.17}$$

$n=1,2,3,...$

$$E_{cm}=\frac{n^2\hbar^2}{4m_eR^2}. \tag{7.18}$$

On the other hand

$$\left\{-\frac{d^2}{d\varphi^2}+\frac{g}{\left|\sin\varphi\right|}\right\}\Phi\left(\varphi\right)=\omega\Phi\left(\varphi\right), \tag{7.19}$$

where

$$g=\frac{2m_eRe^2}{\hbar^2} \tag{7.20}$$

and

$$\omega = \frac{4m_e R^2 E_{rel.}}{\hbar^2} \tag{7.21}$$

Furthermore, since the physical space is $0 \leq \varphi \leq \pi$, we may remove the absolute value sign and write

$$\left\{ -\frac{d^2}{d\varphi^2} + \frac{g}{\sin\varphi} \right\} \Phi(\varphi) = \omega \Phi(\varphi) \tag{7.22}$$

or

$$\left\{ -\frac{d^2}{d\varphi^2} + \frac{g}{\sin\varphi} \right\} \Phi_k(\varphi) = \omega_k \Phi_k(\varphi). \tag{7.23}$$

Although this equation is not amenable to standard methods, our numerically obtained solutions reveal that the dependence of the eigenvalue ω on the scaled coupling g is linear and given by (see figure 36 below)

$$\omega_k = b_k \; g + k^2. \tag{7.24}$$

The coefficients b_k are obtained as slopes of numerically calculated eigenvalues as a function of g. In turn, the eigenvalues ω_k are related to E_{rel}, and therefore E_{total} given by

$$E_{total} = E_{cm} + E_{rel} = \frac{n^2\hbar^2}{4m_e R^2} + \frac{\hbar^2 \omega_k}{4m_e R^2} \tag{7.25}$$

is to a good approximation the total energy of a double excited state of the He atom for appropriately chosen R upto a term $2/R$.

Next we discuss some steps for analytical solution of the eigenvalue equation, the Riccati form of the equation is

$$-y' - y^2 + \frac{g}{\sin\varphi} - \omega(g) = 0. \tag{7.26}$$

Taking derivatives with respect to g yields

$$-y'_g - 2yy_g + \frac{1}{\sin\varphi} - b = 0. \tag{7.27}$$

This equation is first order in y_g, that is,

$$y_g(x;g) = e^{-2\int^x y(s;g)ds}\left\{\int^x dx' e^{2\int^{x'} y(s;g)ds}\left(\frac{1}{\sin x'} - b\right) + C_1(g)\right\}$$

$$y_g(x;0) = e^{-2\int^x y(s;0)ds}\left\{\int^x dx' e^{2\int^{x'} y(s;0)ds}\left(\frac{1}{\sin x'} - b\right) + C_1(0)\right\}$$

Notice also that

$$y(x;0) = \pm n$$

Then

$$y_g(x;0) = \int^x dx'\left(\frac{1}{\sin x'} - b\right) + C_1(0)\, e^{-n^2}$$

Similarly

$$-y'_{gg} - 2y_g^2 - 2yy_{gg} = 0,$$

meaning

$$y_{gg}(x;g) = e^{-2\int^x y(s;g)ds}\left\{\int^x dx' e^{2\int^{x'} y(s;g)ds}\left(-2y_g^2(x';g)\right) + C_2(g)\right\}$$

or

$$y_{gg}(x;0) = -2\int^x dx' y_g^2(x';0) + C_2(g)\, e^{-n^2}.$$

Below are given several generations of derivatives curiously suggestive of how perhaps to find an analytical solution.

$$-y'_{gg} - 2y_g^2 - 2yy_{gg} = 0$$

$$-y'_{ggg} - 6y_g y_{gg} - 2yy_{ggg} = 0$$

$$-y'_{gggg} - 6y_{gg}^2 - 8y_g y_{ggg} - 2yy_{gggg} = 0$$

$$-y'_{ggggg} - 20y_{gg}y_{ggg} - 10y_g y_{gggg} - 2yy_{ggggg} = 0$$

$$-y'_{gggggg} - 20y_{ggg}^2 - 30y_{gg}y_{gggg} - 12y_g y_{ggggg} - 2yy_{gggggg} = 0$$

$$-y'_{ggggggg} - 70y_{ggg}y_{gggg} - 42y_{gg}y_{ggggg} - 14y_g y_{gggggg} - 2yy_{ggggggg} = 0$$

$$-y'_{gggggggg} - 70y_{gggg}^2 - 112y_{ggg}y_{ggggg} - 56y_{gg}y_{gggggg} - 16y_g y_{ggggggg} - 2yy_{gggggggg} = 0$$

$$-y'_{ggggggggg} - 252y_{gggg}y_{ggggg} - 168y_{ggg}y_{gggggg} - 72y_{gg}y_{ggggggg} - 18y_g y_{gggggggg} - 2yy_{ggggggggg} = 0.$$

Finally we solve the eigenvalue Eq. (7.23) numerically using Maple. The boundary conditions are $\Phi_k(\pm\pi/2) = 0$. Figure 36 shows ω_k as a function of g for the first four states $k = 1$, 2 , 3, and 4.

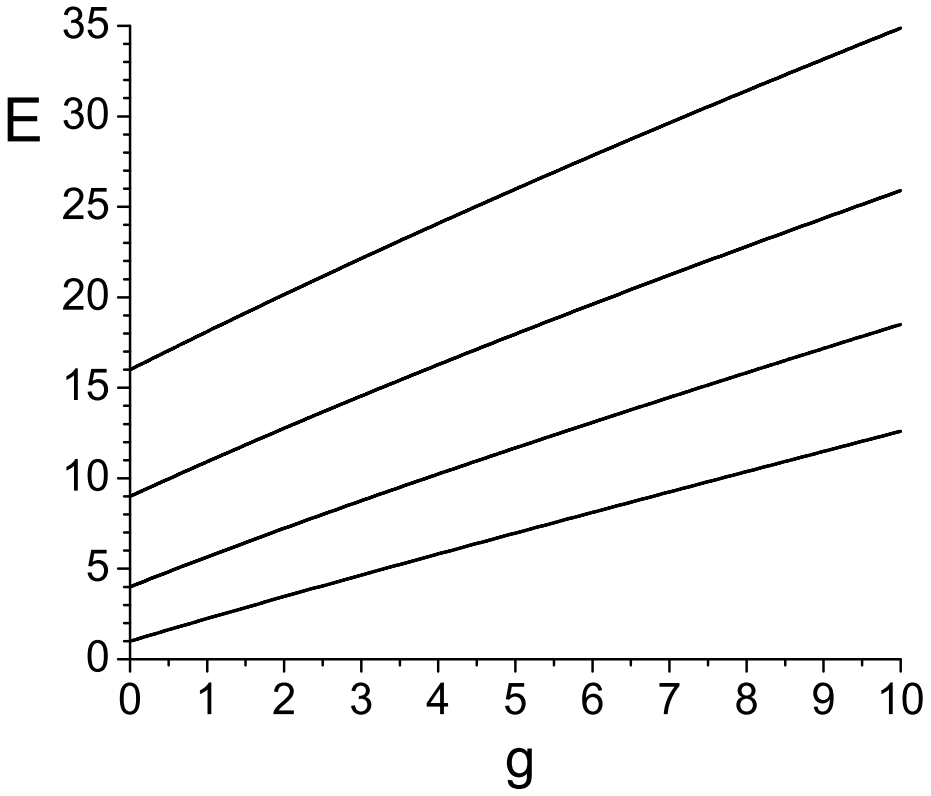

Fig. 36. ω_k as a function of g for $k = 1, 2, 3$ and 4.

CHAPTER VIII

CONCLUSIONS

Here we summarize our findings:

- We applied the interpolated Bohr model for the CH molecule and show that such a simple model yet yields quite accurate potential energy curve for the ground state of CH. This extends the database of molecules for which such an approach has been successfully applied.

- Using the constrained Bohr model with an effective potential we study four-atomic system, such as H_4, and obtained potential energy curves both for linear and square atomic configurations. Our work is the first application of this method for the system of more then three atoms.

- We investigated the accuracy of different methods in calculating the correlation energy and show that the constrained Bohr model approach yields essentially the same accuracy as much more simple molecular axis quantization technique. Therefore, there is no use to go beyond the simple molecular axis quantization model when we are interested in the correlation energy.

- Using the Bohr model we study H_2 molecule in superstrong magnetic fields. We found that magnetic field increases the binding energy and decreases the bond length. Also we found that magnetic field results in appearance of new bound states. Such new states appear only if the field is greater then 5×10^7 G and hence they can not be obtained in a perturbation theory.

- We consider double coupled quantum dots with two electrons in crossed electric and magnetic fields. We applied the Heitler–London molecular method to model

the system and provided a detailed derivation of a general expression for the electron exchange energy.

- We explore the energy of double excited states of the He atom by considering a problem of two electrons in a ring.

REFERENCES

[1] N. Bohr, Phil. Mag. **26**, 1, 476, 857 (1913).

[2] Democritus in *Encyclopaedia Britannica*, vol. VII (J.M. Stoddard, Philadelphia, 1878) 53.

[3] M.C. Nahm, Selections from Early Greek Philosophy, in *The Presocratic Philosophers* edited by G.S. Kirk and J.E. Raven (The University Press, Cambridge, England, 1962)

[4] J.H. Van Vleck, Phil. Mag. **44**, 842-869, 1922.

[5] A. Sommerfeld, *Atomic Structure and Spectral Lines* (E.P. Dutton & Company Publishers, New York, 1923), 3rd Ed., 76-78.

[6] A.A. Svidzinsky, M.O. Scully, and D.R. Herschbach, Phys. Rev. Lett., **95**, 080401 (2005).

[7] A.A. Svidzinsky, M.O. Scully, and D.R. Herschbach, PNAS, **102**, 11985-11988 (2005).

[8] D.R. Herschbach, J. Chem. Phys. **84**, 838 (1986).

[9] J.G. Loeser and D.R. Herschbach, J. Chem. Phys. **84**, 3882 (1986).

[10] J.G. Loeser, J. Chem. Phys. **86**, 5635 (1987).

[11] *Dimensional Scaling in Chemical Physics*, edited by D. R. Herschbach, J. S. Avery and O. Goscinski, (Kluwer Academic Publishers, Dordrecht, 1992).

[12] D.D. Frantz and D.R. Herschbach, Chem. Phys. **126**, 59 (1988).

[13] E. Witten, Phys. Today **33** (7), 38 (1980).

[14] D.Z. Goodson, M. López-Cabrera, D.R. Herschbach and J.D. Morgani III, J. Chem. Phys. **97**, 8481 (1992); Phys. Rev. Lett. **68**, 1992 (1992).

[15] R.D. Harcourt, H. Solomon, J. Beckworth, and L. Chislett, Am. J. Phys. **50**, 557 (1982).

[16] W. Kolos, and C.C.J. Roothaan, Rev. Mod. Phys. **32**, 219 (1960).

[17] W. Heitler and F. London, Zeit. f. Phys. **44**, 455 (1927).

[18] A.A. Svidzinsky, S.A. Chin and M.O. Scully, Phys. Lett. A **355**, 373-377 (2006).

[19] "Exact" energies (solid circles) are taken from a combination of experimental and theoretical sources. The theoretical analyses are typically many term (10-100) configuration interaction computer calculations, see, for example, Ref. [21].

[20] F. Hund and R.S. Mulliken, Phys. Rev. **32**, 186, (1928).

[21] H.F. Schaefer *Quantum Chemistry: The Development of ab initio Methods in Molecular Electronic Structure Theory*, (Oxford: Clarendon Press, 1984).

[22] S.C. Wang, Phys. Rev. **31** 579, (1928).

[23] G. Chen, S.A. Chin, Y. Dou, K.T. Kapale, M. Kim, A.A. Svidzinsky, K. Urtekin, H. Xiong and M.O. Scully, Advances in Atomic, Molecular and Optical Physics, **51**, 93-238 (2005).

[24] J.C. Slater, *Quantum Theory of Molecules and Solids* , (McGraw-Hill, New York, 1963).

[25] L. I. Schiff, H. Snyder, Phys. Rev. , **55**, 59-63, (1939).

[26] N. J. Harrick, R. G. Barnes, P. J. Bray, N. F. Ramsey, Phys. Rev. , **90**, 260-266, (1953).

[27] N. F. Ramsey, Physica, **17**, 388-391, (1951).

[28] T. S. Monteiro, J. Phys. B: At. Mol. Opt. Phys., **25**, L621-L628, (1992).

[29] A.V. Turbiner and J.C. López Vieyra, Physics Reports, **424**, 309-398, (2006).

[30] A. V. Turbiner; J. C. Vieyra; N. L. Guevara, Phys. Rev. A, **72**, 023403, (2005).

[31] Y. P. Kravchenko and M. A. Liberman, Phys. Rev. A, **57**, 3403-3418, (1998).

[32] A. V. Korolev and M. A. Liberman, Phys. Rev. A, **45**, 1762-1766,(1992).

[33] D. Lai and E.E. Salpeter, Phys. Rev. A, **53**, 152-167, (1996).

[34] T. Detmer, P. Schmelcher, F.K. Diakonos, and L. S. Cederbaum, Phys. Rev. A, **56**, 1825-1838, (1997).

[35] M. Encinosa, Phys. Rev. A, **59**, 2521-2523, (1999).

[36] V. K. Khersonskij, Astrophysics and Space Science, **98**, 255-268, (1984).

[37] V. K. Khersonskij, Astrophysics and Space Science, **103**, 357-370, (1984).

[38] V. K. Khersonskii, Astrophysics and Space Science, **117**, 47-64, (1985).

[39] M. S. Kaschiev, S. I. Vinitsky, F. R. Vukajlovic, Phys. Rev. A, **22**,557-559, (1980).

[40] D.P. DiVincenzo, Fortschr. Phys. **48**, 771, (2000).

[41] I.N. Stranski and L. Krastanow, Kl., Abt. IIb **146**, 797, (1938).

[42] L. Goldstein, F. Glas, J.Y. Marzin, M.N. Charasse, and G. Le Roux, Appl. Phys. Lett. **47**, 1099, (1985).

[43] P. Michler, A. Imamoglu, M.D. Mason, P.J. Carson, G.F. Strouse, and S.K. Buratto, Nature **406**, 968, (2000).

[44] L. Landin, M.S. Miller, M.-E. Pistol, C.E. Pryor, L. Samuelson, Science **280**, 262-264, (1998).

[45] J.M. Gerard, B. Gayral, J. Lightwave Technol. **17**, 2089-2095, (1999).

[46] M.S. Sherwin, A. Imamoglu and T. Montroy, Phys. Rev. A **60**, 3508-3514, (1999).

[47] G. Chen, D.A. Church, B-G. Englert and M.S. Zubairy, Mathematical models of contemporary elementary quantum computing devices, in *Quantum Control: Mathematical and Numerical Challenges* edited by A.D. Bandrank, M.C. Delfour and C. Le Bris, CRM Proc. & Lecture Notes, **33**, (Amer. Math. Soc., Providence, R.I., 2003) 79-117.

[48] A. Rauschenbeutel, G. Nogues, S. Osnaghi, P. Bertet, M. Brune, J.M. Raimond, and S. Haroche, Phys. Rev. Lett. **83**, 5166-5169, (1999).

[49] D. Loss and D. DiVincenzo, Phys. Rev. A **57**, 120-126, (1998).

[50] G. Burkard, D. Loss and D. DiVincenzo, Phys. Rev. B **59**, 2070-2078, (1999).

[51] C. Piermarocchi, P. Chen, Y.S. Dale, and L.J. Sham, Phys. Rev. B **65**, 075307, (2002).

[52] J. M. Kikkawa and D. D. Awschalom, Phys. Rev. Lett. **80**, 4313, (1998).

[53] S. Tarucha, D.G. Austing, T. Honda, R.J. van der Hage, and L.P. Houwenhoven, Phys. Rev. Lett. **77**, 3613 (1996); L.P. Kouwenhoven, T.H. Oosterkamp, M.W.S.

Danoesastro, M. Eto, D.G. Austing, T. Honda, and S. Tarucha, Science **278**, 1788 (1997).

[54] G. Burkard, H-A. Engel and D. Loss, Spintronics, quantum computing and quantum communications in quantum dots, in *Fundamentals of Quantum Information* edited by W. Dieter Heiss, (Springer-Verlag, Berlin, 2002) 241-265.

[55] V. Fock, Zeit. Physik **47**, 446, (1928).

[56] C. Darwin, Proc. Cambridge Phil. Soc. **27**, 86, (1930).

[57] M. Abramowitz and I. Stegun, *Handbook of Mathematical Functions*, 9th printing, (Dover, New York, 1970).

[58] I.S. Gradshteyn and I.M. Ryzhik, *Table of Integrals, Series and Products*, 6th edition, (Academic Press, New York, 2000).

APPENDIX A

THE FOCK–DARWIN STATES

The mathematical derivations of (6.4) rely heavily on the Fock–Darwin Hamiltonian, which models the motion of a conduction-band electron confined in a 2-dimensional parabolic potential well in an external magnetic field perpendicular to the 2-dimensional plane:

$$H_{FD} = \frac{1}{2m}\left|\boldsymbol{p} - \frac{e}{c}\boldsymbol{A}\right|^2 + \frac{1}{2M}\omega_0^2 r^2 \qquad (r = (x^2+y^2)^{1/2}); \tag{A.1}$$

where the notation follows that introduced in Section 3. The Fock–Darwin Hamiltonian H_{FD} and its eigenstates have pleasant mathematical properties (Fock [55], Darwin [56]) and may be viewed as a 2-dimensional analog of the simple harmonic oscillator.

From (A.1) and (6.5), we have

$$\begin{aligned} H &= \frac{1}{2m}\left(|\boldsymbol{p}|^2 - 2\frac{e}{c}\boldsymbol{p}\cdot\boldsymbol{A} + \frac{e^2}{c^2}|\boldsymbol{A}|^2\right) + \frac{1}{2}m\omega_0^2(x^2+y^2) \\ &= \frac{|\boldsymbol{p}|^2}{2m} - \frac{1}{2}\frac{eB}{mc}(-p_x y + p_y x) + \frac{e^2B^2}{8mc^2}(x^2+y^2) + \frac{1}{2}m\omega_0^2(x^2+y^2) \\ &= \frac{|\boldsymbol{p}|^2}{2m} + \frac{1}{2}m\left(\omega_0^2 + \frac{\omega_c^2}{4}\right)(x^2+y^2) + \frac{1}{2}\omega_c L_z, \end{aligned} \tag{A.2}$$

where

$\dfrac{eB}{mc} \equiv \omega_c =$ the cyclotron frequency;

$L_z = xp_y - yp_x =$ the z-component of the angular momentum, $\boldsymbol{L} = \boldsymbol{r}\times\boldsymbol{p}$.

Next, from the four independent operators x, y, p_x and p_y, we define four new operators:

$$\left.\begin{aligned} a &= \varepsilon(x - iy) + \eta(ip_x + p_y); \\ a^+ &= \varepsilon(x + iy) + \eta(-ip_x + p_y); \\ b &= \varepsilon(x + iy) + \eta(ip_x - p_y); \\ b^+ &= \varepsilon(x - iy) + \eta(-ip_x - p_y), \end{aligned}\right\} \tag{A.3}$$

where ε and η are real numbers. Using (the commutation relations)

$$[x, p_x] = [y, p_y] = i\hbar, \tag{A.4}$$

$$[x, y] = [x, p_y] = [y, x] = [y, p_x] = 0, \tag{A.5}$$

we can easily show that

$$[a^+, b] = [a, b^+] = [a, b] = [a^+, b^+] = 0, \tag{A.6}$$

and

$$\begin{aligned} [a^+, a] &= \varepsilon\eta[x + iy, ip_x + p_y] + \varepsilon\eta[-ip_x + p_y, x - iy] \\ &= -4\varepsilon\eta\hbar, \end{aligned} \tag{A.7}$$

$$\begin{aligned} [b^+, b] &= \varepsilon\eta[x - iy, ip_x - p_y] + [-ip_x - p_y, x + iy] \\ &= -4\varepsilon\eta\hbar. \end{aligned} \tag{A.8}$$

Thus, if we choose

$$\eta = 1/(4\varepsilon\hbar), \tag{A.9}$$

then

$$\begin{cases} [a, a^+] = [b, b^+] = 1; \\ \text{all other commutators are zero.} \end{cases} \tag{A.10}$$

We obtain

$$\begin{aligned} p_x^2 + p_y^2 &= (ip_x + p_y)(-ip_x + p_y) \\ &= \left(\frac{a - b^+}{2\eta}\right)\left(\frac{a^+ - b}{2\eta}\right); \end{aligned} \tag{A.11}$$

$$\begin{aligned} x^2 + y^2 &= (x + iy)(x - iy) \\ &= \left(\frac{a^+ + b}{2\varepsilon}\right)\left(\frac{a + b^+}{2\varepsilon}\right), \end{aligned} \tag{A.12}$$

and

$$\begin{aligned} L_z = xp_y - yp_x &= \frac{1}{2}[(x + iy)(ip_x + p_y) - (x - iy)(ip_x - ip_y)] \\ &= \frac{1}{2}\left[\left(\frac{a^+ + b}{2\varepsilon}\right)\left(\frac{a - b^+}{2\eta}\right) - \left(\frac{a + b^+}{2\varepsilon}\right)\left(\frac{b - a^+}{2\eta}\right)\right]. \end{aligned} \tag{A.13}$$

Define

$$\Omega^2 = \omega_0^2 + \frac{\omega_c^2}{4}. \tag{A.14}$$

Then

$$\begin{aligned} H &= \frac{1}{2m}\frac{1}{4\eta^2}(a - b^+)(a^+ - b) + \frac{1}{2}m\Omega^2 \cdot \frac{1}{4\varepsilon^2}(a^+ + b)(a + b^+) \\ &\quad + \frac{1}{2}\omega_c \cdot \frac{1}{8\varepsilon\eta}[(a^+ + b)(a - b^-) - (a + b^+)(b - a^+)] \\ &= \frac{1}{8m\eta^2}(aa^+ - ab - b^+a^+ + b^+b) + \frac{m\Omega^2}{8\varepsilon^2}(a^+a + a^+b^+ + ba + bb^+) \\ &\quad + \frac{\omega_c}{16\varepsilon\eta}(a^+a + \cancel{ba} - a^+\cancel{b^+} - bb^+ - \cancel{ab} + aa^+ - b^+b + \cancel{b^+a^+}). \end{aligned} \tag{A.15}$$

Recall from (A.9) that $1/\eta = 4\varepsilon\hbar$. If we further require that

$$\frac{1}{8m\eta^2} = \frac{m\Omega^2}{8\varepsilon^2} = \frac{m\Omega^2}{8}(4\eta\hbar)^2 = 2m\Omega^2\eta^2\hbar^2,$$

i.e.,

$$\eta = \frac{1}{2\sqrt{\hbar m\Omega}}, \tag{A.16}$$

then from (A.15) we see that cross-terms ab, ab^+, a^+b, a^+b^+, etc., cancel out:

$$\begin{aligned}
H &= \frac{\hbar\Omega}{2}\{[aa^+ - \cancel{ab} - \cancel{b^+a} + b^+b] + [a^+a + \cancel{a^+b^+} + \cancel{ba} + bb^+]\} \\
&\quad + \frac{\hbar\omega_c}{4}[\underbrace{a^+a + aa^+}_{2a^+a+\mathbf{1}} \underbrace{-bb^+ - b^+b}_{-2b^+b-\mathbf{1}}] \\
&= \frac{\hbar\Omega}{2}[2a^+a + \mathbf{1} + 2b^+b + \mathbf{1}] + \frac{\hbar\omega_c}{2}[a^+a - b^+b] \\
&= \hbar\left(\Omega + \frac{\omega_c}{2}\right)\left(a^+a + \frac{1}{2}\right) + \hbar\left(\Omega - \frac{\omega_c}{2}\right)\left(b^+b + \frac{1}{2}\right) \\
&= \hbar\omega_+\left[a^+a + \frac{1}{2}\right] + \hbar\omega_-\left[b^+b + \frac{1}{2}\right], \qquad \text{(A.17)}
\end{aligned}$$

where

$$\omega_\pm \equiv \Omega \pm \frac{\omega_c}{2}. \qquad \text{(A.18)}$$

We can now define the Fock–Darwin states

$$|n_+, n_-\rangle = \frac{1}{[(n_+!)(n_-!)]^{1/2}}(a^+)^{n_+}(b^+)^{n_-}|0,0\rangle, \qquad \text{(A.19)}$$

for any integers n_+ and n_-, $n_+ \geq 0$, $n_- \geq 0$, where

$$\begin{cases} a = \varepsilon(x - iy) + \eta(ip_x + p_y), \\ b = \varepsilon(x + iy) + \eta(ip_x - p_y), \end{cases} \qquad \text{(A.20)}$$

with

$$\eta = \frac{1}{2\sqrt{\hbar m\Omega}}, \quad \varepsilon = \frac{1}{4\hbar\eta} = \frac{1}{4\hbar}\cdot 2\sqrt{\hbar m\Omega} = \frac{1}{2}\sqrt{\frac{m\Omega}{\hbar}}. \qquad \text{(A.21)}$$

From (A.17), (A.18) and (A.19), we have

$$H|n_+, n_-\rangle = \left[\hbar\omega_+\left(n_+ + \frac{1}{2}\right) + \hbar\omega_-\left(n_- + \frac{1}{2}\right)\right]|n_+, n_-\rangle, \qquad \text{(A.22)}$$

for integers $n_+ \geq 0, n_- \geq 0$.

Instead of using x and y, we can also use the complex variable z and its conjugate $\bar{z}$:

$$z = x + iy, \quad \bar{z} = x - iy. \tag{A.23}$$

Then

$$\begin{cases} \partial_x = \dfrac{\partial}{\partial x} = \dfrac{\partial z}{\partial x}\dfrac{\partial}{\partial z} + \dfrac{\partial \bar{z}}{\partial x}\dfrac{\partial}{\partial \bar{z}} = \partial_z + \bar{\partial}_z, \\ \partial_y = \dfrac{\partial}{\partial y} = \dfrac{\partial z}{\partial y}\dfrac{\partial}{\partial z} + \dfrac{\partial \bar{z}}{\partial y}\dfrac{\partial}{\partial \bar{z}} = i\partial_z - i\bar{\partial}_z, \end{cases} \tag{A.24}$$

from where we obtain in turn

$$\partial_z = \frac{1}{2}(\partial_x - i\partial_y), \quad \bar{\partial}_z = \frac{1}{2}(\partial_x + i\partial_y). \tag{A.25}$$

From (A.19)–(A.25), we thus have

$$\begin{cases} a = \dfrac{1}{2}\sqrt{\dfrac{m\Omega}{\hbar}}\ \bar{z} + \dfrac{1}{2\sqrt{\hbar m\Omega}} 2\hbar\partial_z = \dfrac{1}{\sqrt{2}}\left[\dfrac{\bar{z}}{2\ell_0} + 2\ell_0\partial_z\right], \\ b = \dfrac{1}{2}\sqrt{\dfrac{m\Omega}{\hbar}}\ z + \dfrac{1}{2\sqrt{\hbar m\Omega}} 2\hbar\bar{\partial}_z = \dfrac{1}{\sqrt{2}}\left[\dfrac{z}{2\ell_0} + 2\ell_0\bar{\partial}_z\right], \end{cases} \tag{A.26}$$

where $\ell_0 \equiv [\hbar/(2m\Omega)]^{1/2}$.

Theorem .5. *The ground state of the Fock–Darwin states are given by*

$$|0,0\rangle = \sqrt{\frac{m\Omega}{\pi\hbar}} e^{-\frac{m\Omega}{2\hbar}(x^2+y^2)}. \tag{A.27}$$

Proof. Since

$$a|0,0\rangle = 0,$$

we have

$$|0,0\rangle = \tilde{c} e^{-\frac{m\Omega}{2\hbar}\bar{z}z}, \tag{A.28}$$

where c is a normalization constant. We also see that (A.28) satisfies

$$b|0,0\rangle = 0.$$

Thus

$$|0,0\rangle = \tilde{c}e^{-\frac{m\Omega}{2\hbar}(x^2+y^2)}.$$

The constant of normalization is easily computed to be $\tilde{c} = [(m\Omega)/(\pi\hbar)]^{1/2}$. The rest can also be easily verified. □

APPENDIX B

EVALUATION OF THE EXCHANGE ENERGY

The point of view taken by Burkard, Loss and DiVincenzo [50] is to regard the coupled two quantum dots as a "molecule" obtained by combining two quantum dots through perturbation with a Fock–Darwin-like ground state as the ground state of the single electron spin on each dot.

Let us rewrite the overall Hamiltonian in (6.10) of the coupled system as

$$H_{\text{orb}} = H_1(\boldsymbol{p}_1, \boldsymbol{r}_1) + H_2(\boldsymbol{p}_2, \boldsymbol{r}_2) + C(\boldsymbol{r}_1, \boldsymbol{r}_2) + W(\boldsymbol{r}_1, \boldsymbol{r}_2), \tag{B.1}$$

$$(\boldsymbol{p}_1 = (p_{x_1}, p_{y_1}, 0), \boldsymbol{r}_1 = (x_1, y_1), \boldsymbol{p}_2 = (p_{x_2}, p_{y_2}, 0), \boldsymbol{r}_2 = (x_2, y_2))$$

$$H_1(\boldsymbol{p}_1, \boldsymbol{r}_1) = \frac{1}{2m}\left|\boldsymbol{p}_1 - \frac{e}{c}\boldsymbol{A}(x_1, y_1, 0)\right|^2 + eEx_1 + \frac{m\omega_0^2}{2}[(x_1 + a)^2 + y_1^2], \tag{B.2}$$

$$H_2(\boldsymbol{p}_2, \boldsymbol{r}_2) = \frac{1}{2m}\left|\boldsymbol{p}_2 - \frac{e}{c}\boldsymbol{A}(x_2, y_2, 0)\right|^2 + eEx_2 + \frac{m\omega_0^2}{2}[(x_2 - a)^2 + y_2^2], \tag{B.3}$$

$$C(\boldsymbol{r}_1, \boldsymbol{r}_2) = \frac{e^2}{\kappa|\boldsymbol{r}_1 - \boldsymbol{r}_2|}, \text{ same as (6.8)}$$

$$W(\boldsymbol{r}_1, \boldsymbol{r}_2) = W_1(x_1) + W_2(x_2), \text{ with} \tag{B.4}$$

$$W_j(x_j) \equiv \frac{m\omega_0^2}{2}\left[\frac{1}{4a^2}(x_j^2 - a^2)^2 - (x_j - a)^2\right], \text{ for } j = 1, 2. \tag{B.5}$$

The H_1 and H_2 given above are not Fock–Darwin Hamiltonians. However, after simple similarity transformations, they become Fock–Darwin plus a constant.

Lemma .1. *Given H_1 and H_2 as in* (B.1) *and* (B.3)*, define*

$$\left.\begin{aligned} \widetilde{H}_1 &= e^{\frac{i}{\hbar}(\frac{e^2BE}{2m\omega_0^2c} + \frac{eBa}{2c})y_1} H_1 e^{-\frac{i}{\hbar}(\frac{e^2BE}{2m\omega_0^2c} + \frac{eBa}{2c})y_1}, \\ \widetilde{H}_2 &= e^{\frac{i}{\hbar}(\frac{e^2BE}{2m\omega_0^2c} - \frac{eBa}{2c})y_2} H_2 e^{-\frac{i}{\hbar}(\frac{e^2BE}{2m\omega_0^2c} - \frac{eBa}{2c})y_2}. \end{aligned}\right\} \tag{B.6}$$

Then

$$\widetilde{H}_j = H_{j,FD} - \left(-\frac{e^2E^2}{2m\omega_0^2} \mp eEa \right); \text{ “}-\text{” for j=1, “}+\text{” for } j = 2, \tag{B.7}$$

where $H_{j,FD}$ is a Fock–Darwin Hamiltonian for $j = 1, 2$ defined by

$$H_{j,FD} = \frac{1}{2m} \left| \boldsymbol{p}_j - \frac{e}{c}\boldsymbol{A}(x_{j\mp}, y_j, 0) \right|^2 + \frac{m\omega_0^2}{2}(x_{j\mp}^2 + y_j^2); \tag{B.8}$$

where

$$x_{j\mp} \equiv x_j - (-1)^j a + \frac{eE}{m\omega_0^2}, \tag{B.9}$$

and “$-$” for $j = 1$ and “$+$” for $j = 2$.

Proof. For $j = 1$, the similarity transformation $(\text{B.6})_1$ effects a translation of p_{y_1}, the y-component of $\boldsymbol{p}_1$, as follows

$$p_{y_1} \longrightarrow p_{y_1} + \frac{e^2BE}{2m\omega_0^2 c} + \frac{eBa}{2c}, \tag{B.10}$$

while the remaining variables x_1, y_1 and p_{x_1} are left unchanged. Thus from (B.6)

$$\begin{aligned} \widetilde{H}_1 = \frac{1}{2m} &\left[\left(p_{x_1} + \frac{eBy_1}{2c} \right)^2 + \left(p_{y_1} - \frac{e^2BE}{2m\omega_0^2 c} + \frac{eBa}{2c} - \frac{eBx_1}{2c} \right)^2 \right] \\ &+ \frac{m\omega_0^2}{2} \left[\left(x_1 - a + \frac{eE}{m\omega_0^2} \right)^2 + y_1^2 \right] - eE \left(\frac{eE}{2m\omega_0^2} - a \right). \end{aligned} \tag{B.11}$$

Define

$$x_1 = x_1 + a + \frac{eE}{m\omega_0^2} \tag{B.12}$$

as in (B.9). Then

$$\widetilde{H}_1 = \frac{1}{2m} \left| \vec{p}_1 - \frac{e}{c}\vec{A}(x_{1-}, y_1, 0) \right|^2 + \frac{m\omega_0^2}{2}(x_{1-}^2 + y_1^2) - \frac{e^2E^2}{2m\omega_0^2} + eEa \tag{B.13}$$

$$\equiv H_{1,FD} + \left(eEa - \frac{e^2E^2}{2m\omega_0^2} \right), \tag{B.14}$$

where $H_{1,FD}$ is a Fock–Darwin Hamiltonian (of variables $\boldsymbol{p}_1, x_{1-}$ and y_1). H_2 and $\widetilde{H}_2$ can be similarly treated. □

We thus have

$$H_1 = e^{-\frac{i}{\hbar}(\frac{e^2BE}{2m\omega_0^2c}-\frac{eBa}{2c})y_1} H_{1,FD} e^{\frac{i}{\hbar}(\frac{e^2BE}{2m\omega_0^2c}-\frac{eBa}{2c})y_1} + \left(eEa - \frac{e^2E^2}{2m\omega_0^2}\right), \tag{B.15}$$

whose eigenstates are

$$e^{-\frac{i}{\hbar}(\frac{e^2BE}{2m\omega_0^2c}-\frac{eBa}{2c})y_1} |n_+^{(1)}, n_-^{(1)}\rangle, \quad \text{cf. (A.22)}, \tag{B.16}$$

with eigenvalues

$$\varepsilon(n_+^{(1)} n_-^{(1)}) \equiv \hbar\omega_+ \left(n_+^{(1)} + \frac{1}{2}\right) + \hbar\omega_- \left(n_-^{(1)} + \frac{1}{2}\right) + \left(eEa - \frac{eE^2}{2m\omega_0^2}\right), \tag{B.17}$$

$$\left(\omega_\omega \equiv \sqrt{\omega_0^2 + \left(\frac{eB}{2mc}\right)^2} \pm \frac{eB}{2mc}\right). \tag{B.18}$$

Similarly, H_2 and $H_{2,FD}$ can be obtained from (B.3), (B.14) and (B.15) by simply replacing the index 1 by 2 and x_- by

$$x_+ \equiv x - a + \frac{eE}{m\omega_0^2}. \tag{B.19}$$

Since the ground state $|0,0\rangle$ of the Fock–Darwin Hamiltonian, H_{FD}, is (cf. (A.27))

$$\Phi_0(x,y) = \sqrt{\frac{m\Omega}{\pi\hbar}} e^{-\frac{m\Omega}{2\hbar}(x^2+y^2)}, \quad \left(\Omega \equiv \sqrt{\omega_0^2 + \left(\frac{eB}{2mc}\right)^2}\right),$$

therefore, the ground state of the Hamiltonians H_1 and H_2 are, respectively,

$$\Phi_0^{(1)}(x,y) = e^{-\frac{i}{\hbar}(\frac{e^2BE}{2m\omega_0^2c}+\frac{eBa}{2c})y} \sqrt{\frac{m\Omega}{\pi\hbar}} e^{-\frac{m\Omega}{2\hbar}(x_-^2+y^2)}, \tag{B.20}$$

$$\Phi_0^{(2)}(x,y) = e^{-\frac{i}{\hbar}(\frac{e^2BE}{2m\omega_0^2c}-\frac{eBa}{2c})y} \sqrt{\frac{m\Omega}{\pi\hbar}} e^{-\frac{m\Omega}{2\hbar}(x_+^2+y^2)}. \tag{B.21}$$

We are now in a position to apply the well known Heitler–London method in quantum molecular chemistry to model the coupled system. The method utilizes

"quantum dot" orbitals:

$$\left.\begin{aligned} a(j) &\equiv \Phi_0^{(1)}(x_j, y_j), \quad j = 1, 2, \\ b(j) &\equiv \Phi_0^{(2)}(x_j, y_j), \quad j = 1, 2, \end{aligned}\right\} \tag{B.22}$$

from which, further define

$$|\Psi_\pm\rangle = \nu[a(1)b(2) \pm a(2)b(1)] \tag{B.23}$$

where ν is the normalization factor. Note that $|\Psi_+\rangle$ is the singlet state, while $|\Psi_-\rangle$ is the triplet state. Note that our notation in (B.21) and (B.23) follows from the convention used by Slater [10, Chap. 3].

Lemma .2. *We have the overlap integral*

$$S \equiv \langle \Phi_0^{(2)} | \Phi_0^{(1)} \rangle = e^{-bd^2 - d^2(b - \frac{1}{b})}, \tag{B.24}$$

where

$$b \equiv \frac{\Omega}{\omega_0}, \quad d = (m\omega_0/\hbar)^{1/2} a. \tag{B.25}$$

Consequently, the normalized singlet and triplet states are

$$|\Psi_\pm\rangle = \frac{1}{\sqrt{2(1 \pm S^2)}}[a(1)b(2) \pm a(2)b(1)], \tag{B.26}$$

satisfying

$$\langle \Psi_+ | \Psi_+ \rangle = 1, \quad \langle \Psi_- | \Psi_- \rangle = 1$$

and

$$\langle \Psi_+ | \Psi_- \rangle = 0.$$

Proof. We evaluate (B.24):

$$
\begin{aligned}
S &\equiv \int_{-\infty}^{\infty}\int_{-\infty}^{\infty} \bar{\Phi}_0^{(2)}(x,y)\Phi_0^{(1)}(x,y)dxdy \\
&= \int_{-\infty}^{\infty}\int_{-\infty}^{\infty} e^{-\frac{i}{\hbar}(\frac{e^2BE}{2m\omega_0^2 c}+\frac{eBa}{2C}-\frac{e^2BE}{2m\omega_0^2 c}+\frac{eBa}{2c})y}\cdot\frac{m\Omega}{\pi\hbar}\cdot e^{-\frac{m\Omega}{\hbar}[(x+\frac{eE}{m\omega_0^2})^2+a^2+y^2]}dxdy \\
&= e^{-\frac{m\Omega}{\hbar}a^2-\frac{e^2B^2a^2}{4\hbar m\Omega c^2}}\left(\frac{m\Omega}{\pi\hbar}\right)\underbrace{\int_{-\infty}^{\infty} e^{-\frac{m\Omega}{\hbar}(x+\frac{eE}{m\omega_0^2})^2}dx}_{\sqrt{\frac{\pi}{(m\Omega/\hbar)}}}\cdot\underbrace{\int_{-\infty}^{\infty} e^{-\frac{m\Omega}{\hbar}(y+i\frac{eBa}{2m\Omega c})^2}dy}_{\sqrt{\frac{\pi}{(m\Omega/\hbar)}}} \\
&= e^{-\frac{m\Omega}{\hbar}a^2-\frac{e^2B^2a^2}{4\hbar m\Omega c^2}} = e^{-bd^2-d^2(b-\frac{1}{2})}.
\end{aligned}
$$

The rest follows from straightforward calculations. □

The exchange energy, by (6.12), now can be written as

$$
\begin{aligned}
J &\equiv \langle\Psi_-|H_{\rm orb}|\Psi_-\rangle - \langle\Psi_+|H_{\rm orb}|\Psi_+\rangle \\
&= \frac{1}{2(1-S^2)}\Big\{\langle a(1)b(2)|H_{\rm orb}|a(1)b(2)\rangle + \langle a(2)b(1)|H_{\rm orb}|a(2)b(1)\rangle \\
&\quad - \langle a(1)b(2)|H_{\rm orb}|a(2)b(1)\rangle - \langle a(2)b(1)|H_{\rm orb}|a(1)b(2)\rangle\Big\} \\
&\quad - \frac{1}{2(1+S^2)}\Big\{\langle a(1)b(2)|H_{\rm orb}|a(1)b(2)\rangle + \langle a(2)b(1)|H_{\rm orb}|a(2)b(1)\rangle \\
&\quad + \langle a(1)b(2)|H_{\rm orb}|a(2)b(1)\rangle + \langle a(2)b(1)|H_{\rm orb}|a(1)b(2)\rangle\Big\} \\
&= \cdots (\text{combining the two parentheses, using (B.1) and expanding}) \\
&= \frac{S^2}{1-S^4}\Bigg\{\Big[\langle a(1)|H_1|a(1)\rangle + \langle a(2)|H_2|a(2)\rangle + \langle b(1)|H_1|b(1)\rangle + \langle a(2)|H_2|a(2)\rangle\Big] \\
&\quad - \frac{1}{S^2}\Big[\langle a(1)|H_1|b(1)\rangle\langle b(2)|a(2)\rangle + \langle b(2)|H_2|a(2)\rangle\langle a(1)|b(1)\rangle \\
&\quad + \langle b(1)|H_1|a(1)\rangle\langle a(2)|b(2)\rangle + \langle a(2)|H_2|b(2)\rangle\langle b(1)|a(1)\rangle\Big] \\
&\quad + [\langle a(1)b(2)|C|a(1)b(2)\rangle + \langle a(2)b(1)|C|a(2)b(1)\rangle] \\
&\quad - \frac{1}{S^2}\Big[\langle a(1)b(2)|C|a(2)b(1)\rangle + \langle a(2)b(1)|C|a(1)b(2)\rangle\Big] \\
&\quad + \Big[\langle a(1)b(2)|W|a(1)b(2)\rangle + \langle a(2)b(1)|W|a(2)b(1)\rangle \\
&\quad - \frac{1}{S^2}\Big(\langle a(1)b(2)|W|a(2)b(1)\rangle + \langle a(2)b(1)|W|a(1)b(2)\rangle\Big)\Big]\Bigg\} \qquad \text{(B.27)} \\
&\equiv \frac{S^2}{1-S^4}\left\{\mathfrak{B}_1 - \frac{1}{S^2}\mathfrak{B}_2 + \mathfrak{B}_3 - \frac{1}{S^2}\mathfrak{B}_4 + \mathfrak{B}_5\right\}, \qquad \text{(B.28)}
\end{aligned}
$$

where each $\mathfrak{B}_j, j = 1, 2, 3, 4$ and 5, represents a square bracket inside the curly parentheses in (B.27) in the correct sequential order. We evaluate these $\mathfrak{B}_j$ one by one below.

Lemma .3. *We have*

$$\mathfrak{B}_1 - \frac{1}{S^2}\mathfrak{B}_2 = 4ma^2\omega_0^2. \qquad \text{(B.29)}$$

Proof. Note the following pairs of cancellations

$$\langle a(1)|H_1|a(1)\rangle - \frac{\langle b(1)|H_1|a(1)\rangle\langle b(2)|a(2)\rangle}{S^2} = 0, \tag{B.30}$$

$$\langle b(2)|H_2|b(2)\rangle - \frac{\langle a(2)|H_2|b(2)\rangle\langle b(1)|a(1)\rangle}{S^2} = 0, \tag{B.31}$$

because

$$H_1|a(1)\rangle = E_0|a(1)\rangle$$

as $|a(1)\rangle$ is the ground state of H_1 and E_0 is the ground state energy (cf. (B.17) with $n_+^{(1)} = n_-^{(1)} = 0$ therein) and so

$$\begin{aligned}\text{Left Hand Side of (B.30)} &= E_0\langle a(1)|a(1)\rangle - \frac{E_0\langle b(1)|a(1)\rangle\langle b(2)|a(2)\rangle}{S^2} \\ &= E_0 - \frac{E_0 \cdot S \cdot S}{S^2} = 0.\end{aligned}$$

Similarly,

$$H_2|b(2)\rangle = E_0|b(2)\rangle,$$

so (B.31) also holds.

For the two remaining terms in $\mathfrak{B}_1$, we have

$$\begin{aligned}&\langle b(1)|H_1|b(1)\rangle + \langle a(2)|H_2|a(2)\rangle \\ =\ & 2\langle b(1)|H_1|b(1)\rangle\end{aligned} \tag{B.32}$$

and by translation along the x_2-axis.

$$2\langle b(1)|H_1|b(1)\rangle = 2\langle b(2)|e^{\frac{i}{\hbar}[(\frac{eBa}{c})y_2 - 2ap_{x_2})]}H_2 e^{-\frac{i}{\hbar}[(\frac{eBa}{c})y_2 - 2ap_{x_2}]}|b(2)\rangle.$$

For $H_2(\boldsymbol{p}_2, \boldsymbol{r}_2)$ in (B.3), we have

$$H_2(p_{x_2}, p_{y_2}, x_2, y_2) = \frac{1}{2m}\left[\left(p_{x_2} + \frac{eB}{2c}y_2\right)^2 + \left(p_{y_2} - \frac{eBa}{2c} + \frac{e^2BE}{2mc\omega_0^2} - \frac{eB}{2c}x_{2+}\right)^2\right] + \frac{m\omega_0^2}{2}(x_{2+}^2 + y_2^2) - eE\left(\frac{eE}{2m\omega_0^2} - a\right),$$

so

$$\begin{aligned} & e^{\frac{i}{\hbar}[(\frac{eBa}{c})y_2 - 2ap_{x_2}]} H_2(p_{x_2}, p_{y_2}, x_2, y_2) e^{-\frac{i}{\hbar}[(\frac{eBa}{c})y_2 - 2ap_{x_2}]} \\ = \; & H_2\left(p_{x_2}, p_{y_2} - \frac{eBa}{c}, x_2 - 2a, y_2\right) \\ = \; & \cdots \text{(substituting and simplifying)} \\ = \; & H_2(p_{x_2}, p_{y_2}, x_2, y_2) + \frac{m\omega_0^2}{2}(4a^2 - 4ax_{2+}). \end{aligned}$$

Therefore

$$\text{(B.32)} = 2\langle b(1)|H_2|b(1)\rangle = 2[\langle b(2)|H_2|b(2)\rangle - 2am\omega_0^2\underbrace{\langle b(2)|x_{2+}|b(2)\rangle}_{=0 \text{ because the integrand is an odd function of } x_{2+}} + 2ma^2\omega_0^2]$$

$$= 2(E_0 + 2ma^2\omega_0^2). \tag{B.33}$$

The remaining terms in $-\frac{1}{S^2}\mathfrak{B}_2$ are

$$\begin{aligned} & -\frac{1}{S^2}[\langle a(1)|H_1|b(1)\rangle S + \langle b(2)|H_2|a(2)\rangle S] \\ = \; & -\frac{S}{S^2}[\langle E_0 a(1)|b(1)\rangle + \langle E_0 b(2)|a(2)\rangle] \\ = \; & -\frac{S}{S^2}\cdot 2E_0 S = -2E_0. \end{aligned} \tag{B.34}$$

By adding (B.33) and (B.34), we obtain (B.29). □

Lemma .4. *We have*

$$\mathfrak{B}_3 - \frac{1}{S^2}\mathfrak{B}_4 = 2\hbar\omega_0 \left[c\sqrt{b}\ e^{-bd^2} I_0(bd^2) - c\sqrt{b}\ e^{d^2(b-\frac{1}{b})} I_0\left(d^2\left(b-\frac{1}{b}\right)\right)\right]. \quad \text{(B.35)}$$

Proof. Note that by the symmetry $C(\boldsymbol{r}_1, \boldsymbol{r}_2) = C(\boldsymbol{r}_2, \boldsymbol{r}_1)$, we have

$$\begin{aligned}
\mathfrak{B}_3 &= 2\langle a(1)b(2)|C|a(1)b(2)\rangle \\
&= \int\limits_{\mathbb{R}^2}\int\limits_{\mathbb{R}^2} \overline{\Phi_0^{(1)}(x_1,y_1)}\ \overline{\Phi_0^{(2)}(x_2,y_2)} \frac{e^2}{\kappa|\vec{r}_1 - \vec{r}_2|} \Phi_0^{(1)}(x_1,y_1)\Phi_0^{(2)}(x_2,y_2)dx_1dy_1dx_2dy_2 \\
&= \left(\frac{m\Omega}{\pi\hbar}\right)^2 \frac{e^2}{\kappa} \int\limits_{\mathbb{R}^2}\int\limits_{\mathbb{R}^2} \frac{1}{|\vec{r}_1 - \vec{r}_2|} e^{-\frac{m\Omega}{\hbar}[(x_1+a+\frac{eE}{m\omega_0^2})^2+y_1^2+(x_2-a+\frac{eE}{m\omega_0^2})^2+y_2^2]} dx_1dy_1dx_2dy_2.
\end{aligned} \quad \text{(B.36)}$$

Introduce the *center of mass coordinates*:

$$\begin{cases} \vec{R} = \dfrac{1}{2}(\vec{r}_1 + \vec{r}_2) & \text{(center of mass)} \\ \vec{r} = \vec{r}_1 - \vec{r}_2 & \text{(relative coordinates)} \end{cases} \quad \text{(B.37)}$$

$$\begin{cases} X = \dfrac{1}{2}(x_1+x_2), Y = \dfrac{1}{2}(y_1+y_2); & X = R\cos\Phi, Y = R\sin\Phi, \\ x = \dfrac{1}{2}(x_1-x_2), y = \dfrac{1}{2}(y_1-y_2); & x = r\cos\phi, y = r\sin\phi. \end{cases} \quad \text{(B.38)}$$

This change of coordinates has Jacobian equal to 1. Then the integral in (B.36)

becomes

$$
\begin{aligned}
\text{(B.36)} = &\left(\frac{m\Omega e}{\pi\hbar}\right)^2 \frac{1}{\kappa} \int\limits_{\mathbb{R}^2}\int\limits_{\mathbb{R}^2} \frac{1}{r} \\
&e^{-\frac{m\Omega}{\hbar}[X^2+xX+\frac{x^2}{4}+(a+\frac{eE}{m\omega_0^2})(2X-x)+(a+\frac{eE}{m\omega_0^2})^2} \\
&\quad +X^2-xX+\frac{x^2}{4}+(\frac{eE}{m\omega_0^2}-a)(2X-x)+(\frac{eE}{m\omega_0^2}-a)^2+Y^2+yY+\frac{y^2}{4}+Y^2-yY+\frac{y^2}{4}]\ r dr d\phi R dR d\Phi \\
= &\left(\frac{m\Omega e}{\pi\hbar}\right)^2 \frac{1}{\kappa} \int_0^{2\pi} d\phi \int_0^{\infty} dr \int_0^{2\pi} d\Phi \int_0^{\infty} dR \cdot R \\
&\times \left\{ e^{-\frac{m\Omega}{\hbar}[2R^2+\frac{r^2}{2}+2(a^2+(\frac{eE}{m\omega_0^2})^2)+2ax+\frac{4eE}{m\omega_0^2}X^2]} \right\} \\
= &\left(\frac{m\Omega e}{\pi\hbar}\right)^2 \frac{1}{\kappa} e^{-\frac{2m\Omega}{\hbar}(a^2+\frac{e^2E^2}{m^2\omega_0^4})} \int_0^{2\pi} d\Phi \int_0^{\infty} dR \quad R \quad e^{-\frac{m\Omega}{\hbar}[2R^2+\frac{4cE}{m\omega_0^2}X]} \\
&\times \int_0^{2\pi}\int_0^{\infty} dr d\phi \cdot e^{-\frac{m\Omega}{\hbar}[\frac{r^2}{2}+2ar\cos\phi]} \\
= &\left(\frac{m\Omega e}{\pi\hbar}\right)^2 \frac{1}{\kappa} e^{-\frac{2m\Omega}{\hbar}(a^2+\frac{e^2E^2}{m^2\omega_0^4})} \left\{ \int_{-\infty}^{\infty} e^{-\frac{m\Omega}{\hbar}[2X^2+\frac{4eE}{m\omega_0^2}X]} \left[\int_{-\infty}^{\infty} e^{-\frac{2m\Omega}{\hbar}Y^2} dY \right] dX \right\} \\
&\times \left\{ \int_0^{\infty} e^{-\frac{m\Omega}{2\hbar}r^2} \underbrace{\left[\int_0^{2\pi} e^{-\frac{2m\Omega a}{\hbar} r\cos\phi}\ d\phi \right]}_{(\mathcal{J}_1)} dr \right\}. \qquad \text{(B.39)}
\end{aligned}
$$

We evaluate the integral $(\mathcal{J}_1)$ above by using the expansion

$$
\begin{aligned}
e^{-(\frac{2m\Omega a}{\hbar} r)\cos\phi} &= \sum_{m=-\infty}^{\infty} (-1)^m I_m\left(\frac{2m\Omega a}{\hbar} r\right) e^{im\phi} \\
&= I_0\left(\frac{2m\Omega a}{\hbar} r\right) + 2\sum_{m=1}^{\infty} I_m\left(\frac{2m\Omega a}{\hbar} r\right)\cos(m\phi)
\end{aligned}
$$

(cf. Abramowitz and Stegun [57, p. 376, Formula 9.6.34])

$$(\mathcal{J}_1) = \int_0^{2\pi} \left\{ I_0\left(\frac{2m\Omega a}{\hbar} r\right) + 2\sum_{m=1}^{\infty} I_m\left(\frac{2m\Omega a}{\hbar} r\right) \cos m\phi \right\} d\phi$$
$$= 2\pi I_0\left(\frac{2m\Omega a}{\hbar} r\right).$$

Substituting $(\mathcal{J}_1)$ into (B.39) above and continuing, we obtain

$$\text{(B.36)} = \left(\frac{m\Omega e}{\pi\hbar}\right)^2 \frac{1}{\kappa} e^{-\frac{2m\Omega}{\hbar}(a^2 + \frac{e^2E^2}{m^2\omega_0^4})} \cdot e^{\frac{2m\Omega}{\hbar}\frac{e^2E^2}{m^2\omega_0^4}} \cdot \underbrace{\int_{-\infty}^{\infty} e^{-\frac{2m\Omega}{\hbar}(X + \frac{eE}{m\omega_0^2})^2} dX}_{\left(\frac{\pi\hbar}{2m\Omega}\right)^{1/2}} \cdot$$
$$\cdot \underbrace{\int_{-\infty}^{\infty} e^{-\frac{2m\Omega}{\hbar}Y^2} dY}_{\left(\frac{\pi\hbar}{2m\Omega}\right)^{1/2}} \cdot 2\pi \underbrace{\int_0^{\infty} e^{-\frac{m\Omega}{2\hbar}r^2} I_0\left(\frac{2m\Omega a}{\hbar} r\right) dr}_{(\mathcal{J}_2)}.$$

To evaluate the integral $(\mathcal{J}_2)$, we use

$$\int_0^{\infty} e^{-ax^2} I_\nu(bx) dx = \frac{1}{2}\sqrt{\frac{\pi}{a}} e^{\frac{b^2}{8a}} I_{\frac{1}{2}\nu}\left(\frac{b^2}{8a}\right) \quad \text{(for Re } \nu > -1, \text{ Re } a > 0)$$

(cf. Abramowitz and Stegun [57, p. 487, Formula 11.4.31]).

Then

$$(\mathcal{J}_2) = \frac{1}{2}\sqrt{\frac{2\hbar\pi}{m\Omega}} e^{\frac{m\Omega a^2}{\hbar}} I_0\left(\frac{m\Omega a^2}{\hbar}\right).$$

Therefore, we have arrived at

$$\mathfrak{B}_3 = 2\langle a(1)b(2)|C|a(1)b(2)\rangle = 2\left(\frac{\pi m\Omega}{2\hbar}\right)^{1/2} \frac{e^2}{\kappa} e^{-\frac{m\Omega a^2}{\hbar}} I_0\left(\frac{m\Omega a^2}{\hbar}\right)$$
$$= 2\hbar\omega_0 c\sqrt{b}\; e^{-bd^2} I_0(bd^2); \quad \left(\text{with } c = \frac{e^2}{\kappa}\frac{1}{\hbar\omega_0}\sqrt{\frac{\pi m\omega_0}{2\hbar}}, \text{ cf. (6.9)}\right). \qquad \text{(B.40)}$$

Next, we proceed to evaluate integral in $\mathfrak{B}_4$:

$$\mathfrak{B}_4 = \langle a(1)b(2)|C|a(2)b(1)\rangle + \langle a(2)b(1)|C|a(1)b(2)\rangle$$
$$= 2\ \mathrm{Re}\langle a(1)b(2)|C|a(2)b(1)\rangle$$

Similarly to (B.36)–(B.39), using the center-of-mass coordinates (B.37) and (B.38),

this may be written

$$\mathfrak{B}_4 = 2\ \mathrm{Re}\left(\frac{m\Omega e}{\pi\hbar}\right)^2 \frac{1}{\kappa} \int_0^{2\pi}\int_0^{2\pi}\int_0^{\infty}\int_0^{\infty} \frac{1}{r} \exp\left\{ i\frac{eBa}{\hbar c}y - \frac{m\Omega}{\hbar}\left[\left(\frac{2X+x}{2}\right)^2 + \left(\frac{2X-x}{2}\right)^2 \right.\right.$$
$$\left.\left. +2a^2 + \left(\frac{2Y+y}{2}\right)^2 + \left(\frac{2Y-y}{2}\right)^2\right]\right\} r\,dr\,R\,dR \cdot d\phi\,d\Phi$$
$$= 2\ \mathrm{Re}\left(\frac{m\Omega e}{\pi\hbar}\right)^2 \frac{1}{\kappa} e^{-\frac{2m\Omega a^2}{\hbar}} \int_0^{2\pi}\int_0^{2\pi}\int_0^{\infty}\int_0^{\infty} e^{\left\{\frac{ieBa}{\hbar c}y - \frac{m\Omega}{\hbar}\left[2X^2+2Y^2+\frac{x^2}{2}+\frac{y^2}{2}\right]\right\}} dr\,R\ dR\ d\phi\ d\Phi$$
$$= 2\ \mathrm{Re}\left(\frac{m\Omega e}{\phi\hbar}\right)^2 \frac{1}{\kappa} e^{-\frac{2m\Omega a^2}{\hbar}} \int_{-\infty}^{\infty} e^{-\frac{2m\Omega}{\hbar}X^2} dX \cdot \int_{-\infty}^{\infty} e^{-\frac{2m\Omega}{\hbar}Y^2} dY$$
$$\cdot \int_0^{\infty} e^{-\frac{m\Omega}{2\hbar}r^2} \underbrace{\left[\int_0^{2\pi} e^{\frac{ieBa}{\hbar c}r\sin\phi} d\phi\right]}_{(\mathcal{J}_3)} dr$$
$$= 2\ \mathrm{Re}\left(\frac{m\Omega e}{\pi\hbar}\right)^2 \frac{1}{\kappa} e^{-\frac{2m\Omega a^2}{\hbar}} \cdot \left(\frac{\pi\hbar}{2m\Omega}\right)^{1/2} \cdot \left(\frac{\pi\hbar}{2m\Omega}\right)^{1/2} \underbrace{\int_0^{\infty} e^{-\frac{m\Omega}{2\hbar}r^2} (\mathcal{J}_3) dr}_{(\mathcal{J}_4)},$$

where

$$(\mathcal{J}_3) = \int_0^{2\pi} e^{\frac{ieBa}{\hbar c}r\sin\phi} d\phi = J_0\left(\frac{eBa}{\hbar c}r\right) \cdot 2\pi$$

(cf. Abramowitz and Stegun [57, p. 360, Formula (9.1.18)])

and

$$(\mathcal{J}_4) = 2\pi \int_0^{\infty} e^{-\frac{m\Omega}{2\hbar}r^2} J_0\left(\frac{eBa}{\hbar c}r\right) dr = 2\pi\sqrt{\frac{\hbar\pi}{2m\Omega}} e^{-(\frac{eBa}{\hbar c})^2 \frac{\hbar}{4m\Omega}} \cdot I_0\left(\left(\frac{eBa}{\hbar c}\right)^2 \frac{\hbar}{4m\Omega}\right)$$

(cf. Gradshteyn and Ryzhik [58, p. 732, Formula (6.618(1))]).

Therefore, we have arrived at

$$\begin{aligned}\mathfrak{B}_4 = 2\ \mathrm{Re}\langle a(1)b(2)|C|a(2)b(1)\rangle \\ &= 2\ \mathrm{Re}\left(\frac{m\Omega}{\hbar}\right)^{1/2}\sqrt{\frac{\pi}{2}}\frac{e^2}{\kappa}e^{-\frac{2m\Omega}{\hbar}a^2-\frac{e^2B^2a^2}{4\hbar c^2 m\Omega}}I_0\left(\frac{e^2B^2a^2}{4\hbar c^2 m\Omega}\right) \\ &= 2\hbar\omega_0 c\sqrt{b}\ e^{-2bd^2}e^{-d^2(b-\frac{1}{b})}I_0\left(d^2\left(b-\frac{1}{b}\right)\right).\end{aligned} \tag{B.41}$$

Using S in (B.24), we obtain from (B.40) and (B.41) that $\mathfrak{B}_3 - (1/S^2)\mathfrak{B}_4$ is indeed equal to (B.35). □

Finally, we evaluate $\mathfrak{B}_5$.

Lemma .5. *We have*

$$\mathfrak{B}_5 = -4m\omega_0^2a^2 + 2\cdot\left(\frac{m\omega_0^2}{2}\right)\left[\frac{3\hbar}{2m\Omega} + 3\left(\frac{eE}{m\omega_0^2}\right)^2 + \frac{3}{2}a^2\right]. \tag{B.42}$$

Proof. First, we want to show that

$$\begin{aligned}&\langle a(1)b(2)|W|a(1)b(2)\rangle + \langle a(2)b(1)|W|a(2)b(1)\rangle \\ =\ & 2\langle a(1)b(2)|W|a(1)b(2)\rangle - 4m\omega_0^2a^2.\end{aligned} \tag{B.43}$$

The first term in $\mathfrak{B}_5$ (and on the left hand side of (B.43)) satisfies

$$\begin{aligned}\langle a(1)b(2)|W|a(1)b(2)\rangle &= \langle a(1)|W_1|a(1)\rangle + \langle b(2)|W_2|b(2)\rangle \qquad \text{(see (B.4), (B.5))} \\ &= \langle b(1)|e^{\frac{i}{\hbar}(\frac{eBa}{c}y_1-2ap_{x_1})}W_1e^{-\frac{i}{\hbar}(\frac{eBa}{c}y_1-2ap_{x_1})}|b(1)\rangle \\ &\quad + \langle a(2)|e^{-\frac{i}{\hbar}(\frac{eBa}{c}y_2-2ap_{x_2})}W_2e^{\frac{i}{\hbar}(\frac{eBa}{c}y_2-2ap_{x_2})}|a(2)\rangle.\end{aligned} \tag{B.44}$$

But

$$W_1(x) = \frac{m\omega_0^2}{2}\left[\frac{1}{4a^2}(x^2-a^2)^2 - (x+a)^2\right],$$

so

$$\begin{aligned} & e^{\frac{i}{\hbar}(\frac{eBa}{c}y_1-2ap_{x_1})}W_1(x_1)e^{-\frac{i}{\hbar}(\frac{eBa}{c}y_1-2ap_{x_1})} = W_1(x_1-2a) \\ = \;& \frac{m\omega_0^2}{2}\left[\frac{1}{4a^2}((x_1-2a)^2-a^2)^2-(x_1-2a+a)^2\right] \\ = \;& \cdots(\text{expanding and regrouping terms}) \\ = \;& W_1(x_1)+\frac{m\omega_0^2}{2}\left[4ax_1-\frac{2}{a}(x_1-a)^3\right]. \end{aligned} \tag{B.45}$$

Similarly, for W_2 given in (B.5),

$$\begin{aligned} & e^{-\frac{i}{\hbar}(\frac{eBa}{c}y_2-2ap_{x_2})}W_2(x_2)e^{\frac{i}{\hbar}(\frac{eBa}{c}y_2-2ap_{x_2})} = W_2(x_2+2a) \\ = \;& W_2(x_2)+\frac{m\omega_0^2}{2}\left[-4ax_2+\frac{2}{a}(x_2+a)^3\right]. \end{aligned} \tag{B.46}$$

Thus, continuing from (B.44) using (B.45) and (B.46), we have

$$\begin{aligned} (\text{B.44}) &= \langle b(1)|W_1|b(1)\rangle + \langle b(1)|\frac{m\omega_0^2}{2}\left[4ax_1-\frac{2}{a}(x_1-a)^3\right]|b(1)\rangle \\ &\quad + \langle a(2)|W_2|a(2)\rangle + \langle a(2)|\frac{m\omega_0^2}{2}\left[-4ax_2+\frac{2}{a}(x_2+a)^3\right]|a(2)\rangle \\ &= \langle b(1)a(2)|W|b(1)a(2)\rangle + 2m\omega_0^2 a[\langle b(1)|x_1|b(1)\rangle - \langle a(2)|x_2|a(2)\rangle] \\ &\quad + \frac{m\omega_0^2}{a}[\langle a(2)|(x_2+a)^3|a(2)\rangle - \langle b(1)|(x_1-a)^3|b(1)\rangle] \\ &= \langle b(1)a(2)|W|b(1)a(2)\rangle + 2m\omega_0^2 a\left[\langle b(1)|(x_1)_+ + a - \frac{eE}{m\omega_0^2}|b(1)\rangle\right. \end{aligned}$$

$$
\begin{aligned}
&-\langle a(2)|(x_2)_- - a - \frac{eE}{m\omega_0^2}|a(2)\rangle\Bigg] \\
&+\frac{m\omega_0^2}{a}\left[\langle a(2)|\left((x_2)_- - \frac{eE}{m\omega_0^2}\right)^3|a(2)\rangle - \langle b(1)|\left((x_1)_+ - \frac{eE}{m\omega_0^2}\right)^3|b(1)\rangle\right] \\
&\text{(where, recall that } x_+ = x - a + \frac{eE}{m\omega_0^2} \text{ and } x_- = x + a + \frac{eE}{m\omega_0^2}\text{)} \\
&= \langle b(1)a(2)|W|b(1)a(2)\rangle + 4m\omega_0^2 a^2 \\
&+\frac{m\omega_0^2}{a}\left[\langle a(2)|(x_2)_-^3 - \frac{3eE}{m\omega_0^2}(x_2)_-^2 + 3\left(\frac{eE}{m\omega_0^2}\right)^2(x_2)_- - \left(\frac{eE}{m\omega_0}\right)^3|a(2)\rangle\right. \\
&\left.-\langle b(1)|(x_1)_+^3 - 3\frac{eE}{m\omega_0^2}(x_1)_+^2 + 3\left(\frac{eE}{m\omega_0^2}\right)^2(x_1)_+ - \left(\frac{eE}{m\omega_0}\right)^3|b(1)\rangle\right] \\
&= \langle b(1)a(2)|W|b(1)a(2)\rangle + 4m\omega_0^2 a^2. \qquad \text{(B.47)}
\end{aligned}
$$

By (B.44) and (B.47), we have confirmed (B.43). So our objective now is to evaluate

$\langle a(1)b(2)|W|a(1)b(2)\rangle$:

$$
\langle a(1)b(2)|W|a(1)b(2)\rangle = \langle a(1)|W_1|a(1)\rangle + \langle b(2)|W_2|b(2)\rangle; \qquad \text{(B.48)}
$$

$$
\begin{aligned}
\langle a(1)|W_1|a(1)\rangle &= \frac{m\Omega}{\pi\hbar}\int_{-\infty}^{\infty}\int_{-\infty}^{\infty} e^{-\frac{m\Omega}{\hbar}[(x_1+a+\frac{eE}{m\omega_0^2})^2+y_1^2]}\cdot \\
&\quad\cdot\frac{m\omega_0^2}{2}\left[\frac{1}{4a^2}(x_1^2-a^2)^2 - (x_1+a)^2\right] \quad dx_1dy_1 \equiv f(a);
\end{aligned}
\qquad \text{(B.49)}
$$

$$
\begin{aligned}
\langle b(2)|W_2|b(2)\rangle &= \frac{m\Omega}{\pi\hbar}\int_{-\infty}^{\infty}\int_{-\infty}^{\infty} e^{-\frac{m\Omega}{\hbar}[(x_2-a+\frac{eE}{m\omega_0^2})^2+y_2^2]}\cdot \\
&\quad\cdot\frac{m\omega_0^2}{2}\left[\frac{1}{4a^2}(x_2^2-a^2)^2 - (x_2-a)^2\right]dx_2dy_2. \qquad \text{(B.50)}
\end{aligned}
$$

By comparing (B.49) and (B.50), we see that if the outcome of (B.49) is $f(a)$ (with all the parameters other than a being fixed), then the outcome of (B.50) will be $f(-a)$.

Similarly,

$$\langle a(1)|W_1|b(1)\rangle = \frac{m\Omega}{\pi\hbar}\int_{-\infty}^{\infty}\int_{-\infty}^{\infty} e^{\frac{i}{\hbar}\frac{eBa}{c}y_1} e^{-\frac{m\Omega}{\hbar}[(x_1+\frac{eE}{m\omega_0^2})^2+a^2+y_1^2]}\cdot$$
$$\cdot\frac{m\omega_0^2}{2}\left[\frac{1}{4a^2}(x_1^2-a^2)^2-(x_1+a)^2\right]dx_1dy_1 \equiv g(a), \tag{B.51}$$

then

$$\langle b(2)|W_2|a(2)\rangle = \frac{m\Omega}{\pi\hbar}\int_{-\infty}^{\infty}\int_{-\infty}^{\infty} e^{-\frac{i}{\hbar}\frac{eBa}{c}y_2} e^{-\frac{m\Omega}{\hbar}[(x_2+\frac{eE}{m\omega_0^2})^2+a^2+y_2^2]}\cdot$$
$$\cdot\frac{m\omega_0^2}{2}\left[\frac{1}{4a^2}(x_2^2-a^2)^2-(x_2-a)^2\right]dx_2dy_2 = g(-a). \tag{B.52}$$

By translating $x \mapsto x - a - \frac{eE}{m\omega_0^2}$, we have

$$\langle a(1)|W_1|a(1)\rangle = \text{(B.49)} = \frac{m\Omega}{\pi\hbar}\left[\int_{-\infty}^{\infty} e^{-\frac{m\Omega}{\hbar}y^2}dy\right]\left[\int_{-\infty}^{\infty} e^{-\frac{m\Omega}{\hbar}x^2} W_1\left(x-a-\frac{eE}{m\omega_0^2}\right)dx\right]. \tag{B.53}$$

Here

$$W_1\left(x-a-\frac{eE}{m\omega_0^2}\right) = W_1(x-a-\beta) \quad \left(\beta \equiv \frac{eE}{m\omega_0^2}\right) \tag{B.54}$$
$$= \frac{m\omega_0^2}{2}\left\{\frac{1}{4a^2}[(x-a-\beta)^2-a^2]^2-(x-\beta)^2\right\}$$
$$= \frac{m\omega_0^2}{2}\left[\frac{1}{4a^2}(x-\beta)^4-\frac{1}{a}(x-\beta)^3\right]$$
$$= \frac{m\omega_0^2}{2}\left[\frac{1}{4a^2}x^4-\left(\frac{\beta}{a^2}+\frac{1}{a}\right)x^3+\left(\frac{3}{2}\frac{\beta^2}{a^2}+\frac{3\beta}{a}\right)x^2\right.$$
$$\left.-\left(\frac{\beta^3}{a^2}+\frac{3\beta^2}{a}\right)x+\left(\frac{\beta^4}{4a^2}+\frac{\beta^3}{a}\right)\right]. \tag{B.55}$$

Recall the formulas for Gaussian integrals

$$\int_{-\infty}^{\infty} x^{2n} e^{-\alpha x^2} dx = -\left(\frac{\partial}{\partial \alpha}\right)^n \int_{-\infty}^{\infty} e^{-\alpha x^2} dx = \left(-\frac{\partial}{\partial \alpha}\right)^n \sqrt{\frac{\pi}{\alpha}}$$

$$= \left[\prod_{k=1}^{n} \left(\frac{1}{2} + k - 1\right)\right] \left(\frac{1}{\alpha^n}\sqrt{\frac{\pi}{\alpha}}\right), \quad \text{for} \quad n = 1, 2, \ldots, \tag{B.56}$$

$$\int_{-\infty}^{\infty} x^{2n+1} e^{-\alpha x^2}\ dx = 0, \quad \text{for} \quad n = 0, 1, 2, \ldots, \tag{B.57}$$

from (B.53), (B.55)–(B.57) we obtain

$$\begin{aligned}
\langle a(1)|W_1|a(1)\rangle &= \frac{m\Omega}{\pi\hbar}\left(\frac{\pi\hbar}{m\Omega}\right)^{1/2}\left(\frac{m\omega_0^2}{2}\right) \\
&\quad \times \left[\frac{1}{4a^2}\frac{\partial^2}{\partial\alpha^2} - \left(\frac{3\beta^2}{2a^2} + \frac{3\beta}{a}\right)\frac{\partial}{\partial\alpha} + \left(\frac{\beta^4}{4a^2} + \frac{\beta^3}{a}\right)\right]\left(\sqrt{\frac{\pi}{\alpha}}\right) \\
&\quad (\text{where } \alpha \equiv m\Omega/\hbar) \\
&= \frac{m\Omega}{\pi\hbar}\left(\frac{\pi\hbar}{m\Omega}\right)^{1/2}\frac{m\omega_0^2}{2}\left(\frac{\pi\hbar}{m\Omega}\right)^{1/2} \\
&\quad \times \left[\frac{1}{4a^2}\frac{3\hbar^2}{4m^2\Omega^2} + \frac{1}{2}\left(\frac{3\beta^2}{2a^2} + \frac{3\beta}{a}\right)\frac{\hbar}{m\Omega} + \frac{\beta^4}{4a^2} + \frac{\beta^3}{a}\right] \\
&= \frac{m\omega_0^2}{2}\left[\frac{3\hbar^2}{16m^2\Omega^2a^2} + \left(\frac{3\beta^2}{4a^2} + \frac{3\beta}{2a}\right)\frac{\hbar}{m\Omega} + \frac{\beta^4}{4a^2} + \frac{\beta^3}{a}\right] \\
&= f(a); \qquad \text{cf. (B.49).}
\end{aligned}$$

Then $\langle b(2)|W_2|b(2)\rangle = f(-a)$ and so from (B.48), we obtain

$$\langle a(1)b(2)|W|a(2)b(1)\rangle = \frac{m\omega_0^2}{2}\left[\frac{3\hbar^2}{8m^2\Omega^2a^2} + \frac{3\beta^2\hbar}{2a^2m\Omega} + \frac{\beta^4}{2a^2}\right]. \tag{B.58}$$

Next, repeat similar procedures,

$$
\begin{aligned}
(\text{B.51}) &= \frac{m\Omega}{\pi\hbar} e^{-\frac{m\Omega}{\hbar}a^2} \left[\int_{-\infty}^{\infty} e^{\frac{i}{\hbar}\frac{eBa}{c}y - \frac{m\Omega}{\hbar}y^2}\, dy \right] \left[\int_{-\infty}^{\infty} e^{-\frac{m\Omega}{\hbar}x^2} W_1(x-\beta)dx \right] \\
&= \frac{m\Omega}{\pi\hbar} e^{-\frac{m\Omega}{\hbar}a^2} \left[\int_{-\infty}^{\infty} e^{-\frac{m\Omega}{\hbar}(y - i\frac{eBa}{2m\Omega c})^2 - \frac{m\Omega}{\hbar}\frac{e^2B^2a^2}{4m^2\Omega^2c^2}} dy \right] \\
&\quad \cdot \int_{-\infty}^{\infty} e^{-\frac{m\Omega}{\hbar}x^2} \cdot \frac{m\omega_0^2}{2} \left[\frac{1}{4a^2}(x-\beta+a)^4 - \frac{1}{a}(x-\beta+a)^3 \right] dx \\
&= \left(\frac{m\Omega}{\pi\hbar} \right) e^{-\frac{m\Omega}{\hbar}a^2 - \frac{e^2B^2a^2}{4\hbar m\Omega c^2}} \left(\frac{\pi\hbar}{m\Omega} \right)^{1/2} \cdot \left(\frac{\pi\hbar}{m\Omega} \right)^{1/2} \cdot \frac{m\omega_0^2}{2} \cdot \\
&\quad \left\{ \frac{3\hbar^2}{16m^2\Omega^2a^2} + \left[\frac{3(\beta-a)^2}{4a^2} + \frac{3(\beta-a)}{2a} \right] \frac{\hbar}{m\Omega} + \frac{(\beta-a)^4}{4a^2} + \frac{(\beta-a)^3}{a} \right\} = g(a).
\end{aligned}
\tag{B.59}
$$

Therefore,

$$
\begin{aligned}
\langle a(1)b(2)|W|a(2)b(1)\rangle &= \langle a(1)|W_1|b(1)\rangle\langle b(2)|a(2)\rangle + \langle a(1)|b(1)\rangle \cdot \langle b(2)|W_2|a(2)\rangle \\
&= S[\langle a(1)|W_1|b(1)\rangle + \langle b(2)|W_2|a(2)\rangle] \\
&= S[g(a) + g(-a)] \qquad (\text{by (B.52)}) \\
&= S \cdot e^{-\frac{a^2}{\hbar}(m\Omega + \frac{e^2B^2}{4m\Omega c^2})} \frac{m\omega_0^2}{2} \left[\frac{3\hbar^2}{8m^2\Omega^2a^2} + \left(\frac{3\beta^2}{2a^2} + \frac{3}{2} - 3 \right) \frac{\hbar}{m\Omega} \right. \\
&\quad \left. + \frac{\beta^4}{2a^2} + 3\beta^2 + \frac{a^2}{2} - 6\beta^2 - 2a^2 \right] \quad (\text{by (B.58) and (B.52)}).
\end{aligned}
$$

But the factor $e^{-\frac{a^2}{\hbar}(m\Omega + \frac{e^2B^2}{4m\Omega c^2})}$ behind S is just S itself by (B.24). Thus

$$
\frac{1}{S^2}\langle a(1)b(2)|W|a(2)b(1)\rangle = \frac{m\omega_0^2}{2} \left[\frac{3\hbar^2}{8m^2\Omega^2a^2} + \frac{3}{2}\left(\frac{\beta^2}{a^2} - 1 \right) \frac{\hbar}{m\Omega} + \frac{\beta^4}{2a^2} - 3\beta^2 - \frac{3}{2}a^2 \right].
\tag{B.60}
$$

Summarizing (B.43), (B.58) and (B.60), we have

$$\begin{aligned}\mathfrak{B}_5 &= 2\langle a(1)b(2)|W|a(1)b(2)\rangle - 4m\omega_0^2 a^2 \\ &\quad - 2\ \mathrm{Re}\cdot\frac{1}{S^2}\langle a(1)b(2)|W|a(2)b(1)\rangle \\ &= -4m\omega_0^2 a^2 + 2\cdot\left(\frac{m\omega_0^2}{2}\right)\left(\frac{3\hbar}{2m\Omega} + 3\beta^2 + \frac{3}{2}a^2\right).\end{aligned}$$

This is (B.42). □

We can now combine all the preceding lemmas and finally obtain the following.

Theorem .6. *The exchange energy is given by*

$$\begin{aligned}J &= \langle\Psi_-|H_{orb}|\Psi_-\rangle - \langle\Psi_+|H_{orb}|\Psi_+\rangle \\ &= (6.4).\end{aligned}$$

Proof. We only need note that with S given in (B.24), we have

$$\frac{S^2}{1-S^4} = \frac{1}{S^{-2}-S^2} = \frac{1}{2\sinh(2d^2(2b-\frac{1}{b}))}.$$

Thus, the coefficient outside the parentheses in (B.28) is determined as above. We now collect all the terms in (B.29), (B.35), and (B.42), noting the cancellation of the terms $4ma^2\omega_0^2$ and $-4ma^2\omega_0^2$ in (B.28) and (B.42), and then simplify (just a little). We then obtain (6.4). □

VITA

Kerim Urtekin

Address:

Texas A&M University

Physics Department

College Station, TX

77843-4242

Degrees received:

B.S. in Physics, Bogazici University, Istanbul, Turkey, 1994;

Ph.D. in Physics, Texas A&M University, 2006

Publications include:

G. Chen, S.A. Chin, Y. Dou, K.T. Kapale, M. Kim, A.A. Svidzinsky, K. Urtekin, H. Xiong and M.O. Scully, Advances in Atomic, Molecular and Optical Physics, **51**, 93-238 (2005).

G. Chen, Z. Diao, J. U. Kim, A. Neogi, K. Urtekin, Z. Zhang, International Journal of Quantum Information, **4**, 233-296, (2006)